DYNAMIC MODELLING AND CONTROL OF A TWO-AXIS GIMBAL SYSTEM WITH MODEL REFERENCE ADAPTIVE CONTROL

A THESIS SUBMITTED TO
THE GRADUATE SCHOOL OF NATURAL AND APPLIED SCIENCES
OF
MIDDLE EAST TECHNICAL UNIVERSITY

BY

ÖMER FARUK BARLAS

IN PARTIAL FULFILLMENT OF THE REQUIREMENTS
FOR
THE DEGREE OF MASTER OF SCIENCE
IN
MECHANICAL ENGINEERING

APRIL 2023

Approval of the thesis:

DYNAMIC MODELLING AND CONTROL OF A TWO-AXIS GIMBAL SYSTEM WITH MODEL REFERENCE ADAPTIVE CONTROL

submitted by **ÖMER FARUK BARLAS** in partial fulfillment of the requirements for the degree of **Master of Science in Mechanical Engineering, Middle East Technical University** by,

Prof. Dr. Halil Kalıpçılar
Dean, Graduate School of **Natural and Applied Sciences** _____

Prof. Dr. M. A. Sahir Arıkan
Head of the Department, **Mechanical Engineering, METU** _____

Prof. Dr. Yiğit Yazıcıoğlu
Supervisor, **Mechanical Engineering, METU** _____

Examining Committee Members:

Prof. Dr. R. Tuna Balkan
Mechanical Engineering, METU _____

Prof. Dr. Yiğit Yazıcıoğlu
Mechanical Engineering, METU _____

Assoc. Prof. Dr. Ulaş Yaman
Mechanical Engineering, METU _____

Assist. Prof. Dr. Hakan Çalışkan
Mechanical Engineering, METU _____

Assoc. Prof. Dr. Bülent Özkan
Mechanical Engineering., Gazi Uni. _____

Date: 14.04.2023

I hereby declare that all information in this document has been obtained and presented in accordance with academic rules and ethical conduct. I also declare that, as required by these rules and conduct, I have fully cited and referenced all material and results that are not original to this work.

Name Last name : Ömer Faruk Barlas

Signature :

ABSTRACT

DYNAMIC MODELLING AND CONTROL OF A TWO-AXIS GIMBAL SYSTEM WITH MODEL REFERENCE ADAPTIVE CONTROL

Barlas, Ömer Faruk
Master of Science, Mechanical Engineering
Supervisor: Prof. Dr. Yiğit Yazıcıoğlu

April 2023, 132 pages

Providing high-speed and uninterrupted communication has become primary demands of today. Out of the coverage area, it is needed to establish a communication path with the satellites in space. Thus, gimbal systems were developed, that direct the antennas to the satellites with desired position accuracy. Application areas and performance criteria determine the design specifications of gimbal systems. In this study, the gimbal system assembled to the naval platform and used in the orientation and stabilization of a antenna was discussed.

In this thesis, a detailed mathematical model was obtained by expressing kinematic relations with Denavit-Hartenberg convention and dynamic relations with Newton-Euler method of a statically-balanced but dynamically-unbalanced two-axis gimbal system. Therefore, a nonlinear equation of motion was obtained, and the system was linearized and expressed in state space representation. According to the system identification tests on physical system, it was realized that the linearized system model has differences due to the modeling uncertainties and the structural flexibility of the mechanical system. The model reference adaptive control (MRAC) method was used by considering these differences in the control system design. Additionally, the control system was developed using the full-state feedback control method that

was used both for comparison of the controllers and as reference model in the MRAC method. Further to these control methods, cascaded PI control method, being frequently used in the industry, was developed using a straightforward gimbal model and compared with other methods. Finally, experiments and simulation studies were carried out and the results were examined and discussed.

Keywords: Gimbal Systems, Mathematical Model, System Identification, Model Reference Adaptive Control (MRAC), Full-State Feedback Control

ÖZ

İKİ EKSEN BİR GİMBAL SİSTEMİNİN DİNAMİK MODELLENMESİ VE MODEL REFERANS ADAPTİF KONTROL İLE KONTROLÜ

Barlas, Ömer Faruk
Yüksek Lisans, Makina Mühendisliği
Tez Yöneticisi: Prof. Dr. Yiğit Yazıcıoğlu

Nisan 2023, 132 sayfa

Haberleşmenin yüksek hızda ve kesintisiz olarak sağlanabilmesi günümüzdeki en önemli ihtiyaçlardan biri haline gelmiştir. Yerleşim bölgeleri dışında haberleşme kapsama alanının dışına çıkılması, uzayda yer alan haberleşme uyduları ile farklı bir iletişim yolu kurmayı gerektirmektedir. Bu amaçla kullanılan haberleşme antenlerini uydulara belirli konum hassasiyeti içerisinde yönlendirecek gimbal sistemler geliştirilmektedir. Uygulama alanları ve istenilen performans kriterleri gimbal sistemlerin tasarım isterlerini belirlemektedir. Bu çalışmada deniz platformuna bağlanacak olan ve bir haberleşme anteninin yönlendirilmesi ve stabilizasyonunda kullanılacak olan gimbal sistem ele alınmıştır.

Bu tezde önce statik olarak dengede fakat dinamik olarak dengesiz, iki eksenli bir gimbal sistemin Denavit-Hartenberg ve Newton-Euler yaklaşımlarıyla kinematik ve dinamik ilişkileri ifade edilerek detaylı matematik modeli elde edilmiştir. Matematik model sonucu lineer olmayan bir hareket denklemine ulaşılmıştır ve bu denklemden yola çıkarak sistem lineerleştirilmiş ve durum uzayı gösteriminde ifade edilmiştir. Gerçekte üretilmiş sistem üzerinde yapılan sistem tanımlama çalışmaları sonucuna göre lineerleştirilmiş sistem modelinin modelleme belirsizlikleri ve mekanik

sistemin yapısal esnekliğinden dolayı farklılıklar gösterdiği anlaşılmıştır. Kontrol sistem tasarımında bu farklılıklar göz önüne alınarak model referans adaptif kontrol yöntemi kullanılmıştır. Ayrıca tam durum geri besleme kontrol yöntemi kullanılarak geliştirilen kontrol sistemi hem karşılaştırma amaçlı kullanılmış hem de model referans adaptif kontrol yönteminde referans model olarak kullanılmıştır. Bu kontrol yöntemlerine ilave olarak endüstride sıklıkla kullanılan kaskad yapıda PI kontrol yöntemi, basitleştirilmiş bir gimbal modeli kullanılarak geliştirilmiş ve diğer yöntemlerle karşılaştırılmıştır. Son olarak deney ve benzetim çalışmaları gerçekleştirilmiş; sonuçlar incelenerek, tartışılmıştır.

Anahtar Kelimeler: Gimbal Sistemleri, Matematik Model, Sistem Tanımlama, Model Referans Adaptif Kontrol, Tam Durum Geri Besleme

To my family and my love Aynur

ACKNOWLEDGMENTS

Firstly, I would like to thank my supervisor Prof. Dr. Yiğit Yazıcıoğlu for his guidance and support throughout the thesis.

I would like to express my appreciations to Emre Aynagöz, who I had the opportunity to work with at the beginning of my career and contributed endlessly both in this study and in my engineering life. I also thank my friends Akın Arslan and Otur Ata for their support during this period.

I would like to thank my manager Dr. Akif Türker Gürer and ASELSAN Inc. for its support in my graduate education.

I am very grateful to my family for their invaluable support not only during my education, but also throughout my life.

Finally, I would like to thank my lovely wife, Aynur, for her great support and understanding at every stage of my life.

TABLE OF CONTENTS

LIST OF TABLES

TABLES

LIST OF FIGURES

FIGURES

LIST OF ABBREVIATIONS

ABBREVIATIONS

LOS: Line of sight

MRAC: Model reference adaptive control

FSFC: Full-state feedback control

DH: Denavit-Hartenberg

FRF: Frequency response functions

LIST OF SYMBOLS

SYMBOLS

θ_1: Angular position variable of azimuth axis

$\dot{\theta}_1$: Angular velocity variable of azimuth axis

θ_2: Angular position variable of elevation axis

$\dot{\theta}_2$: Angular velocity variable of elevation axis

$\mathcal{F}_k(O_k)$: Reference frame of $k-th$ link whose origin is at point O_k

$\vec{u}_j^{(k)}$: j-th basis vector of the k-th reference frame

$\hat{C}^{(i,j)}$: Transformation matrix of reference frame from $\mathcal{F}_i$ to $\mathcal{F}_j$

$\vec{\omega}_k$: Angular velocity of the k-th body

$\vec{v}_k$: Velocity of the $k-th$ body origin with respect to $\mathcal{F}_0(O_0)$

$\vec{\alpha}_k$: Angular acceleration of the $k-th$ body origin with respect to $\mathcal{F}_0(O_0)$

$\vec{a}_k$: Angular acceleration of the $k-th$

m_1: Mass of the body 1

m_2: Mass of the body 2

$\hat{J}_1^{(1)}$: Inertia matrix of the body 1 with respect to $\mathcal{F}_1(O_1)$

$\hat{J}_2^{(2)}$: Inertia matrix of the body 1 with respect to $\mathcal{F}_2(O_2)$

$\vec{F}_{jk}$: Force acting on body k from body j

$\vec{T}_{jk}$: Torque acting on body k from body j

M_{jk}: Reaction moment acting on body k from body j

$\hat{J}_{outer}^{(1)}$: Inertia matrix of the outer gimbal body with respect to $\mathcal{F}_1(O_1)$

$\hat{J}_{inner}^{(1)}$: Inertia matrix of the inner gimbal body with respect to $\mathcal{F}_2(O_2)$

CHAPTER 1

INTRODUCTION

Although communication technologies are highly developed today, communication coverage areas are mostly limited to residential areas [1]. However, the need for communication continues, and a way to communicate with satellites in space is required in order to maintain communication. These satellites are always located at a fixed point in space, and the line of sight (LOS) of the antennas must be directed to this point. Nevertheless, looking at the same point while on a moving object is quite difficult compared to antenna systems placed on a fixed platform. For this purpose, the antennas are assembled on a movable mechanical structure called gimbal and directed to a fixed point according to the inertial reference system.

Gimbal usually consists of mechanical elements such as electric motor, bearings, gyroscope, encoders [2]. It is used to direct the objects which are expressed as payloads placed on it to the desired position. Although the gimbal system examined in this thesis includes an antenna as a payload, it has many different usage areas. These include target tracking with camaras, guidance of missiles, turret control, astronomical telescopes; one of the best-known examples is the Hubble space telescope. This telescope is used to orient distant stars and galaxies very precisely and to take images while maintaining its position [2]. The area where the gimbal will be used is one of the most important factors affecting its mechanical design. Issues such as the useful load it carries, the disturbance effects from platform on which it is placed, and the desired orientation accuracy directly determine the gimbal design. Similarly, the structural dynamics, friction, mass unbalance properties of the gimbal system are decisive for the controller design. [3]

The gimbal system used in this study is product of ASELSAN company, carries an antenna as specified and will be mounted on a marine platform as demonstrated in Figure 1. Since it is necessary to have at least two degrees of freedom to look at a point in space, this gimbal system also has two degrees of freedom called azimuth (yaw) and elevation (pitch) axes. These are the rotation freedoms in the direction of two axes perpendicular to each other; the position and speed variables of the system are measured by encoder and gyro sensors respectively. The system consists of two direct drive brushless DC motors for actuation purposes.

Although it requires kinematically and dynamically complex mathematical expressions, a mathematical model to be created in line with the obtaining of these expressions provides benefits in the design and control of gimbal systems [4]. In systems that have not yet reached the mechanical design stage and have not been physically manufactured, it provides benefits for the design of the control system as well as the applicability of model-based control algorithms. Today's high-capacity computing power enables numerous controller design trials. Therefore, a linearized system model was obtained by analytical mathematical expression in this study. Model reference adaptive control (MRAC), which is a control method that makes use of this linearized model, was used in the control system design. This control method includes an adaptive control algorithm that changes its control signal to converge the response of the system to be controlled to the response of the model called reference model [5]. In addition, a full-state feedback control (FSFC) method was developed using the linearized model and the control system obtained by this method was used as a reference model in the model reference adaptive control method. Also, cascade PI control method designed with a linear decoupled gimbal model obtained with the assumption of independent gimbal masses. Thus, these three methods were compared with each other.

1.1 Literature Survey

Kinematic and dynamic relations of the gimbal system are discussed when obtaining a mathematical model. At this stage, different methods are followed in the expression of relations. In the representation of kinematic relationships, the Denavit-Hartenberg approach, which is generally used in robotic systems, can be used, as well as the Lagrangian's and Newton-Euler methods for dynamic relations. The equations of motion obtained by using these relations are expressed as a set of first order ordinary differential equations with state space representation;thus, the linear system model is obtained. The advantage of obtaining a linear model is that it allows the use of linear control system design methods. There are many studies that have been carried out in the literature on gimbal systems. Some of them are as follows.

In [6], the gimbal, which has a two-axis yaw-pitch configuration, is handled statically and dynamically unbalance, with both Lagrangian and Newton-Euler approaches. In addition, the terms of the obtained equations of motion were expressed under two types of disturbance terms as a result of an appropriate grouping, making the factors affecting the gimbal system more understandable and interpretable. The researcher evaluates the eliminability of these disturbance terms and proposes the feedforward control technique as a solution example. As another solution proposal, it is stated that the cross-coupling behavior between the motion axes can be prevented as a result of balancing the system so as to eliminate the non-zero product of inertia terms.

In [7], the mechanisms of the gimbal systems used in imaging systems were compared, and the kinematic analysis of these mechanisms was performed. Within the scope of a sample flight scenario of the aircraft discussed in the study, these mechanisms were encountered through simulation. Optimum gimballed mechanism configurations were explained according to the purposes of the gimbal systems. Although the purpose and working scenario of the gimbal system were different from the one in this thesis, the kinematic analysis of the gimbal mechanisms in different configurations contributed to this study.

In [8], the Denavit-Hartenberg approach was used to obtain kinematic relationships also worked on the gimbal, which carries a camera system and stabilizes it with the PID control method. In this study, PID tuning methods were focused on, and it was stated that particle swarm optimization method gave the best results among the genetic algorithm, Ziegler Nichols methods. Another study, [9], using the Denavit-Hartenberg approach to obtain kinematic relationships, and the Lagrangian approach for dynamic relationships. Statically balanced but dynamically unbalanced gimbal structure has been studied. Equation of motion is linearized by state space representation; it was used to design the PI control method. The studies were limited to simulation as prototype was not available to use.

In [10], a statically and dynamically unbalanced two-axis gimbal is discussed. In addition, platform movements are included when modeling the gimbal system and the performance of the designed/implemented controllers is also evaluated according to the platform movements. The Lagrangian approach is used to obtain the equations of motion. Cascaded PI is used as the controller, and it is stated that it is successful against base acceleration changes. In addition, in [11], the gimbal system is modeled with four degrees of freedom, where two of the freedom come from gimbal and the other two come from platform movements included in the system model. However, in this study, it is discussed that the mass distribution in the gimbal axes was equal and statically and dynamically balanced; these effects were evaluated as disturbances, and it is aimed to eliminate this effect among the control performance targets.

The controllers used in gimbal systems are usually PI/D. This method, which is frequently used due to its ease of application and adequate performance in most cases, can include adapted and improved PID solutions in gimbal systems [12]. Some of these are PII controllers with two integrals [13] and dual cascaded inner PI and outer PID stabilization controllers [14]. They state that with such approaches, they reduce steady state error and improve disturbance rejection characteristic. In addition, in the studies [15][16], traditional methods designed to eliminate disturbance effects such as mechanical vibrations and signal noises arising from the

platform on which the system mounted were discussed and their comparisons were made by simulation. The effect of control system loop number on performance was also investigated by adapting conventional methods (such as LPV, PID) to single and double loop control systems. In this thesis, a linear decoupled gimbal model was obtained, and a two-layer control system was developed to compare the performance of this common method in the literature. PI controller was used in the inner control loop and the P controller is used in the outer control loop.

There are also controller studies that use the LQG/LTR method as an alternative to PID and require a mathematical model of the system. It has been stated that the LQG/LTR controller is a better alternative as the system becomes nonlinear and complicated [17].

In addition to classical control methods, intelligent control methods have also been applied to gimbals. [18] proposed the fuzzy-knowledge-based control method by stating that classical control methods ignore high order dynamics and lose performance when the system shows nonlinear behavior. They stated that classical control methods respond faster when there are no nonlinear effects, but when nonlinear effects and disturbances are involved, the fuzzy controller gives a similar performance. However, they emphasized the difficulty of fuzzy controller application and the importance of the performance effect of fuzzy variable selection. Therefore, they stated that the system-specific controller design should be carefully selected. [19] applied the fuzzy sliding mode control method to a three-axis gimbal system and stated that it is successful against disturbances. They also stated that this controller suppresses the coupling effect between the control axes. They designed a PI controller for comparison and emphasized that the proposed method is successful against disturbance and coupling effects.

In [20], an adaptive controller is used to take into account system uncertainties and various disturbance effects. Adaptive control based on Radial Basis Function Neural Network has improved stabilization. It is stated that they used this method together with state feedback control and combined both signals. According to the researchers,

the proposed method not only increases the stabilization sensitivity but also provides a more fluent motor voltage when compared to the case using only state feedback.

[21] studied the model reference adaptive control method used with PID to improve the effects of nonlinear and time-varying mass unbalanced torque disturbances on the gimbal system. They state that the method proposed in this study improved robustness and tracking accuracy by 50% compared to the PID controller. In addition, as shown in the experimental results, it is observed that the PID controller has a faster response time but has more overshoot; Although the rising time decreased in the MRAC/PID method, it was stated that there was a significant improvement in the overshoot feature.

As shown experimentally in the SYSTEM IDENTIFICATION Chapter, the gimbal system studied in this thesis is structurally flexible. Figure 23 shows how much the mathematical model obtained with the assumptions of viscous friction and rigid body by ignoring structural flexibility reflects the real system. In [22], researchers expressed the effects of the poor dynamic properties of servo systems with structural flexibility on the performance of the control system. They also stated that only PI/D controllers were not sufficient to suppress the vibrations of the mechanical system in its natural frequencies, and additional feedback signals might be required, but this time the transient response deteriorated. In [23], they studied on a gimbal system used for tracking objective and developed a vibration suppression controller for this system. However, it is stated that the source of the vibration here is not the gimbal system but a flexible spacecraft platform to which the gimbal system is connected. In addition, their main motivation for controlling vibration is to reduce the disturbance effects to be transferred to spacecraft, apart from the orientation (tracking) accuracy. For this purpose, a robust controller was preferred and as a result, they used the H_2/H_∞ control method and stated that they had a successful result except for some singularity problems. In [24], researchers studied on a vibration suppression controller for the gimbal system mounted on a flexible spacecraft. Modal model of the flexible platform is obtained, and the mathematical expression of the vibration is focused via that model. The researchers, who stated that they aimed to

design a simple controller to suppress the vibration, used an extension of a PD type controller. They expressed that they achieved an improvement in the stabilization performance of the gimbal system, yet the method should be modified according to actuator saturation limits for improvement in the tracking performance in the future. It can be examined as another study [25], which works on the vibration problem caused by the effects of flexible mounting dynamics and proposes PI as a control method. There are some studies that work directly on the flexibility of the gimbal system rather than the flexible platform dynamics [26], [27] . The researchers, who preferred the robust control method for multi frequency band disturbance of a flexible gimbal system with high stabilization performance, used the robust disturbance observer and H_∞ optimal vibration controller methods [26]. However, controlling vibrations generated at high frequencies resulted in a motor current saturation situation, thus deteriorating the tracking accuracy. It is understood that controlling vibrations at high frequencies might cause tracking errors, although stabilization performance improves. Therefore, the control system should be designed for the flexible mechanical system by determining the purpose and bandwidth accordingly. High bandwidth may be desired for the system where stabilization is major criterian, but as in this study, if the tracking is a major concern, the bandwidth should be determined according to the transient response requirements, and additional improvements should be evaluated according to the stability of the system [28].

1.2 Problem Definition and Motivation

The gimbal system studied in this thesis; is aimed at orienting the satellite communication antenna on a moving platform to the satellites in space as a primary objective. That objective in gimbal systems can be expressed as tracking. The antenna needs to be oriented within a certain angular position with an accuracy determined by the communication frequency band and the mechanical properties of the antenna used[1]. In this study, it is required that both azimuth and elevation

gimbal control axis tracks the reference input position within a certain position deviation ($\pm 0.5°$). Communication performance decreases in the case of position deviation higher than this value. The criterion of communication performance is to minimize radio frequency signal power loss. Therefore, the antenna, which is the payload carried by the gimbal system, should not have an orientation error of more than the specified angle range.

On the other hand, if the antenna is directed to a satellite and wants to be directed to a different location in order to establish communication with another satellite, it is aimed to be oriented to the new position within 0.5 seconds for both azimuth and elevation gimbal axis. This criterion must be verified with a step response.

In addition to changes in the position and orientation of the platform, it must also maintain its orientation against disturbance effects such as the vibration of a nearby engine that can be transferred from the platform to the system. That can be considered as the second objective of the gimbal system, which is the stabilization or disturbance rejection. As can be seen in the mathematical modeling chapter, the effect of the movement of the platform on the gimbal system was considered as a disturbance effect and the robustness of the control system is expected to overcome this effect. For this reason, the performance criteria of the controller include keeping the gimbal system within the desired orientation range if the platform was exposed to $12°$ of movement with a period of 8 seconds in all three rotating axes.

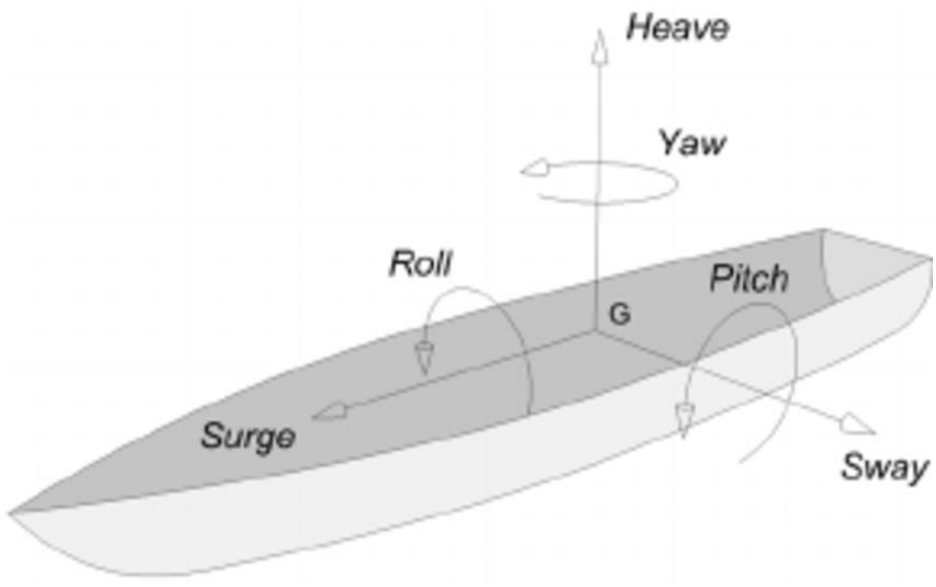

Figure 1: Marine vehicle motions [29]

According to the results obtained in the MATHEMATICAL MODELLING and SYSTEM IDENTIFICATION Chapters, it can be observed that the gimbal system in real behaves differently than it was defined by analytical methods due to its many nonlinear characteristics. As mentioned in the following chapters, the main nonlinearities are friction behavior and flexible structural property of the mechanical system. Even if the mathematical model was obtained very close to the real system, manufacturing tolerances and assembly process of the products caused model discrepancies. These effects are inherent in many real-life control systems, and after the linearized system is obtained and the controller is developed, it is tried to be adapted to by methods such as fine-tuning, which involves adaptation of controller gains manually on the real system. However, this method requires that each product be reviewed and adapted separately; and causes the system to be weak against the effects that are not encountered or unpredictable during fine-tuning process, but that the system will be exposed to during the future working life. Therefore, mentioned nonlinearities dominate the system behavior and result in unpredictable system response. Conventional control methods that consider only the modeled dynamics of the system and ignore the mentioned nonlinearities have lower performance than expected on the real system. In response to this problem, this thesis proposes a

method for the antenna gimbal system, model reference adaptive control, that will perform this operation autonomously and act against structural flexibilities and friction nonlinearities by regarding them as unmodeled disturbances while still using the linearized system in its control structure. Improving the performance of the gimbal control system with MRAC method is the main motivation of this study.

As seen in the Literature Survey section, although there are applications of MRAC method for compensation of mass unbalanced torque disturbance [21], or regarding structural flexibility of gimbal systems with different types of control methods [23], [24], [25], [26], [27]; the proposed MRAC method with full-state feedback controller was to be developed for the structurally flexible antenna gimbal system with the assumption of viscous friction, static mass balanced, dynamically unbalanced.

1.3 Outline of the Thesis

The structure of the thesis is as follows.

In Chapter 2, the two-axis gimbal system was first expressed in kinematic relations using the Denavit-Hartenberg convention and dynamic relationships using the Newton-Euler method in order to obtain a mathematical model of coupled nonlinear three-dimensional gimbal system. Later, a nonlinear equation of motion that governs the coupled gimbal model was derived from these relations. Besides, decoupled linear gimbal model was derived with the assumption of independent gimbal bodies to observe the validity of the very simple model for the specific gimbal system. The responses of the gimbal models were obtained to compare with each other and validate as well as the real physical system. Using the nonlinear equation of motion, the coupled system was linearized around the equilibrium point and expressed as state space representation. The bode plot of the linearized system is shown to express the characteristics of the system.

In Chapter 3, frequency response function identification tests (FRF) were performed to see how well the linear system model obtained analytically in Chapter 2 reflected

the real system. After expressing the properties of the sine swept excitation signal used in the test performed, FRF plots of the actual system were shown. In addition, the bode plots shown in Chapter 2 and the FRF plots obtained in this chapter were compared with each other.

In Chapter 4, the control system was developed using three different control methods. These methods are full-state feedback control, model reference adaptive control and cascade PI control methods. In developing the first, the linearized coupled system model obtained in chapter 2 was used. With the pole placement technique, the state feedback controller was determined to meet the desired specifications. The control system designed with this method was used as the reference model in the model reference adaptive control method. In addition, the full-state feedback controller was also used as a nominal controller in the MRAC method. Then, MRAC update law, determined according to Lyapunov stability criteria, was adapted and designed for the gimbal system. Lastly, a cascade PI control method was designed by using the decoupled gimbal model.

In Chapter 5, The control systems designed in the previous chapter were experimentally applied to the real system; and those were compared and evaluated with the simulation results. Also, the linearized and nonlinear coupled gimbal models were tested against the real system test conditions to observe the validity of the control systems based on mathematical models.

Chapter 6, the work carried out in this thesis is summarized and future works were evaluated.

CHAPTER 2

MATHEMATICAL MODELLING

The mathematical model describes the behavior of the gimbal system in terms of set of equations is to obtained in this chapter. It enables to a better understanding of the system and puts relations between external excitations of the system and response of the system. Although a mathematical model of a real-world system is non-linear in almost all of the cases, it can be linearized around a suitable working condition to use control of it by linear techniques. Therefore, it is worthwhile to obtain a mathematical model even if it is usually a challenging producere. Here, the mathematical modelling of the three-dimensional two-axis gimbal system was achieved for both non-linear and linear representations. Besides, a very simple gimbal model was obtained by ignoring the interaction between the gimbal masses. This decoupled gimbal model was linear and governed by two independent equations of motion. That assumption was then compared to the coupled nonlinear 3D model and the real system and also used in the control design.

2.1 Description of the System

The two-axis gimbal system consists of three bodies, two of which are rotating bodies and the other one is base (reference) body, and two gimbal axis (joints) which represent degrees of freedom. These two revolute joints were denoted as azimuth axis and elevation axis. The azimuth axis enables relative rotation between body 0 (base) and body 1 (azimuth body); similarly, the elevation axis enables relative rotation between body 1 (azimuth body) and body 2 (elevation body). The payload is, in this case, elevation body which is a satellite antenna and to be oriented as a purpose of the system. The system is composed of two direct drive brushless DC

motors as actuators and two encoders as a position sensors, all of which placed joints. Besides, a gyroscope is assembled on the elevation body to measure the angular velocity of the payload. Three ball bearings, one for the azimuth body at point O, two for the elevation body at points A and C are used. The following figures describe the gimbal system with appropriate reference frames attached on bodies and were explained in the Kinematic Analysis section.

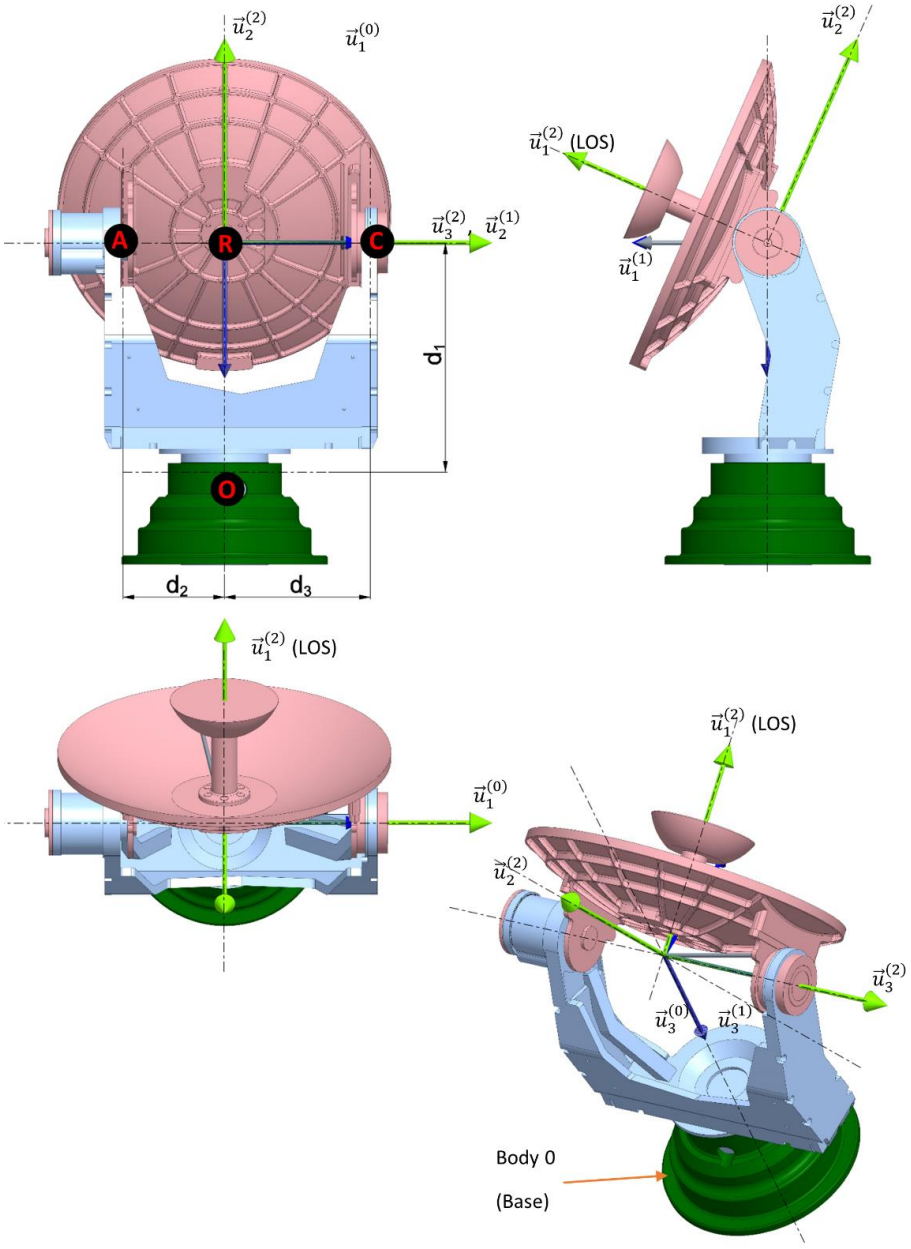

Figure 2: General description of the gimbal system

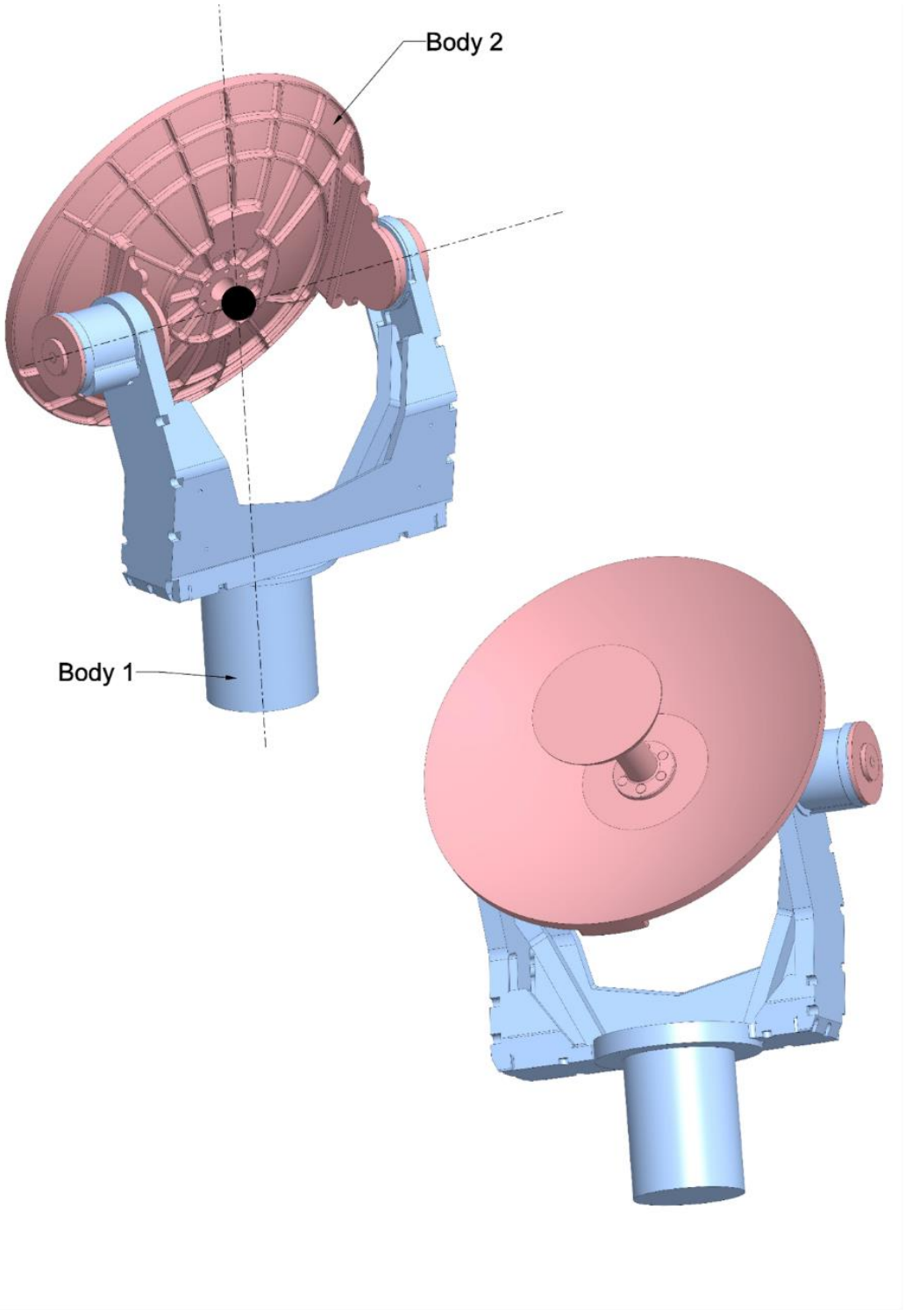

Figure 3: Rotating bodies of the gimbal system

2.2 Kinematic Analysis

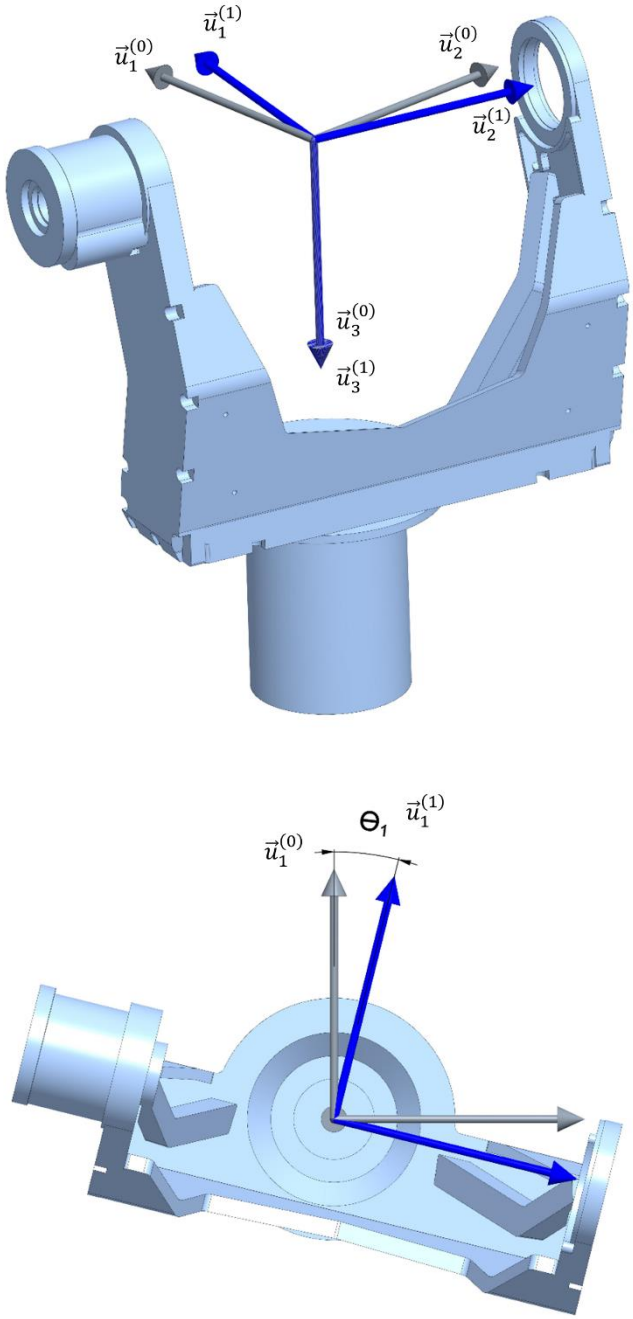

Figure 4: Kinematic representation of the body 1 (azimuth body)

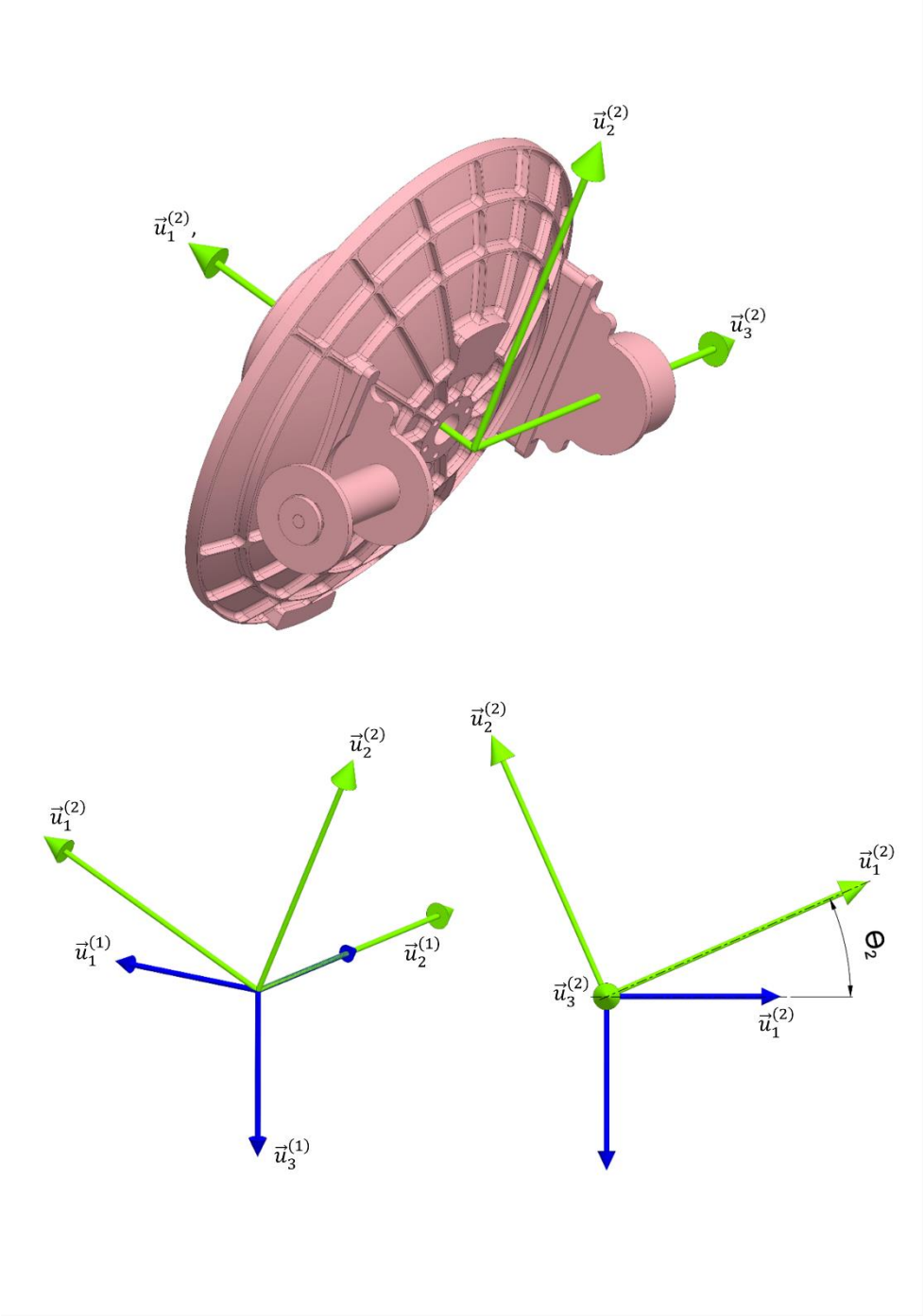

Figure 5: Kinematic representation of the body 2 (elevation body)

Rotating bodies shown in the figures Figure 4 and Figure 5. Besides, angular rotation angles θ_1 and θ_2 are denoted on the coordinate axes of the bodies. Selection rule of

the coordinate axes based on Denavit Hartenberg convention described in the next section 2.2.1.

2.2.1 Denavit-Hartenberg (DH) Convention

A two-axis inertially stabilized platform could be considered as a robotic manipulator. The gimbal is an open kinematic chain that its rigid bodies (links) connected to each other by revolute joints where the DC motors drive and give actuation energy. The end effector of the gimbal can be considered as its payload which is antenna in this study. Due to the special motion task of the gimbal, robotic manipulator, its link lengths are zero so that only the orientation of the antenna is allowed to manipulate.

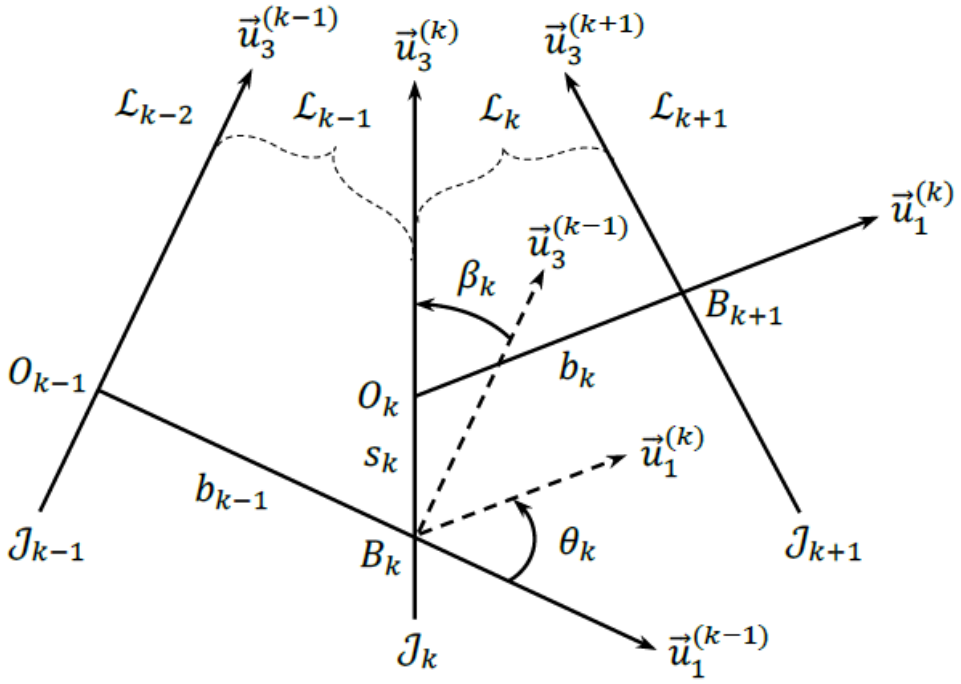

Figure 6: Denavit-Hartenberg convention [30]

Denavit-Hartenberg (DH) convention is used to express kinematic relations of the two-axis gimbal system. The DH convention is applied according to the [30]. There is a general guideline to describe kinematics of connected rigid bodies. The links and

joints are numbered from 1 to m where m is the total number of links, $i-th$ joint connects the links $i-1$ and i. A reference frame is attached to each rigid bodies, and $0-th$ reference frame indicates the inertial or base reference frame. A reference frame and origin of $k-th$ link are, respectively, $\mathcal{F}_k$ and O_k denoted as following,

$$\mathcal{F}_k(O_k)$$

Basis vectors of the reference frame $\mathcal{F}_k$ are denoted as following,

$$\left\{\vec{u}_1^{(k)}, \vec{u}_2^{(k)}, \vec{u}_3^{(k)}\right\}; where\ upperscript\ indicates\ k-th\ reference\ frame$$

Basis vectors can be expressed in vector equations as follows.

$$\bar{u}_1 = \begin{bmatrix}1\\0\\0\end{bmatrix}, \qquad \bar{u}_2 = \begin{bmatrix}0\\1\\0\end{bmatrix}, \qquad \bar{u}_3 = \begin{bmatrix}0\\0\\1\end{bmatrix}$$

Selection of the reference frame components is done in compliance with DH convention as well. Frame origins can be selected freely. $\vec{u}_3^{(k)}$ is assigned to axis of the joint-revolute joints in this case- with freely selected direction. $\vec{u}_1^{(k)}$ is assigned to the common normal N_k between $\vec{u}_3^{(k-1)}$ and $\vec{u}_3^{(k)}$. Since joint axes of the gimbal bodies intersecting, direction of the $\vec{u}_1^{(k)}$ is selected freely. Second basis vector $\vec{u}_2^{(k)}$ is determined due to right-handed property of the reference frame; such that,

$$\vec{u}_2^{(k)} = \vec{u}_3^{(k)} \times \vec{u}_1^{(k)}$$

Joint variables are rotation angle θ_{ij} between $\vec{u}_1^{(i)}$and $\vec{u}_1^{(j)}$; and distance $d_{ij} = O_iO_j$ is a constant parameter. For the sake of simplicity, only the $j-th$ subscript is used. That is,

$$\theta_1 = \theta_{01}:\ rotation\ angle\ of\ the\ azimuth\ axis$$

$$\theta_2 = \theta_{12}:\ rotation\ angle\ of\ the\ elevation\ axis$$

$$d_{01} = d_1:\ distance\ of\ the\ azimuth\ axis$$

$$d_{12} = d_2:\ distance\ of\ the\ elevation\ axis$$

There are four DH parameters need to be defined before using the DH convention.

- The twist angle, β_k, between the axes of $\vec{u}_3^{(k-1)}$ and $\vec{u}_3^{(k)}$.
- Rotation angle, θ_k, between the common normal $\vec{u}_1^{(k-1)}$ and $\vec{u}_1^{(k)}$.
- The offset, s_k, between the common normal $\vec{u}_1^{(k-1)}$ and $\vec{u}_1^{(k)}$.
- The effective link length, b_k, between the axes of $\vec{u}_3^{(k-1)}$ and $\vec{u}_3^{(k)}$.

The parameters β_k and b_k are always constant. Since the gimbal system has only revolute joint, the parameter s_k is constant, too. The following table consists of link frame origins and the four DH parameters for the studied gimbal.

Table 1: Denavit-Hartenberg parameters

Twist Angles		
$\beta_1 = 0$	$\beta_2 = -\pi/2$	
Rotation Angles (jv: joint variable)		
$\theta_1 = jv$	$\theta_2 = jv$	
Constant Offsets		
$s_1 = d_1$	$s_2 = 0$	
Effective Link Lengths		
$b_0 = 0$	$b_1 = 0$	$b_2 = 0$
Link Frame Origins		
$O_0 = R$	$O_1 = R$	$O_2 = R$

2.2.2 Geometric Relations of the Gimbal System

Geometrical parameters of the gimbal system are provided below.

Link lengths and distances indicating center of gravity,

$$\begin{gathered} d_1 = 261\ mm \\ c_{azi2} = 20\ mm \\ c_{azi3} = 67\ mm \\ c_2 = 18\ mm \\ d_2 = 115\ mm \\ d_3 = 167\ mm \end{gathered} \tag{2.1}$$

$$\vec{r}_{OC_{azi}} = -c_{azi2}\vec{u}_2^{(1)} - c_{azi3}\vec{u}_3^{(1)} \Rightarrow \bar{r}_{OC_{azi}}^{(1)} = \begin{bmatrix} 0 \\ -c_{azi2} \\ -c_{azi3} \end{bmatrix} \tag{2.2}$$

$$\vec{r}_{OA} = -d_2\vec{u}_2^{(1)} - d_1\vec{u}_3^{(1)} \Rightarrow \bar{r}_{OA}^{(1)} = -\begin{bmatrix} 0 \\ d_2 \\ d_1 \end{bmatrix} \tag{2.3}$$

$$\begin{gathered} \vec{r}_{C_{azi}A} = (c_{azi2} - d_2)\vec{u}_2^{(1)} + (c_{azi3} - d_1)\vec{u}_3^{(1)} \Rightarrow \bar{r}_{C_{azi}A}^{(1)} \\ = \begin{bmatrix} 0 \\ -d_2 + c_{azi2} \\ c_{azi3} - d_1 \end{bmatrix} \end{gathered} \tag{2.4}$$

$$\vec{r}_{AR} = d_2\vec{u}_2^{(1)} = d_2\vec{u}_3^{(2)} \Rightarrow \bar{r}_{AR}^{(1)} = \begin{bmatrix} 0 \\ d_2 \\ 0 \end{bmatrix} \tag{2.5}$$

$$\vec{r}_{AC_{ele}} = (c_2 + d_2)\vec{u}_2^{(1)} = (c_2 + d_2)\vec{u}_3^{(2)} \Rightarrow \bar{r}_{AC_{ele}}^{(1)} = \begin{bmatrix} 0 \\ c_2 + d_2 \\ 0 \end{bmatrix} \tag{2.6}$$

$$\vec{r}_{AC} = (d_2 + d_3)\vec{u}_2^{(1)} = (d_2 + d_3)\vec{u}_3^{(2)} \Rightarrow \bar{r}_{AC}^{(1)} = \begin{bmatrix} 0 \\ d_2 + d_3 \\ 0 \end{bmatrix} \tag{2.7}$$

$$\vec{r}_{C_{ele}C} = (d_3 - c_2)\vec{u}_2^{(1)} = (d_3 - c_2)\vec{u}_3^{(2)} \Rightarrow \bar{r}_{C_{ele}C}^{(2)} = \begin{bmatrix} 0 \\ 0 \\ d_3 - c_2 \end{bmatrix} \tag{2.8}$$

$$\begin{gathered} \vec{r}_{C_{azi}C} = (d_3 + c_{azi2})\vec{u}_2^{(1)} + (c_{azi3} - d_1)\vec{u}_3^{(1)} \Rightarrow \bar{r}_{C_{azi}C}^{(1)} \\ = \begin{bmatrix} 0 \\ d_3 + c_{azi2} \\ c_{azi3} - d_1 \end{bmatrix} \end{gathered} \tag{2.9}$$

$$\begin{gathered} \vec{r}_{OC_{ele}} = \vec{r}_{OA} + \vec{r}_{AC_{ele}} = -d_2\vec{u}_2^{(1)} - d_1\vec{u}_3^{(1)} + (c_2 + d_2)\vec{u}_2^{(1)} \\ \Rightarrow \bar{r}_{OC_{ele}}^{(1)} = \begin{bmatrix} 0 \\ c_2 \\ -d_1 \end{bmatrix} \end{gathered} \tag{2.10}$$

2.2.3 Body-to-Body Orientation

Transformation matrices between reference frames, $\hat{C}^{(i,j)}$, denotes transformation of reference frame from $\mathcal{F}_i$ to $\mathcal{F}_j$ and is calculated as following.

$$\hat{C}^{(i,j)} = e^{\tilde{u}_1 \beta_{01}} e^{\tilde{u}_3 \theta_{01}} \tag{2.11}$$

Exponential terms of (2.11) are the rotation matrix and basic rotation matrix are expressed as followings.

$$\hat{R}_1(\theta) = e^{\tilde{u}_1 \theta} = \begin{bmatrix} 1 & 0 & 0 \\ 0 & \cos\theta & -\sin\theta \\ 0 & \sin\theta & \cos\theta \end{bmatrix} \tag{2.12}$$

$$\hat{R}_2(\theta) = e^{\tilde{u}_2 \theta} = \begin{bmatrix} \cos\theta & 0 & \sin\theta \\ 0 & 1 & 0 \\ -\sin\theta & 0 & \cos\theta \end{bmatrix} \tag{2.13}$$

$$\hat{R}_3(\theta) = e^{\tilde{u}_3 \theta} = \begin{bmatrix} \cos\theta & -\sin\theta & 0 \\ \sin\theta & \cos\theta & 0 \\ 0 & 0 & 1 \end{bmatrix} \tag{2.14}$$

2.2.4 Angular Velocities of the Bodies

Angular velocity, $\vec{\omega}_k = \vec{\omega}_{k/0}$, of the $k-th$ body with respect to the inertial reference frame $\mathcal{F}_0$ can be expressed as following recursive vector.

$$\vec{\omega}_k = \sum_{m=1}^{k-1} \vec{\omega}_{m/m-1}, \qquad where\ \vec{\omega}_0 = 0 \tag{2.15}$$

It is known that, according to the DH convention, rotation axes of the bodies are along $\vec{u}_3^{(k)}$. Therefore,

$$\vec{\omega}_{k/k-1} = \dot{\theta}_k \vec{u}_3^{(k)} \tag{2.16}$$

(2.15) can be written as the following matrix equation in inertial reference frame.

$$\bar{\omega}_k{}^{(0)} = \bar{\omega}_k = \bar{\omega}_{k-1}{}^{(0)} + \dot{\theta}_k \bar{u}_3^{(k/0)} \Rightarrow$$

$$\bar{\omega}_k = \bar{\omega}_{k-1}{}^{(0)} + \dot{\theta}_k \hat{C}^{(0,k)} \bar{u}_3 \tag{2.17}$$

2.2.5 Velocities of the Body Frame Origins

Velocity, $\vec{v}_k = \vec{v}_{k/0}$, of the $k-th$ body frame origin with respect to the inertial reference frame origin $\mathcal{F}_0(O_0)$ can be expressed as following recursive vector.

$$\vec{v}_k = D_0\vec{r}_k = \sum_{m=1}^{k-1} D_0\vec{r}_{m/m-1}\,, \qquad where\ \vec{v}_0 = 0 \tag{2.18}$$

$D_0\vec{r}_k$ term in above equation express that time derivative of position vector of the $k-th$ body frame origin, $\vec{r}_k$, with respect to the inertial reference frame $\mathcal{F}_0(O_0)$.

2.2.6 Angular Acceleration of the Bodies

Angular acceleration, $\vec{\alpha}_k = \vec{\alpha}_{k/0}$, of the $k-th$ body with respect to the inertial reference frame $\mathcal{F}_0$ can be expressed as following recursive vector.

$$\vec{\alpha}_k = \sum_{m=1}^{k-1} \vec{\alpha}_{m/m-1}\,, \qquad where\ \vec{\alpha}_0 = 0 \tag{2.19}$$

Recalling the relation between angular acceleration and angular velocity,

$$\vec{\alpha}_k = D_0\vec{\omega}_{k/0}$$

2.2.7 Acceleration of the Body Frame Origins

Angular acceleration, $\vec{a}_k = a_{k/0}$, of the $k-th$ body frame origin with respect to the inertial reference frame origin $\mathcal{F}_0(O_0)$ can be expressed as following recursive vector.

$$\vec{a}_k = D_0\vec{a}_k = \sum_{m=1}^{k-1} D_0\vec{v}_{m/m-1}\,, \qquad where\ \vec{a}_0 = 0 \tag{2.20}$$

2.2.8 Kinematic Relations of the Gimbal System

Kinematic relations of the studied gimbal are to be expressed in this section.

Transformation matrices between successive gimbal bodies can be expressed as follows.

$$\hat{C}^{(0,1)} = e^{\tilde{u}_1\beta_1}e^{\tilde{u}_3\theta_1} = e^{\tilde{u}_3\theta_1} \tag{2.21}$$

$$\hat{C}^{(1,2)} = e^{\tilde{u}_1\beta_2}e^{\tilde{u}_3\theta_2} = e^{-\tilde{u}_1\pi/2}e^{\tilde{u}_3\theta_2} \tag{2.22}$$

$$\begin{aligned}\hat{C} = \hat{C}^{(0,2)} &= \hat{C}^{(0,1)}\hat{C}^{(1,2)} = e^{\tilde{u}_3\theta_1}e^{-\tilde{u}_1\pi/2}e^{\tilde{u}_3\theta_2} \\ &= e^{\tilde{u}_3\theta_1}e^{\tilde{u}_2\theta_2}e^{-\tilde{u}_1\pi/2}\end{aligned} \tag{2.23}$$

Calculating transformation matrices by using the equations (2.21), (2.22), and (2.23),

$$\hat{C}^{(0,1)} = \begin{bmatrix}\cos\theta_1 & -\sin\theta_1 & 0\\ \sin\theta_1 & \cos\theta_1 & 0\\ 0 & 0 & 1\end{bmatrix} \tag{2.24}$$

$$\hat{C}^{(1,2)} = \begin{bmatrix}1 & 0 & 0\\ 0 & 0 & 1\\ 0 & -1 & 0\end{bmatrix}\begin{bmatrix}\cos\theta_2 & -\sin\theta_2 & 0\\ \sin\theta_2 & \cos\theta_2 & 0\\ 0 & 0 & 1\end{bmatrix} \Rightarrow$$

$$\hat{C}^{(1,2)} = \begin{bmatrix}\cos\theta_2 & -\sin\theta_2 & 0\\ 0 & 0 & 1\\ -\sin\theta_2 & -\cos\theta_2 & 0\end{bmatrix} \tag{2.25}$$

$$\hat{C}^{(0,2)} = \begin{bmatrix}\cos\theta_1 & -\sin\theta_1 & 0\\ \sin\theta_1 & \cos\theta_1 & 0\\ 0 & 0 & 1\end{bmatrix}\begin{bmatrix}\cos\theta_2 & -\sin\theta_2 & 0\\ 0 & 0 & 1\\ -\sin\theta_2 & -\cos\theta_2 & 0\end{bmatrix} \Rightarrow$$

$$\hat{C}^{(0,2)} = \begin{bmatrix}\cos\theta_1\cos\theta_2 & -\cos\theta_1\sin\theta_2 & -\sin\theta_1\\ \sin\theta_1\cos\theta_2 & -\sin\theta_1\sin\theta_2 & \cos\theta_1\\ -\sin\theta_2 & -\cos\theta_2 & 0\end{bmatrix} \tag{2.26}$$

Angular velocity and acceleration of the antenna (second body) can be expressed as follows by recalling (2.17).

$$\bar{\omega}_1 = \bar{\omega}_{1/0}{}^{(0)} = \dot{\theta}_1\bar{u}_3 \Rightarrow$$

$$\bar{\omega}_1 = \begin{bmatrix} 0 \\ 0 \\ \dot{\theta}_1 \end{bmatrix} \tag{2.27}$$

$$\bar{\omega}_2 = \bar{\omega}_{2/0}{}^{(0)} = \bar{\omega}_{1/0}{}^{(0)} + \bar{\omega}_{2/1}{}^{(0)} \Rightarrow$$

$$\bar{\omega}_2 = \dot{\theta}_1 \bar{u}_3 + \dot{\theta}_2 e^{\tilde{u}_3 \theta_1} \bar{u}_2 \Rightarrow$$

$$\bar{\omega}_2 = \dot{\theta}_1 \bar{u}_3 + \dot{\theta}_2 (\bar{u}_2 \cos\theta_1 - \bar{u}_1 \sin\theta_1) \Rightarrow$$

$$\bar{\omega}_2 = -\dot{\theta}_2 \sin\theta_1 \, \bar{u}_1 + \dot{\theta}_2 \cos\theta_1 \, \bar{u}_2 + \dot{\theta}_1 \bar{u}_3 \Rightarrow$$

$$\bar{\omega}_2 = \begin{bmatrix} -\dot{\theta}_2 \sin\theta_1 \\ \dot{\theta}_2 \cos\theta_1 \\ \dot{\theta}_1 \end{bmatrix} \tag{2.28}$$

$$\bar{\alpha}_1 = \bar{\alpha}_{1/0}{}^{(0)} = \dot{\bar{\omega}}_1 \Rightarrow$$

$$\bar{\alpha}_1 = \begin{bmatrix} 0 \\ 0 \\ \ddot{\theta}_1 \end{bmatrix} \tag{2.29}$$

$$\bar{\alpha}_2 = \bar{\alpha}_{2/0}{}^{(0)} = \dot{\bar{\omega}} = \begin{bmatrix} -\dot{\theta}_1 \dot{\theta}_2 \cos\theta_1 - \ddot{\theta}_2 \sin\theta_1 \\ -\dot{\theta}_1 \dot{\theta}_2 \sin\theta_1 + \ddot{\theta}_2 \cos\theta_1 \\ \ddot{\theta}_1 \end{bmatrix} \tag{2.30}$$

Location, velocity, and acceleration of the wrist point (point R) on antenna (second body) can be expressed as follows.

$$\vec{r} = \vec{r}_{OR} = \vec{r}_{OA} + \vec{r}_{AR} \Rightarrow$$

$$\vec{r} = \mathrm{d}_1 \vec{u}_3^{(0)} \tag{2.31}$$

Expressing as column matrix representation in base reference frame,

$$\bar{r} = \mathrm{d}_1 \bar{u}_3 = \begin{bmatrix} 0 \\ 0 \\ d_1 \end{bmatrix} \tag{2.32}$$

$$\vec{v}_{\mathrm{r}} = \vec{v}_{OB} = 0 \Rightarrow \bar{v}_r = \begin{bmatrix} 0 \\ 0 \\ 0 \end{bmatrix} \tag{2.33}$$

$$\vec{a}_{\mathrm{r}} = \vec{a}_{OB} = 0 \Rightarrow \bar{a}_R = \begin{bmatrix} 0 \\ 0 \\ 0 \end{bmatrix} \tag{2.34}$$

Location, velocity and acceleration of the mass center of the body 1:

$$\bar{r}_{OC_{azi}}^{(1)} = \begin{bmatrix} 0 \\ -c_{azi2} \\ -c_{azi3} \end{bmatrix} \Rightarrow$$

$$\bar{r}_{OC_{azi}}^{(0)} = \hat{C}^{(0,1)} \bar{r}_{OC_{azi}}^{(1)} = e^{\tilde{u}_3 \theta_1} (-c_{azi2} \bar{u}_2 - c_{azi3} \bar{u}_3) \Rightarrow$$

$$\bar{r}_{OC_{azi}}^{(0)} = c_{azi2} \sin\theta_1 \, \bar{u}_1 - c_{azi2} \cos\theta_1 \, \bar{u}_2 - c_{azi3} \bar{u}_3 \tag{2.35}$$

$$\vec{v}_{azi} = \vec{v}_{OC_{azi}} = \mathrm{D}_0 \vec{r}_{OC_{azi}} \Rightarrow$$

$$\bar{v}_{azi} = \dot{\bar{r}}_{OC_{azi}}^{(0)} = c_{azi2} \dot{\theta}_1 \cos\theta_1 \, \bar{u}_1 + c_{azi2} \dot{\theta}_1 \sin\theta_1 \, \bar{u}_2 \Rightarrow$$

$$\bar{v}_{azi} = \begin{bmatrix} c_{azi2} \dot{\theta}_1 \cos\theta_1 \\ c_{azi2} \dot{\theta}_1 \sin\theta_1 \\ 0 \end{bmatrix} \tag{2.36}$$

$$\vec{a}_{\mathrm{azi}} = \vec{a}_{OC_{azi}} = \mathrm{D}_0 \vec{v}_{azi} \Rightarrow$$

$$\bar{a}_{azi} = \dot{\bar{v}}_{azi} = c_{azi2} (\ddot{\theta}_1 \cos\theta_1 - \dot{\theta}_1^2 \sin\theta_1) \bar{u}_1 + c_{azi2} (\ddot{\theta}_1 \sin\theta_1 + \dot{\theta}_1^2 \cos\theta_1) \bar{u}_2 \Rightarrow$$

$$\vec{a}_{\mathrm{azi}} = \begin{bmatrix} c_{azi2} \left(\ddot{\theta}_1 \cos\theta_1 - \dot{\theta}_1^2 \sin\theta_1 \right) \\ c_{azi2} \left(\ddot{\theta}_1 \sin\theta_1 + \dot{\theta}_1^2 \cos\theta_1 \right) \\ 0 \end{bmatrix} \tag{2.37}$$

Location, velocity and acceleration of the COG of the body 2:

$$\bar{r}_{OC_{ele}}^{(1)} = \begin{bmatrix} 0 \\ c_2 \\ -d_1 \end{bmatrix} \Rightarrow$$

$$\bar{r}_{OC_{ele}}^{(0)} = \hat{C}^{(0,1)} \bar{r}_{OC_{ele}}^{(2)} = e^{\tilde{u}_3 \theta_1} (c_2 \bar{u}_2 - d_1 \bar{u}_3) \Rightarrow$$

$$\vec{r}_{OC_{ele}} = -c_2 \sin\theta_1 \, \vec{u}_1^{(0)} + c_2 \cos\theta_1 \, \vec{u}_2^{(0)} - d_1 \vec{u}_3^{(0)} \Rightarrow$$

$$\bar{r}_{OC_{ele}}^{(0)} = -c_2 \sin\theta_1 \, \bar{u}_1 + c_2 \cos\theta_1 \, \bar{u}_2 - d_1 \bar{u}_3 \tag{2.38}$$

$$\vec{v}_{OC_{ele}} = \mathrm{D}_0 \vec{r}_{OC_{ele}} = -c_2 \dot{\theta}_1 \cos\theta_1 \, \vec{u}_1^{(0)} - c_2 \dot{\theta}_1 \sin\theta_1 \, \vec{u}_2^{(0)} \Rightarrow$$

$$\bar{v}_{OC_{ele}}^{(0)} = \begin{bmatrix} -c_2\dot{\theta}_1 \cos\theta_1 \\ -c_2\dot{\theta}_1 \sin\theta_1 \\ 0 \end{bmatrix} \tag{2.39}$$

$$\begin{aligned} \vec{a}_{OC_{ele}} &= \mathrm{D}_0\vec{v}_{ele} \\ &= \left(-c_2\ddot{\theta}_1 \cos\theta_1 + c_2\dot{\theta}_1^2 \sin\theta_1\right)\vec{u}_1^{(0)} \\ &\quad - \left(c_2\ddot{\theta}_1 \sin\theta_1 + c_2\dot{\theta}_1^2 \cos\theta_1\right)\vec{u}_2^{(0)} \Rightarrow \end{aligned}$$

$$\bar{a}_{OC_{ele}}^{(0)} = \begin{bmatrix} -c_2\ddot{\theta}_1 \cos\theta_1 + c_2\dot{\theta}_1^2 \sin\theta_1 \\ -c_2\ddot{\theta}_1 \sin\theta_1 - c_2\dot{\theta}_1^2 \cos\theta_1 \\ 0 \end{bmatrix} \tag{2.40}$$

2.3 Dynamic Analysis

Dynamic analysis describes the relation between acting forces-moments and motion variables that are analyzed in Kinematic Analysis section. There are two well-known dynamic analysis methods which are Newton-Euler and Lagrange's methods. Newton-Euler method directly uses force-moment relations; that is why it is also called force and moment equation method, while Lagrange's method uses energy relations to obtain equation of motion. The Newton-Euler method is used in the thesis.

According to the CAD models, mass and inertia values are as follows. Noting that inertia matrices of the bodies are defined in their own reference frame.

$$m_1 = 6.212\ kg \tag{2.41}$$

$$m_2 = 6.377\ kg \tag{2.42}$$

$$\begin{aligned} \hat{J}_1^{(1)} &= \begin{bmatrix} J_{111} & J_{112} & J_{113} \\ J_{112} & J_{122} & J_{123} \\ J_{113} & J_{123} & J_{133} \end{bmatrix} \\ &= \begin{bmatrix} 1.275e-1 & 7.956e-3 & -7.703e-3 \\ 7.956e-3 & 8.141e-2 & -1.047e-2 \\ -7.703e-3 & -1.047e-2 & 7.207e-2 \end{bmatrix} kgm^2 \end{aligned} \tag{2.43}$$

$$\hat{J}_2^{(2)} = \begin{bmatrix} J_{211} & J_{212} & J_{213} \\ J_{212} & J_{222} & J_{223} \\ J_{213} & J_{223} & J_{233} \end{bmatrix} = \begin{bmatrix} 6.891e-2 & -2.880e-3 & -9.234e-4 \\ -2.880e-3 & 8.077e-2 & -2.006e-3 \\ -9.234e-4 & -2.006e-3 & 5.732e-2 \end{bmatrix} kgm^2 \quad (2.44)$$

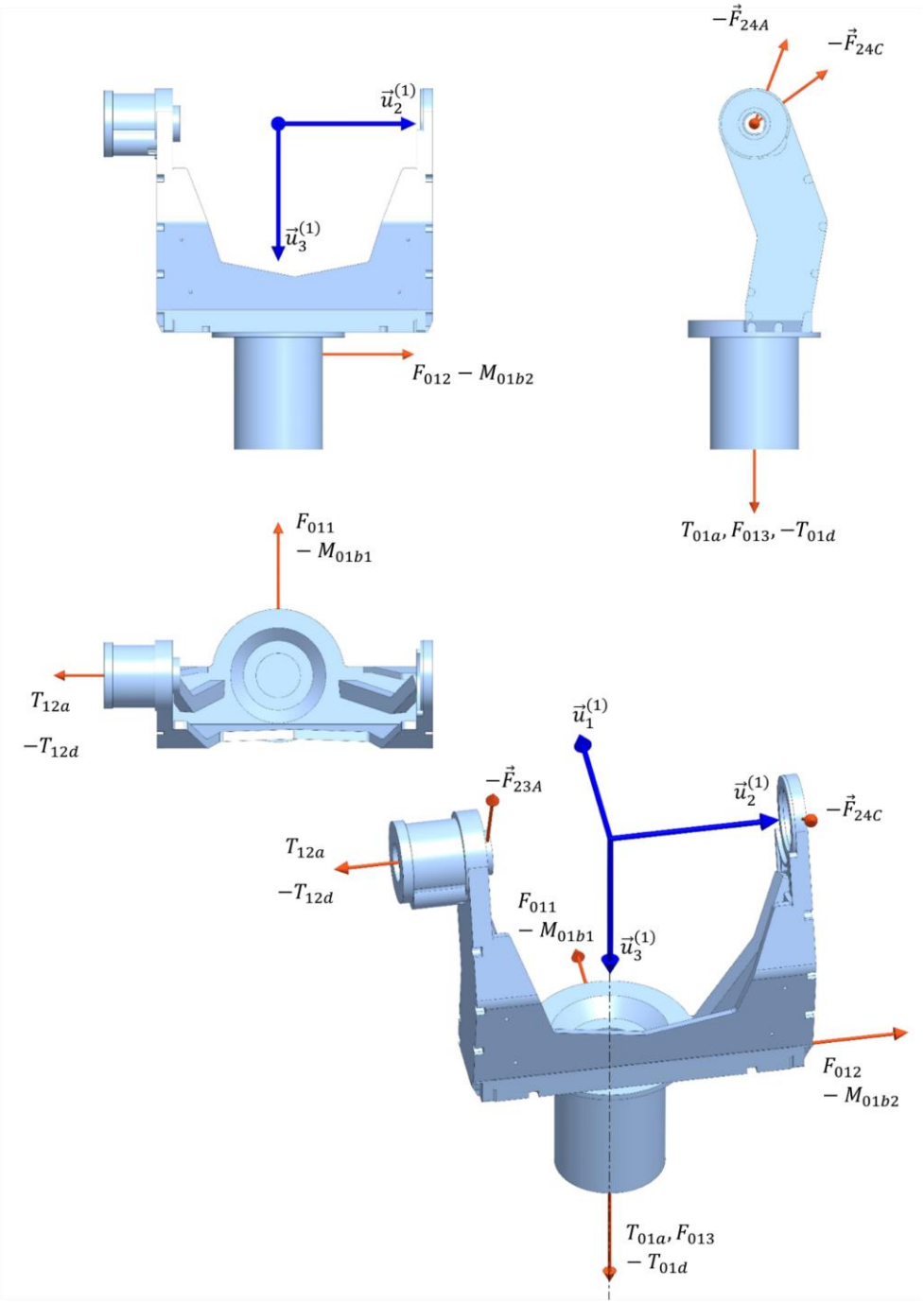

Figure 7: Free-body diagram of the azimuth body

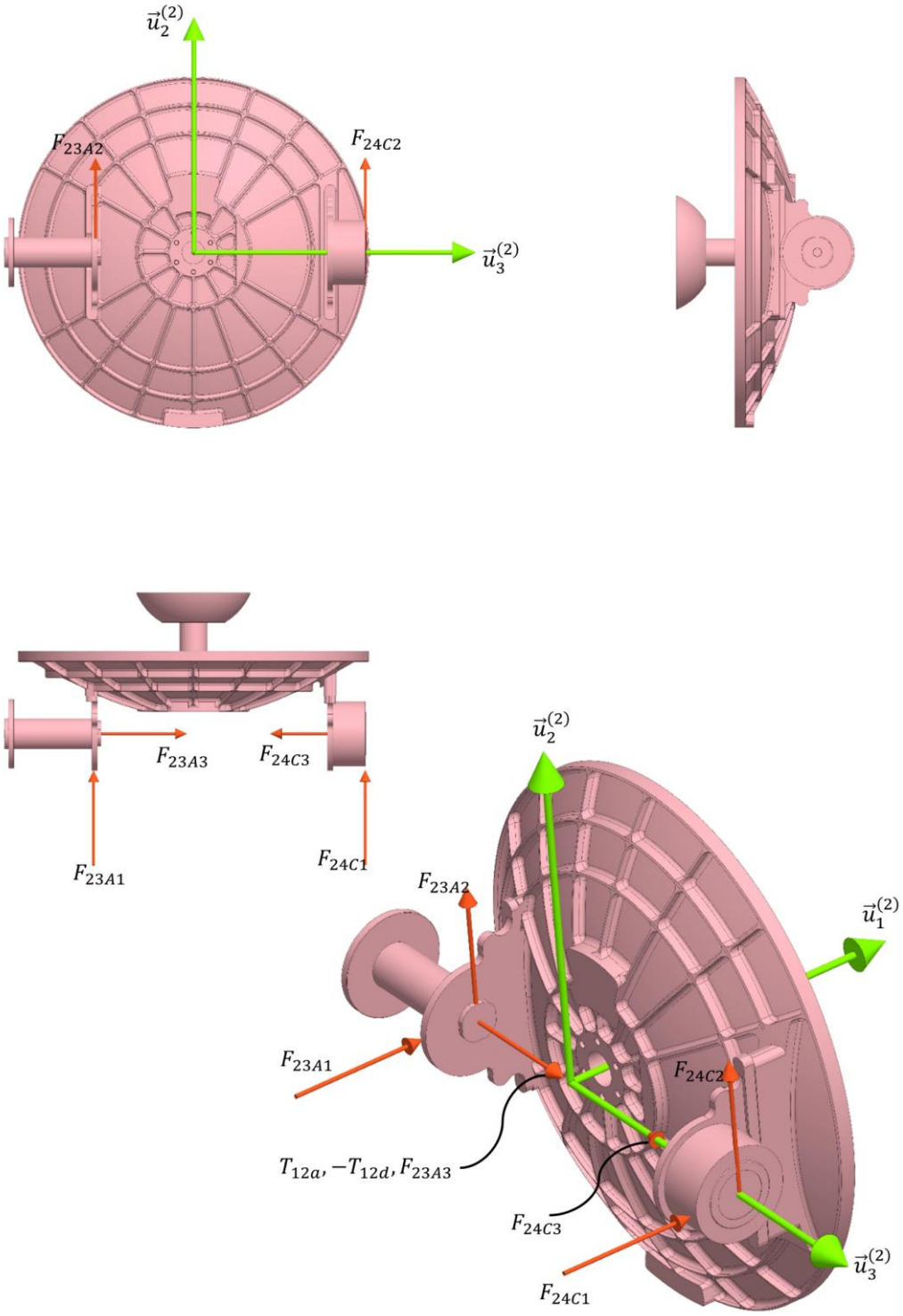

Figure 8: Free-body diagram of the elevation body

Forces and moments shown in free body diagrams are indicated below. A force or moment notation such as $\vec{F}_{01}$ states that force acting on body 1 from body 0. Resolving force and moment relations:

$$\vec{F}_{01} = F_{011}\vec{u}_1^{(1)} + F_{012}\vec{u}_2^{(1)} + F_{013}\vec{u}_3^{(1)} \tag{2.45}$$

$$\vec{T}_{01a} = T_{01a}\vec{u}_3^{(1)} \tag{2.46}$$

$$\vec{T}_{01d} = -T_{01d}\vec{u}_3^{(1)};\quad T_{01d} = c_{01d}\dot{\theta}_1 \tag{2.47}$$

$$\vec{M}_{01b} = -M_{01b1}\vec{u}_1^{(1)} - M_{01b2}\vec{u}_2^{(1)} \tag{2.48}$$

$$\vec{F}_{12A} = F_{12A1}\vec{u}_1^{(2)} + F_{12A2}\vec{u}_2^{(2)} + F_{12A3}\vec{u}_3^{(2)} \tag{2.49}$$

$$\vec{F}_{12C} = F_{12C1}\vec{u}_1^{(2)} + F_{12C2}\vec{u}_2^{(2)} \tag{2.50}$$

where $F_{12C3} = 0$ assumed bearing located at point C has larger axial space than the on at point A.

$$\vec{T}_{12a} = T_{12a}\vec{u}_3^{(2)} = T_{12a}\vec{u}_2^{(1)} \tag{2.51}$$

$$\vec{T}_{12d} = -T_{12d}\vec{u}_3^{(2)};\quad T_{12d} = c_{12d}\dot{\theta}_3 \tag{2.52}$$

2.3.1 Newton-Euler Equations for Body 1

Force equation:

$$m_1\vec{a}_{azi} = m_1\vec{g} + \vec{F}_{01} - \vec{F}_{12A} - \vec{F}_{12C} \Rightarrow$$

Expressing in matrix representation in base reference frame,

$$m_1\hat{C}^{(1,0)}\begin{bmatrix} c_{azi2}\left(\ddot{\theta}_1\cos\theta_1 - \dot{\theta}_1^2\sin\theta_1\right) \\ c_{azi2}\left(\ddot{\theta}_1\sin\theta_1 + \dot{\theta}_1^2\cos\theta_1\right) \\ 0 \end{bmatrix}$$

$$= m_1\hat{C}^{(1,0)}\begin{bmatrix}0\\0\\g\end{bmatrix} + \begin{bmatrix}F_{011}\\F_{012}\\F_{013}\end{bmatrix} - \hat{C}^{(1,2)}\begin{bmatrix}F_{12A1}\\F_{12A2}\\F_{12A3}\end{bmatrix} - \hat{C}^{(1,2)}\begin{bmatrix}F_{12C1}\\F_{12C2}\\0\end{bmatrix} \Rightarrow$$

where,

$$\begin{bmatrix} \cos\theta_1 & \sin\theta_1 & 0 \\ -\sin\theta_1 & \cos\theta_1 & 0 \\ 0 & 0 & 1 \end{bmatrix} \begin{bmatrix} c_{azi2}\left(\ddot{\theta}_1 \cos\theta_1 - \dot{\theta}_1^2 \sin\theta_1\right) \\ c_{azi2}\left(\ddot{\theta}_1 \sin\theta_1 + \dot{\theta}_1^2 \cos\theta_1\right) \\ 0 \end{bmatrix} = c_{azi2} \begin{bmatrix} \ddot{\theta}_1 \\ \dot{\theta}_1^2 \\ 0 \end{bmatrix}$$

$$\begin{bmatrix} \cos\theta_2 & -\sin\theta_2 & 0 \\ 0 & 0 & 1 \\ -\sin\theta_2 & -\cos\theta_2 & 0 \end{bmatrix} \begin{bmatrix} F_{12A1} + F_{12C1} \\ F_{12A2} + F_{12C2} \\ F_{12A3} \end{bmatrix}$$

$$= \begin{bmatrix} (F_{12A1} + F_{12C1})\cos\theta_2 - (F_{12A2} + F_{12C2})\sin\theta_2 \\ F_{12A3} \\ -(F_{12A1} + F_{12C1})\sin\theta_2 - (F_{12A2} + F_{12C2})\cos\theta_2 \end{bmatrix}$$

$$m_1 c_{azi2} \begin{bmatrix} \ddot{\theta}_1 \\ \dot{\theta}_1^2 \\ 0 \end{bmatrix} = m_1 \begin{bmatrix} 0 \\ 0 \\ g \end{bmatrix} + \begin{bmatrix} F_{011} \\ F_{012} \\ F_{013} \end{bmatrix}$$

$$- \begin{bmatrix} (F_{23A1} + F_{12C1})\cos\theta_2 - (F_{23A2} + F_{12C2})\sin\theta_2 \\ F_{23A3} \\ -(F_{23A1} + F_{12C1})\sin\theta_2 - (F_{23A2} + F_{12C2})\cos\theta_2 \end{bmatrix} \Rightarrow$$

Writing as separate equations,

$$m_1 c_{azi2} \ddot{\theta}_1 = F_{011} - (F_{12A1} + F_{12C1})\cos\theta_2 + (F_{12A2} + F_{12C2})\sin\theta_2 \tag{2.53}$$

$$m_1 c_{azi2} \dot{\theta}_1^2 = F_{012} - F_{12A3} \tag{2.54}$$

$$0 = m_1 g + F_{013} + (F_{12A1} + F_{12C1})\sin\theta_2 + (F_{12A2} + F_{12C2})\cos\theta_2 \tag{2.55}$$

Moment equation:

$$\begin{aligned} \check{J}_1 \cdot \vec{\alpha}_1 + \vec{\omega}_1 \times \check{J}_1 \cdot \vec{\omega}_1 &= \vec{M}_{01b} + \vec{T}_{01a} - \vec{T}_{12a} + \vec{T}_{01d} - \vec{T}_{12d} \\ &+ \vec{r}_{C_{azi}O} \times \vec{F}_{01} + \vec{r}_{C_{azi}A} \times (-\vec{F}_{12A}) \\ &+ \vec{r}_{C_{azi}C} \times (-\vec{F}_{12C}) \end{aligned} \tag{2.56}$$

The moment equation can be written as column matrix equations as follows. Manipulations of the equation are provided in Appendix A.

$$\begin{bmatrix} J_{113}\ddot{\theta}_1 \\ J_{123}\ddot{\theta}_1 \\ J_{133}\ddot{\theta}_1 \end{bmatrix} + \begin{bmatrix} -J_{123}\dot{\theta}_1^2 \\ -J_{113}\dot{\theta}_1^2 \\ 0 \end{bmatrix}$$

$$= \begin{bmatrix} -M_{01b1} \\ -M_{01b2} - T_{12a} + k_{12s}\theta_3 + c_{12d}\dot{\theta}_3 \\ T_{01a} - c_{01d}\dot{\theta}_1 \end{bmatrix} + \begin{bmatrix} c_{azi2}F_{013} - c_{azi3}F_{012} \\ c_{azi3}F_{011} \\ -c_{azi2}F_{011} \end{bmatrix}$$

$$- \begin{bmatrix} F_{12A3}(d_1 - c_{azi3}) + (d_2 - c_{azi2})(F_{12A1}\sin\theta_2 + F_{12A2}\cos\theta_2) \\ (c_{azi3} - d_1)(F_{12A1}\cos\theta_2 - F_{12A2}\sin\theta_2) \\ (d_2 - c_{azi2})(F_{12A1}\cos\theta_2 - F_{12A2}\sin\theta_2) \end{bmatrix}$$

$$- \begin{bmatrix} -(d_3 + c_{azi2})(F_{24C1}\sin\theta_2 + F_{24C2}\cos\theta_2) \\ (c_{azi3} - d_1)(F_{12C1}\cos\theta_2 - F_{12C2}\sin\theta_2) \\ -(d_3 + c_{azi2})(F_{12C1}\cos\theta_2 - F_{12C2}\sin\theta_2) \end{bmatrix}$$

Writing as separate equations,

$$\begin{aligned} J_{113}\ddot{\theta}_1 - J_{123}\dot{\theta}_1^2 = {} & -M_{01b1} + c_{azi2}F_{013} - c_{azi3}F_{012} \\ & - F_{12A3}(d_1 - c_{azi3}) \\ & - (d_2 - c_{azi2})(F_{12A1}\sin\theta_2 + F_{12A2}\cos\theta_2) + (d_3 \\ & + c_{azi2})(F_{24C1}\sin\theta_2 + F_{24C2}\cos\theta_2) \end{aligned} \tag{2.57}$$

$$\begin{aligned} J_{123}\ddot{\theta}_1 - J_{113}\dot{\theta}_1^2 & \\ = {} & -M_{01b2} - T_{12a} + k_{12s}\theta_3 + c_{12d}\dot{\theta}_3 + c_{azi3}F_{011} \\ & - (c_{azi3} - d_1)(F_{12A1}\cos\theta_2 - F_{12A2}\sin\theta_2) \\ & - (c_{azi3} - d_1)(F_{12C1}\cos\theta_2 - F_{12C2}\sin\theta_2) \end{aligned} \tag{2.58}$$

$$\begin{aligned} J_{133}\ddot{\theta}_1 = {} & T_{01a} - c_{01d}\dot{\theta}_1 - c_{azi2}F_{011} \\ & - (d_2 - c_{azi2})(F_{12A1}\cos\theta_2 - F_{12A2}\sin\theta_2) \\ & + (d_3 + c_{azi2})(F_{12C1}\cos\theta_2 - F_{12C2}\sin\theta_2) \end{aligned} \tag{2.59}$$

2.3.2 Newton-Euler Equations for Body 2

Force equation:

$$m_2\vec{a}_2 = m_2\vec{g} + \vec{F}_{12A} + \vec{F}_{12C} \Rightarrow$$

Expressing in matrix representation in base reference frame,

$$m_2\bar{a}_{2/0}^{(2)} = m_2\bar{g}^{(2)} + \bar{F}_{12A}^{(2)} + \bar{F}_{12C}^{(2)} \Rightarrow$$

$$m_2\hat{C}^{-1}\bar{a}_{2/0}^{(0)} = m_2\hat{C}^{-1}\bar{g}^{(0)} + \begin{bmatrix} F_{12A1} \\ F_{12A2} \\ F_{12A3} \end{bmatrix} + \begin{bmatrix} F_{12C1} \\ F_{12C2} \\ 0 \end{bmatrix} \Rightarrow$$

$$m_2 \begin{bmatrix} \cos\theta_1\cos\theta_2 & \sin\theta_1\cos\theta_2 & -\sin\theta_2 \\ -\cos\theta_1\sin\theta_2 & -\sin\theta_1\sin\theta_2 & -\cos\theta_2 \\ -\sin\theta_1 & \cos\theta_1 & 0 \end{bmatrix} \begin{bmatrix} -c_2\ddot{\theta}_1\cos\theta_1 + c_2\dot{\theta}_1^2\sin\theta_1 \\ -c_2\ddot{\theta}_1\sin\theta_1 - c_2\dot{\theta}_1^2\cos\theta_1 \\ 0 \end{bmatrix}$$

$$= m_2 \begin{bmatrix} \cos\theta_1\cos\theta_2 & \sin\theta_1\cos\theta_2 & -\sin\theta_2 \\ -\cos\theta_1\sin\theta_2 & -\sin\theta_1\sin\theta_2 & -\cos\theta_2 \\ -\sin\theta_1 & \cos\theta_1 & 0 \end{bmatrix} \begin{bmatrix} 0 \\ 0 \\ g \end{bmatrix} + \begin{bmatrix} F_{12A1} \\ F_{12A2} \\ F_{12A3} \end{bmatrix}$$

$$+ \begin{bmatrix} F_{12C1} \\ F_{12C2} \\ 0 \end{bmatrix} \Rightarrow$$

$$m_2 \begin{bmatrix} -c_2\cos\theta_2\,\ddot{\theta}_1 \\ c_2\sin\theta_2\,\ddot{\theta}_1 \\ -c_2\dot{\theta}_1^2 \end{bmatrix} = m_2 \begin{bmatrix} -g\sin\theta_2 \\ -g\cos\theta_2 \\ 0 \end{bmatrix} + \begin{bmatrix} F_{12A1} \\ F_{12A2} \\ F_{12A3} \end{bmatrix} + \begin{bmatrix} F_{12C1} \\ F_{12C2} \\ 0 \end{bmatrix}$$

Writing as separate equations,

$$-m_2c_2\cos\theta_2\,\ddot{\theta}_1 = -m_2g\sin\theta_2 + F_{12A1} + F_{12C1} \tag{2.60}$$

$$m_2c_2\sin\theta_2\,\ddot{\theta}_1 = -m_2g\cos\theta_2 + F_{12A2} + F_{12C2} \tag{2.61}$$

$$-m_2c_2\dot{\theta}_1^2 = F_{12A3} \tag{2.62}$$

Moment equation:

$$\check{J}_2\cdot\vec{\alpha}_2 + \vec{\omega}_2\times\check{J}_2\cdot\vec{\omega}_2 = \vec{T}_{12a} + \vec{T}_{12d} + \vec{r}_{C_{ele}A}\times\vec{F}_{12A} + \vec{r}_{C_{ele}C}\times\vec{F}_{12C} \tag{2.63}$$

The moment equation can be written as column matrix equations as follows. Manipulations of the equation are provided in Appendix A.

$$\begin{bmatrix} \ddot{\theta}_1(-J_{211}\sin\theta_2 - J_{212}\cos\theta_2) + \ddot{\theta}_2(J_{213}) + \left(-J_{211}\cos\theta_2\,\dot{\theta}_1\dot{\theta}_2 + J_{212}\sin\theta_2\,\dot{\theta}_1\right) \\ \ddot{\theta}_1(-J_{212}\sin\theta_2 - J_{222}\cos\theta_2) + \ddot{\theta}_2(J_{223}) + (-J_{212}\cos\theta_2\,\dot{\theta}_1\dot{\theta}_2 + J_{222}\sin\theta_2\,\dot{\theta}_1) \\ \ddot{\theta}_1(-J_{213}\sin\theta_2 - J_{223}\cos\theta_2) + \ddot{\theta}_2(J_{233}) + (-J_{213}\cos\theta_2\,\dot{\theta}_1\dot{\theta}_2 + J_{223}\sin\theta_2\,\dot{\theta}_1) \end{bmatrix}$$

$$+ \begin{bmatrix} J_{223}\left(\dot{\theta}_1^2\cos^2\theta_2 - \dot{\theta}_2^2\right) + J_{212}\dot{\theta}_1\dot{\theta}_2\sin\theta_2 \\ -J_{213}\left(\dot{\theta}_1^2\sin^2\theta_2 + \dot{\theta}_2^2\right) + \dot{\theta}_1\dot{\theta}_2\sin\theta_2\,(J_{211} + J_{233}) \\ J_{212}\left(\dot{\theta}_1^2\cos^2\theta_2 - \dot{\theta}_1^2\sin^2\theta_2\right) + \dot{\theta}_1^2\sin\theta_2\cos\theta_2\,(J_{211} - J_{222}) \end{bmatrix}$$

$$+ \begin{bmatrix} J_{213}\dot{\theta}_1^2\sin\theta_2\cos\theta_2 - \dot{\theta}_1\dot{\theta}_2\cos\theta_2\,(J_{233} - J_{222}) \\ J_{212}\dot{\theta}_1\dot{\theta}_2\cos\theta_2 - J_{223}\dot{\theta}_1^2\sin\theta_2\cos\theta_2 \\ -J_{213}\dot{\theta}_1\dot{\theta}_2\cos\theta_2 + J_{223}\dot{\theta}_1\dot{\theta}_2\sin\theta_2 \end{bmatrix}$$

$$= \begin{bmatrix} 0 \\ 0 \\ T_{12a} - c_{12d}\dot{\theta}_2 \end{bmatrix} + \begin{bmatrix} (c_2 + d_2)F_{12A2} \\ -(c_2 + d_2)F_{12A1} \\ 0 \end{bmatrix} + \begin{bmatrix} (c_2 - d_3)F_{12C2} \\ (d_3 - c_2)F_{12C1} \\ 0 \end{bmatrix} \Rightarrow$$

Writing as separate equations,

$$\begin{aligned} &\ddot{\theta}_1(-J_{211}\sin\theta_2 - J_{212}\cos\theta_2) + \ddot{\theta}_2(J_{213}) \\ &\quad + \left(-J_{211}\cos\theta_2\,\dot{\theta}_1\dot{\theta}_2 + J_{212}\sin\theta_2\,\dot{\theta}_1\right) \\ &\quad + J_{223}\left(\dot{\theta}_1^2\cos^2\theta_2 - \dot{\theta}_2^2\right) + J_{212}\dot{\theta}_1\dot{\theta}_2\sin\theta_2 \\ &\quad + J_{213}\dot{\theta}_1^2\sin\theta_2\cos\theta_2 - \dot{\theta}_1\dot{\theta}_2\cos\theta_2\,(J_{233} - J_{222}) \\ &\quad = (c_2 + d_2)F_{12A2} + (c_2 - d_3)F_{12C2} \end{aligned} \tag{2.64}$$

$$\begin{aligned} &\ddot{\theta}_1(-J_{212}\sin\theta_2 - J_{222}\cos\theta_2) + \ddot{\theta}_2(J_{223}) \\ &\quad + \left(-J_{212}\cos\theta_2\,\dot{\theta}_1\dot{\theta}_2 + J_{222}\sin\theta_2\,\dot{\theta}_1\right) \\ &\quad - J_{213}\left(\dot{\theta}_1^2\sin^2\theta_2 + \dot{\theta}_2^2\right) \\ &\quad + \dot{\theta}_1\dot{\theta}_2\sin\theta_2\,(J_{211} + J_{233}) + J_{212}\dot{\theta}_1\dot{\theta}_2\cos\theta_2 \\ &\quad - J_{223}\dot{\theta}_1^2\sin\theta_2\cos\theta_2 \\ &\quad = -(c_2 + d_2)F_{12A1} + (d_3 - c_2)F_{12C1} \end{aligned} \tag{2.65}$$

$$\begin{aligned} &\ddot{\theta}_1(-J_{213}\sin\theta_2 - J_{223}\cos\theta_2) + \ddot{\theta}_2(J_{233}) \\ &\quad + \left(-J_{213}\cos\theta_2\,\dot{\theta}_1\dot{\theta}_2 + J_{223}\sin\theta_2\,\dot{\theta}_1\right) \\ &\quad + J_{212}\left(\dot{\theta}_1^2\cos^2\theta_2 - \dot{\theta}_1^2\sin^2\theta_2\right) \\ &\quad + \dot{\theta}_1^2\sin\theta_2\cos\theta_2\,(J_{211} - J_{222}) - J_{213}\dot{\theta}_1\dot{\theta}_2\cos\theta_2 \\ &\quad + J_{223}\dot{\theta}_1\dot{\theta}_2\sin\theta_2 = T_{12a} - c_{12d}\dot{\theta}_2 \end{aligned} \tag{2.66}$$

Equation of the motion can be obtained from the above Newton-Euler equations. Manipulations of those were provided Appendix B. The nonlinear equation of motion is as follows.

$$\begin{bmatrix} 1 & 0 & 0 & 0 \\ 0 & CONS_{31} & 0 & CONS_{32} \\ 0 & 0 & 1 & 0 \\ 0 & CONS_{41} & 0 & CONS_{42} \end{bmatrix} \begin{bmatrix} \dot{\theta}_1 \\ \ddot{\theta}_1 \\ \dot{\theta}_2 \\ \ddot{\theta}_2 \end{bmatrix} = - \begin{bmatrix} \dot{\theta}_1 \\ CONS_{33} \\ \dot{\theta}_2 \\ CONS_{43} \end{bmatrix} \tag{2.67}$$

Defining the matrices,

$$[N_1] = \begin{bmatrix} 1 & 0 & 0 & 0 \\ 0 & CONS_{31} & 0 & CONS_{32} \\ 0 & 0 & 1 & 0 \\ 0 & CONS_{41} & 0 & CONS_{42} \end{bmatrix} \; and \; [N_2] = - \begin{bmatrix} \dot{\theta}_1 \\ CONS_{33} \\ \dot{\theta}_2 \\ CONS_{43} \end{bmatrix}$$

It is observed that equation of motion is nonlinear differential equation; besides, it depends on the elevation axis variable, θ_2 as can be seen from relations in Appendix. $[N_1]$ matrix should be non-singular; otherwise, equation of motion cannot be calculated. Note that variations of the $[N_1]$ with respect to other joint variables such as $\theta_1, \dot{\theta}_1, \dot{\theta}_2$ are also analyzed; and it is observed that $[N_1]$ is independent of them. The dependency of the $[N_1]$ to θ_2 is because of inertial change of the total rotating mass around azimuth axis as elevation position changes.

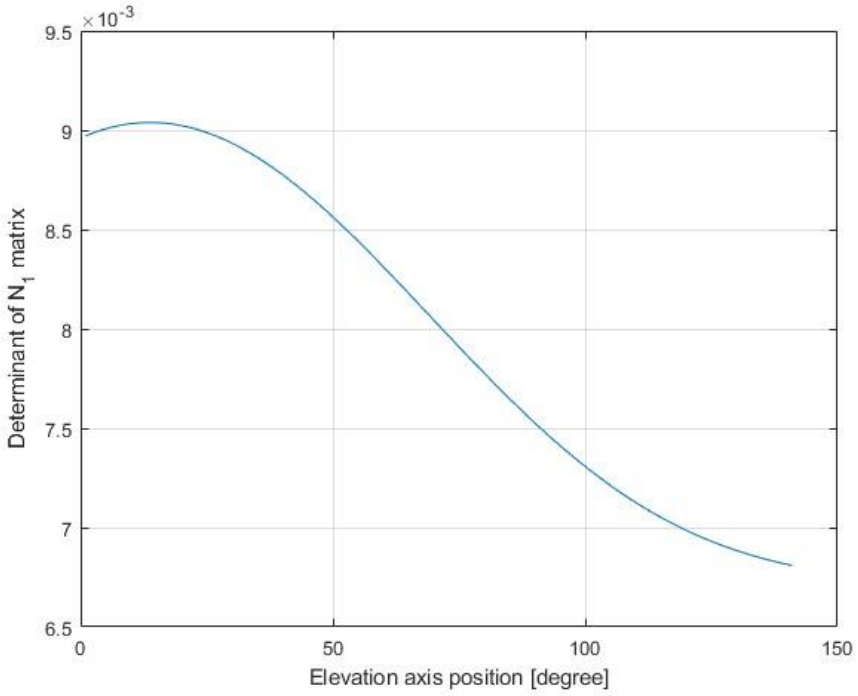

Figure 9: Determinant of augmented matrix N_1

2.4 Decoupled Equation of Motion

It has been shown in the previous section that the equations of motion are coupled. As can be seen, it was quite difficult to obtain these coupled equations of motion. Coupling of the gimbal axis emerges from nonzero off-diagonal product of inertia terms and coriolis and centrifugal forces. The coupled situation might be negligible or small when the nonzero off-diagonal product of inertia terms and the rotation velocities are very low. This simplifies the modeling considerably. Many gimbal studies are modeled using this simplified decoupled gimbal approach. As observed in (3.2)(3.3), a similar situation might be valid in the gimbal system used in this study. In this study, the gimbal system was modeled with the decouple approach and compared with the coupled model.

In addition to the zero off-diagonal product of inertia terms, decoupled gimbal axis model consists of the following approaches. In the previous sections, the interactions of the moving bodies with each other were expressed by reaction forces such as F_{12A}. Assuming that the position change of the elevation body was small such that change in these forces is negligible, or if the elevation inertia matrix at different angles is constant, these two azimuth and elevation masses can be considered and modeled as a lumped outer gimbal mass as seen in the Figure 11. Besides, the mass named body 2 in the coupled 3D gimbal model constructs the inner gimbal by also consisting of the kinematic and dynamic independency of body 1, which can be shown in the Figure 10 All these assumptions greatly reduce computing power and especially the modeling complexity. In this way, the moment equations, expressed simply along the rotational motion axes, form equations of the motion of the inner and outer gimbal masses, which are independent of each other.

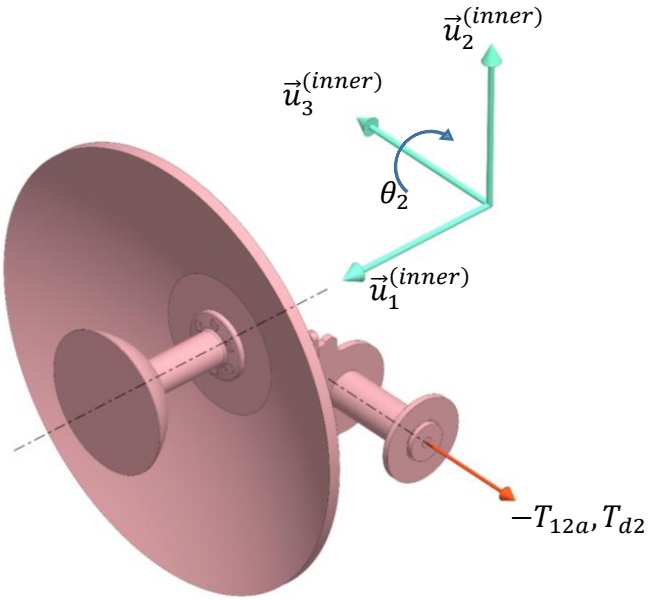

Figure 10: Free body diagram of the decoupled inner gimbal

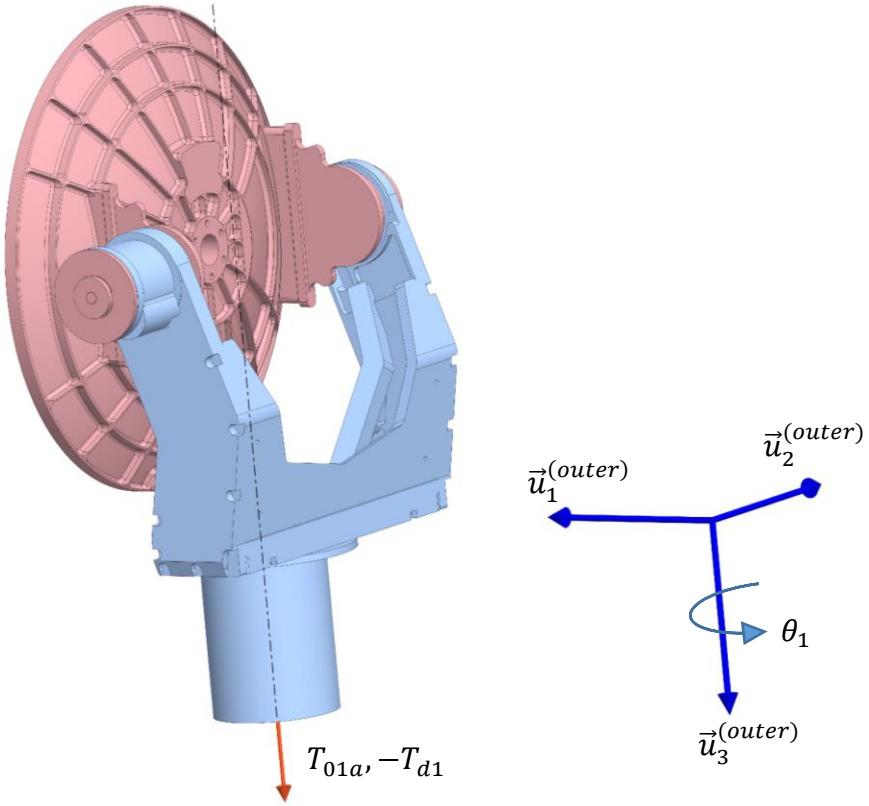

Figure 11: Free body diagram of the decoupled outer gimbal

The outer gimbal, composed of the azimuth body and the elevation body which is considered in a constant position ($\theta_2 = 0$) for mass calculation of the outer gimbal, has a static balance. Therefore, the decoupled equations of motion are calculated by considering the mass and inertia values as follows.

Decoupled inertia matrices:

$$\hat{J}_{outer}^{(1)} = J_{outer} = 15.284e-2\ kgm^2 \tag{2.68}$$

$$\hat{J}_{inner}^{(2)} = J_{inner} = 5.732e-2\ kgm^2 \tag{2.69}$$

Moment equation and equation of motion of the outer gimbal in the rotation axis:

$$J_{outer}\ddot{\theta}_1 = T_{01a} - c_{01d}\dot{\theta}_1 \tag{2.70}$$

Moment equation and equation of motion of the inner gimbal in the rotation axis:

$$J_{inner}\ddot{\theta}_2 = T_{12a} - c_{12d}\dot{\theta}_2 \tag{2.71}$$

Laplace transform can be applied on decoupled gimbal equations of motion because they are linear second order nonhomogeneous differential equations. For the zero initial conditions, decoupled outer gimbal plant dynamics can be expressed as follows where G_{outerP} represents transfer function between $\Theta_1(s)$ and T_{01a}, G_{outerP} represents transfer function between $\dot{\Theta}_1(s)$ and $T_{01a}(s)$.

$$\Theta_1(s)(J_{outer}s^2 + c_{01d}s) = T_{01a} \tag{2.72}$$

$$G_{outerP} = \frac{\Theta_1(s)}{T_{01a}(s)} = \frac{1}{s(J_{outer}s + c_{01d})} \tag{2.73}$$

$$G_{outerR} = \frac{\dot{\Theta}_1(s)}{T_{01a}(s)} = \frac{s\Theta_1(s)}{T_{01a}(s)} = \frac{1}{J_{outer}s + c_{01d}} \tag{2.74}$$

Similarly, decoupled inner gimbal plant dynamics can be expressed as follows where G_{innerP} represents transfer function between $\Theta_2(s)$ and T_{12a}, G_{innerP} represents transfer function between $\dot{\Theta}_2(s)$ and $T_{12a}(s)$.

$$J_{inner}\ddot{\theta}_2 = T_{12a} - c_{12d}\dot{\theta}_2 \tag{2.75}$$

$$\Theta_2(s)(J_{inner}s^2 + c_{12d}s) = T_{12a} \tag{2.76}$$

$$G_{innerP} = \frac{\Theta_2(s)}{T_{12a}(s)} = \frac{1}{s(J_{inner}s + c_{12d})} \tag{2.77}$$

$$G_{innerR} = \frac{\dot{\Theta}_2(s)}{T_{12a}(s)} = \frac{s\Theta_2(s)}{T_{12a}(s)} = \frac{1}{J_{inner}s + c_{12d}} \tag{2.78}$$

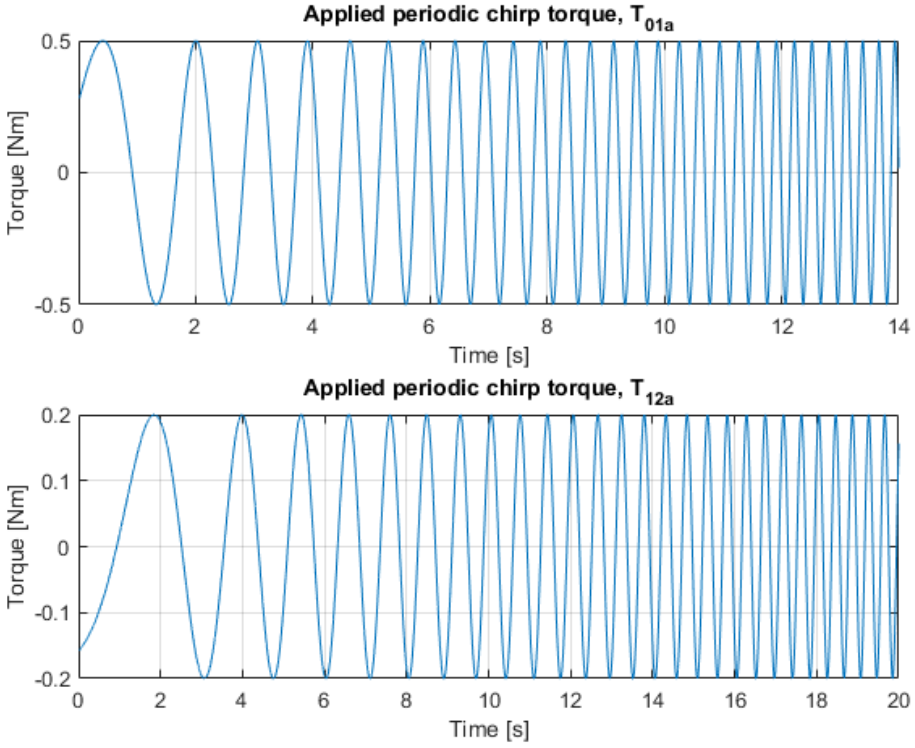

Figure 12: Excitation torques for model verification

The validity of the mathematical models, which are coupled and decoupled models tested by applying time domain chirp signal shown in Figure 12 That signal was applied as input torques (T_{01a} and T_{12a}) on both the mathematical models and real gimbal system simultaneously and responses were given in Figure 13 and Figure 14. As observed in the figures, both mathematical models contain differences. However, the decoupled gimbal model behaves more inconsistently than the real system. This difference is mainly due to the simultaneous application of torque to both gimbal

axes, which arises the effect of the cross-coupling behavior of the gimbal axis; therefore, the coupled model represents real system more accurately. However, although the decoupled model is obtained with a very simple approach, it gives very close results. This was actually expected because the gimbal system in this study was specifically designed to converge to decouple assumptions. In the mechanical design phase, the static and dynamic distribution of the masses were tried to be balanced. Therefore, the decoupled gimbal model seems useful for using the early stages of the design and for quick and rough calculations. In the following sections, the cascade PI control system was developed and tested for comparison purposes by using the decoupled model. However, since this thesis focuses on the more general 3D coupled mathematical model approach, the coupled gimbal model was taken as a basis in the following sections.

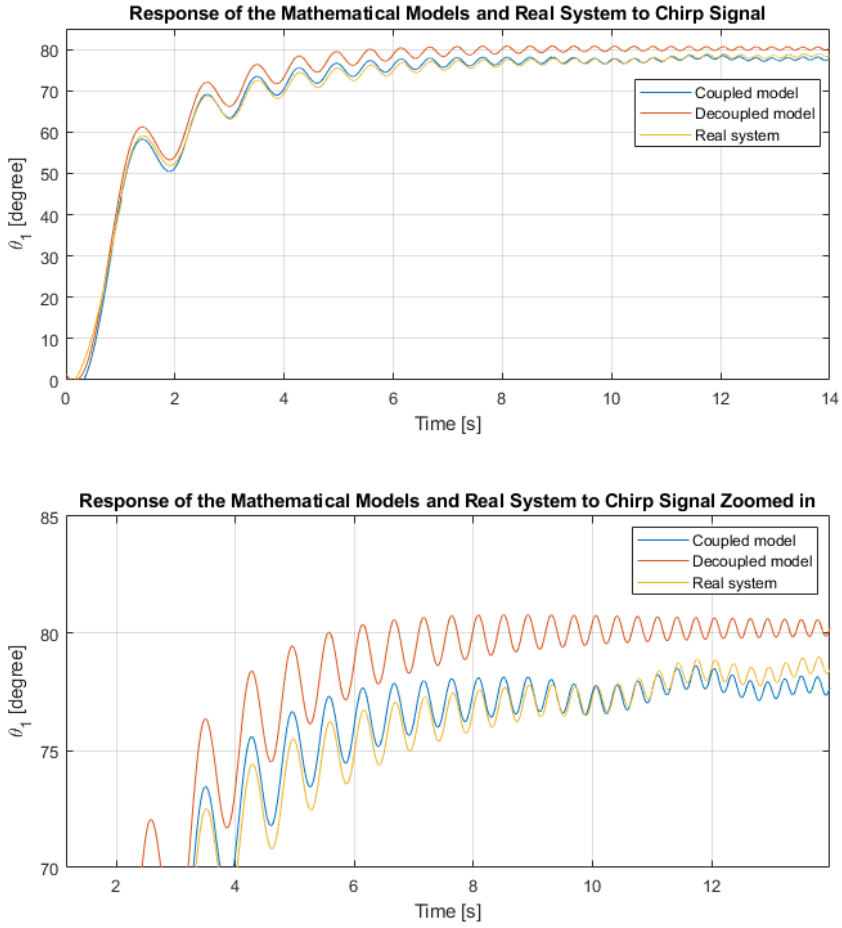

Figure 13: θ_1 response of the mathematical models and real system to chirp signal

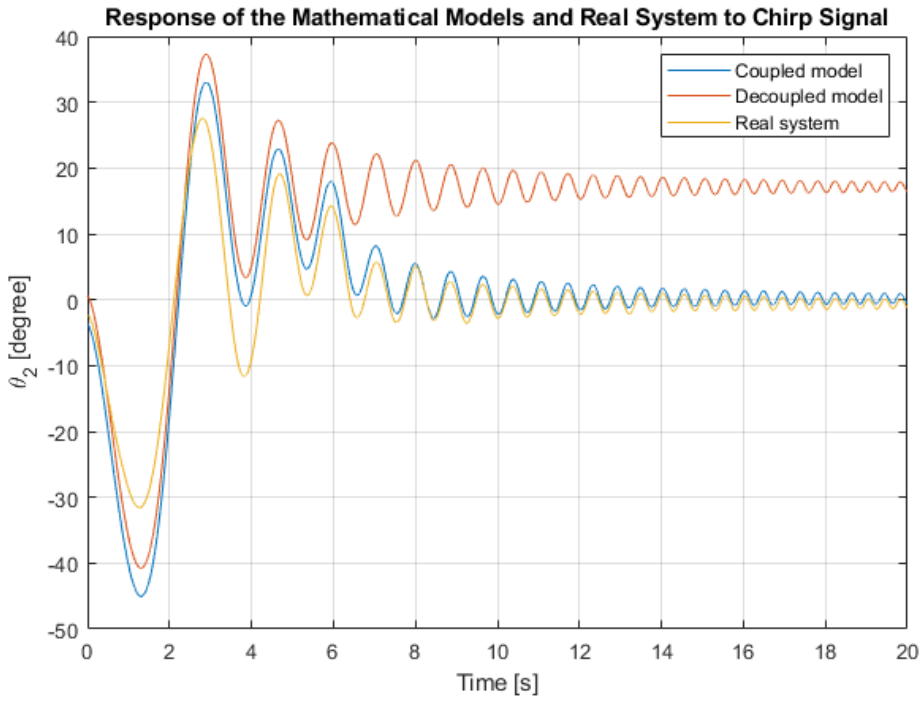

Figure 14: θ_2 response of the mathematical models and real system to chirp signal

2.5 Linearization

In this section, the 3D coupled model was linearized. The decoupled gimbal model has very simple equations of motion, as seen in the previous section. In addition, since the thesis proceeded by considering a more general mathematical model, the 3D coupled gimbal model was taken as a basis in the following sections.

2.5.1 Equilibrium point

The nonlinear equation of motion should be linearized around an equilibrium point to express as linear time-invariant system. Variables defining a system's state do not change over time around an equilibrium point. That is, state derivative with respect to time is zero.

States, x, of the gimbal system are rotation angles and velocities of the body 1 and 2. Inputs, u, are dc motor torques for each rotation degree. Therefore, they can be expressed as,

$$x = \begin{bmatrix} x_1 \\ x_2 \\ x_3 \\ x_4 \end{bmatrix} = \begin{bmatrix} \theta_1 \\ \dot{\theta}_1 \\ \theta_2 \\ \dot{\theta}_2 \end{bmatrix} \tag{2.79}$$

$$u = \begin{bmatrix} T_{01a} \\ T_{12a} \end{bmatrix} \tag{2.80}$$

State changes can be expressed as,

$$\dot{x} = \begin{bmatrix} \dot{x}_1 \\ \dot{x}_2 \\ \dot{x}_3 \\ \dot{x}_4 \end{bmatrix} = \begin{bmatrix} \dot{\theta}_1 \\ \ddot{\theta}_1 \\ \dot{\theta}_2 \\ \ddot{\theta}_2 \end{bmatrix} \tag{2.81}$$

It can be related to the equation of motion found in previous section.

$$\begin{bmatrix} 0 & 1 & 0 & 0 \\ 0 & CONS_{31} & 0 & CONS_{32} \\ 0 & 0 & 0 & 1 \\ 0 & CONS_{41} & 0 & CONS_{42} \end{bmatrix} \dot{x} = -\begin{bmatrix} \dot{\theta}_1 \\ CONS_{33} \\ \dot{\theta}_2 \\ CONS_{43} \end{bmatrix} \Rightarrow$$

$$\dot{x} = -f(x,u) \tag{2.82}$$

$$where, \qquad f(x,u) = -\begin{bmatrix} 0 & 1 & 0 & 0 \\ 0 & CONS_{31} & 0 & CONS_{32} \\ 0 & 0 & 0 & 1 \\ 0 & CONS_{41} & 0 & CONS_{42} \end{bmatrix}^{-1} \begin{bmatrix} \dot{\theta}_1 \\ CONS_{33} \\ \dot{\theta}_2 \\ CONS_{43} \end{bmatrix}$$

The manipulated nonlinear equation of motion is $4x1$ matrix and it is dependent on states and inputs of the gimbal system.

$f(x,u)$ can be partitioned as follows.

$$f(x,u) = \begin{bmatrix} f_1 \\ f_2 \\ f_3 \\ f_4 \end{bmatrix} \tag{2.83}$$

The state changes are zero at equilibrium point; therefore,

$$\dot{x} = f(x_e, u_e) = 0 \tag{2.84}$$

An equilibrium point that satisfies the above condition is chosen as:

$$x_e = \begin{bmatrix} 0 \\ 0 \\ 0 \\ 0 \end{bmatrix} \tag{2.85}$$

$$where, \qquad [N_2]|_{x_e} = 0 \Rightarrow f(x_e, u_e)|_{x_e} = 0$$

It is observed that equilibrium points are independent of angular position variables because of the fact that the gimbal system is statically balanced.

2.5.2 State space representation

Mathematical model of a linear time invariant system can be denoted as state space representation, according to [31].

$$\dot{x}(t) = Ax(t) + Bu(t) \tag{2.86}$$

$$y = Cx(t) + Du(t) \tag{2.87}$$

where x and u are state vector and input vector respectively as defined above, y is output vector, A is state matrix, B is input matrix, $C$is output matrix and D is direct transmission (disturbance output) matrix. If the system has n number of state variables, m number of control input variable, q number of output variables, dimensions of the matrices are then:

- $\dim(A) = \mathbb{R}^{nxn}$
- $\dim(B) = \mathbb{R}^{nxm}$

- $\dim(C) = \mathbb{R}^{qxn}$
- $\dim(D) = \mathbb{R}^{qxm}$

The gimbal state space representation variables are as follows.

- $n = 4 \Rightarrow x(t)$ is a $4x1$ vector
- $m = 2 \Rightarrow \mathrm{u}(t)$ is a $2x1$ vector
- $q = 4 \Rightarrow y(t)$ is $4x1$ vector
- A is a $4x4$ matrix
- B is a $4x2$ matrix
- C is a $4x4$ matrix
- D is a $4x2$ matrix

The nonlinear equation of motion that describes the state changes is to be used to obtain linearized state space matrices around the equilibrium point for the gimbal system.

$$A = \frac{\partial f}{\partial x}\Big|_{x_e,u_e} = \begin{bmatrix} \frac{\partial f_1}{\partial x_1} & \frac{\partial f_1}{\partial x_2} & \frac{\partial f_1}{\partial x_3} & \frac{\partial f_1}{\partial x_4} \\ \frac{\partial f_2}{\partial x_1} & \frac{\partial f_2}{\partial x_2} & \frac{\partial f_2}{\partial x_3} & \frac{\partial f_2}{\partial x_4} \\ \frac{\partial f_3}{\partial x_1} & \frac{\partial f_3}{\partial x_2} & \frac{\partial f_3}{\partial x_3} & \frac{\partial f_3}{\partial x_4} \\ \frac{\partial f_4}{\partial x_1} & \frac{\partial f_4}{\partial x_2} & \frac{\partial f_4}{\partial x_3} & \frac{\partial f_4}{\partial x_4} \end{bmatrix}_{x_e,u_e} \tag{2.88}$$

$$B = \frac{\partial f}{\partial u}\Big|_{x_e,u_e} = \begin{bmatrix} \frac{\partial f_1}{\partial u_1} & \frac{\partial f_1}{\partial u_2} \\ \frac{\partial f_2}{\partial u_1} & \frac{\partial f_2}{\partial u_2} \\ \frac{\partial f_3}{\partial u_1} & \frac{\partial f_3}{\partial u_2} \\ \frac{\partial f_4}{\partial u_1} & \frac{\partial f_4}{\partial u_2} \end{bmatrix}_{x_e,u_e} \tag{2.89}$$

Controlled output of the gimbal system includes all the state variables; thus, output matrix is:

$$C = \begin{bmatrix} 1 & 0 & 0 & 0 \\ 0 & 1 & 0 & 0 \\ 0 & 0 & 1 & 0 \\ 0 & 0 & 0 & 1 \end{bmatrix} \tag{2.90}$$

The direct transmission matrix is zero matrix; that is,

$$D = \begin{bmatrix} 0 & 0 \\ 0 & 0 \\ 0 & 0 \\ 0 & 0 \end{bmatrix} \tag{2.91}$$

State space matrices are found as follows by computing the partial differentiations at equilibrium points.

$$A = \begin{bmatrix} 0 & 1 & 0 & 0 \\ 0 & -0.0636 & 0 & 0.0022 \\ 0 & 0 & 0 & 1 \\ 0 & 0.0022 & 0 & -0.1745 \end{bmatrix} \tag{2.92}$$

$$B = \begin{bmatrix} 0 & 0 \\ 6.35 & -0.22 \\ 0 & 0 \\ -0.22 & 17.45 \end{bmatrix} \tag{2.93}$$

2.5.3 Frequency Response of the Linearized Gimbal System

Frequency responses of the linearized gimbal system can be represented with bode plots. The following figures include frequency responses for all combined input-output pairs. Those can also be related to open loop position/velocity dynamics or plant dynamics. As observed in Figure 15 and Figure 17, position variables cannot be controlled by open loop control method due to phase and gain margins. These imply that they can only be controlled for very low frequencies; however desired settling time requirement needs to have larger bandwidth, as seen in SYSTEM

IDENTIFICATION. Besides, it is known that control systems should have phase and gain margins for robustness against disturbance and model uncertainties.

Bode plots of the linearized system were used in SYSTEM IDENTIFICATION for comparison with the real system. The differences can be observed Figure 23.

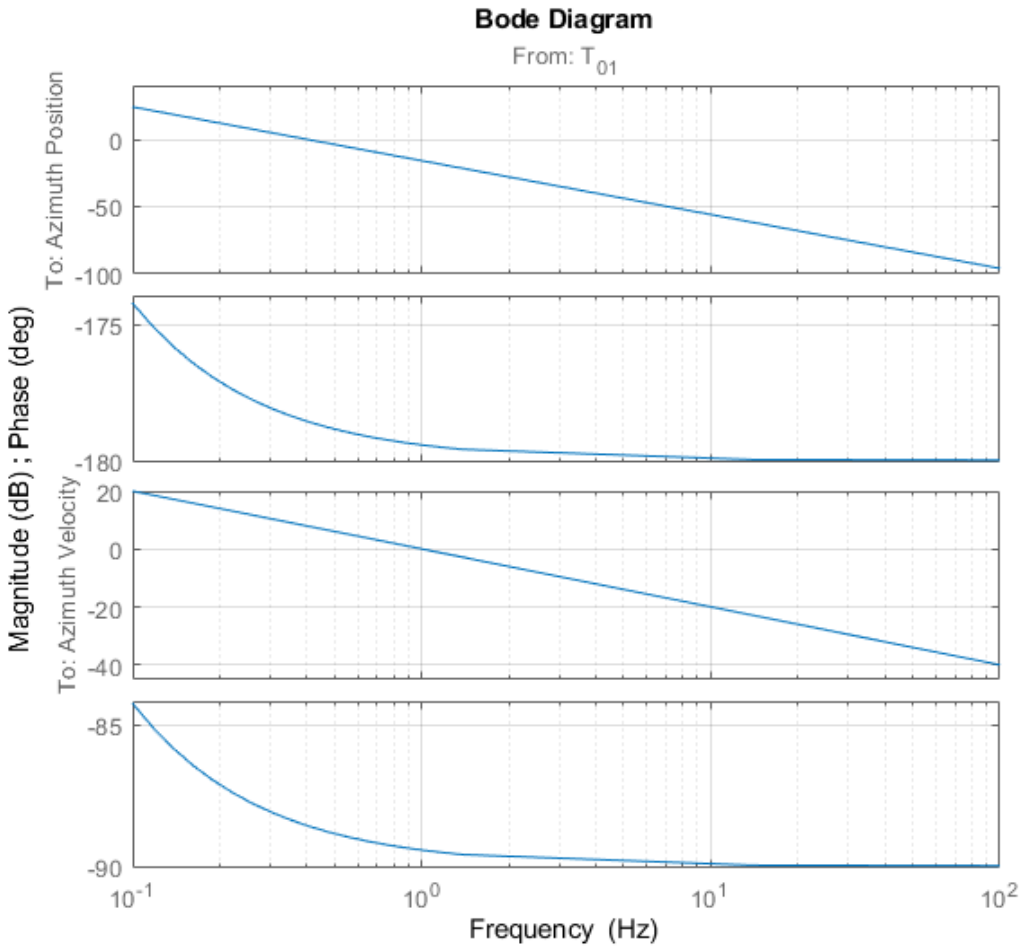

Figure 15: Bode plot from T_{01a} to θ_1 and $\dot{\theta}_1$

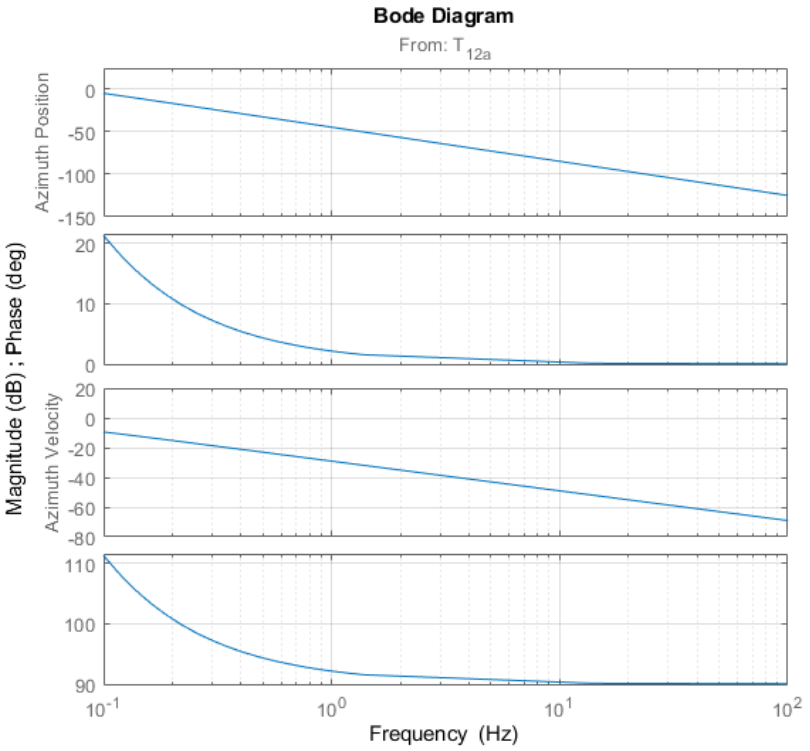

Figure 16: Bode plot from T_{12a} to θ_1 and $\dot{\theta}_1$

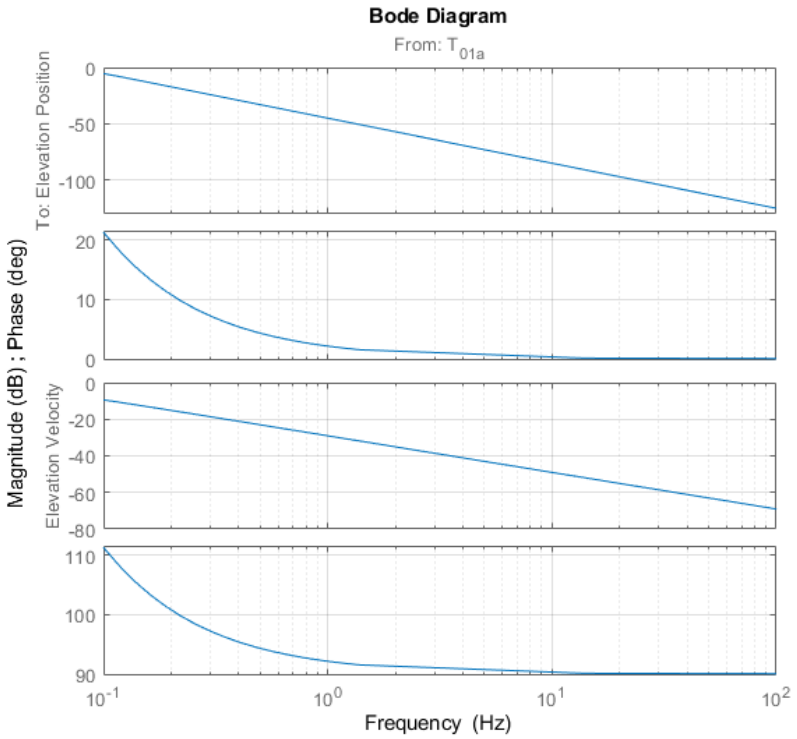

Figure 17: Bode plot from T_{01a} to θ_2 and $\dot{\theta}_2$

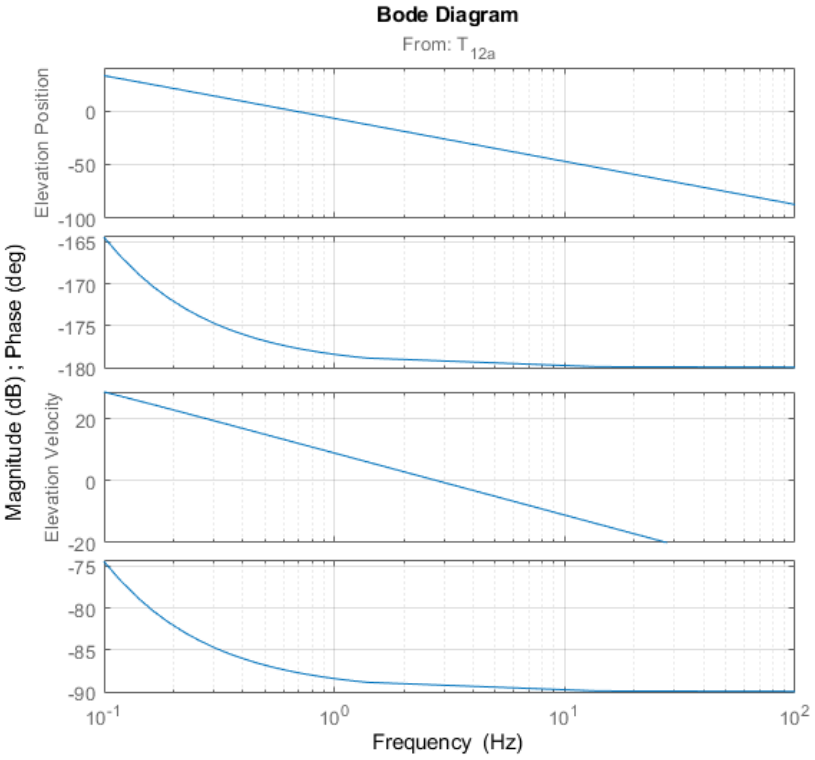

Figure 18: Bode plot from T_{12a} to θ_2 and $\dot{\theta}_2$

CHAPTER 3

SYSTEM IDENTIFICATION

It is known that the gimbal system has several nonlinearities, most of which are not suitable for analytically expressing or are quite complicated to solve. It is clearly observed in the nonlinear equation of motion, (2.67), obtained in the MATHEMATICAL MODELLING – even the gimbal system modeled by ignoring most nonlinearities such as coulomb friction, structural flexibilities, sensor, actuator nonlinearities, and so on. Thus, the dynamics of the linearized gimbal system should be compared and validated by means of frequency response function (FRF) identification tests.

There are various FRF identification test methods according to the types of the excitation signal type, such as swept sine, multi-sine, square sweep, and pseudo-random sequences. Swept sine is one of the most straightforward and used FRF identification method. As the name suggests, it is a sine function where the frequency of the excitation signal increases or decreases between interested frequencies. The swept sine identification method is used for the gimbal system with the following excitation signal.

$$u(t) = Asin(\omega(t)t) \tag{3.1}$$

where A is the amplitude of the excitation signal in Nm, $\omega(t)$ is variable frequency in Hz. The signal is designed with the following properties:

- $A = 0.5\ Nm$ and $A = 0.3\ Nm$ for the DC motor corresponds to azimuth and elevation axis.
- Excitation frequency ranges are $1 < \omega(t) < 100$ in Hz and distributed linearly.
- Sampling frequency of the system is $1\ kHz$.

The gimbal system is excited with the signal represented in (3.1), and the response is saved with the corresponding time information. Two independent tests are carried out for each input channel, and two FRFs are identified for each test; therefore, four FRFs are identified in total. Those are represented from Figure 19 to Figure 22.

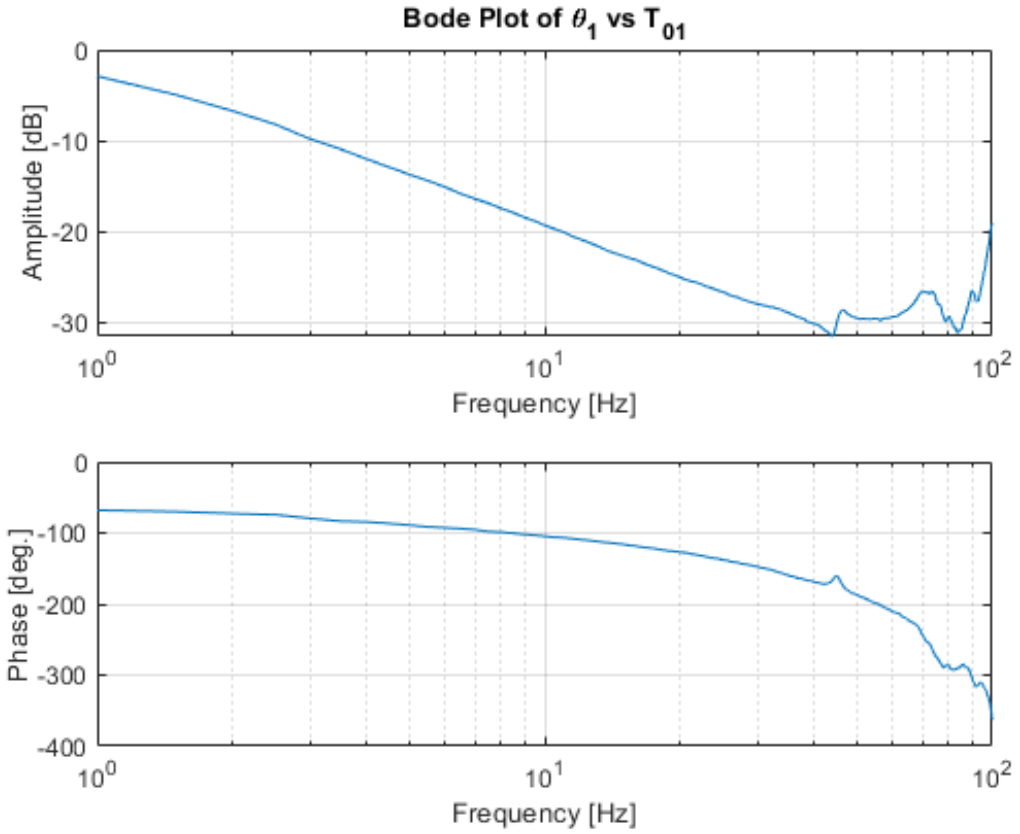

Figure 19: Bode plot of the measured real system between θ_1 vs T_{01}

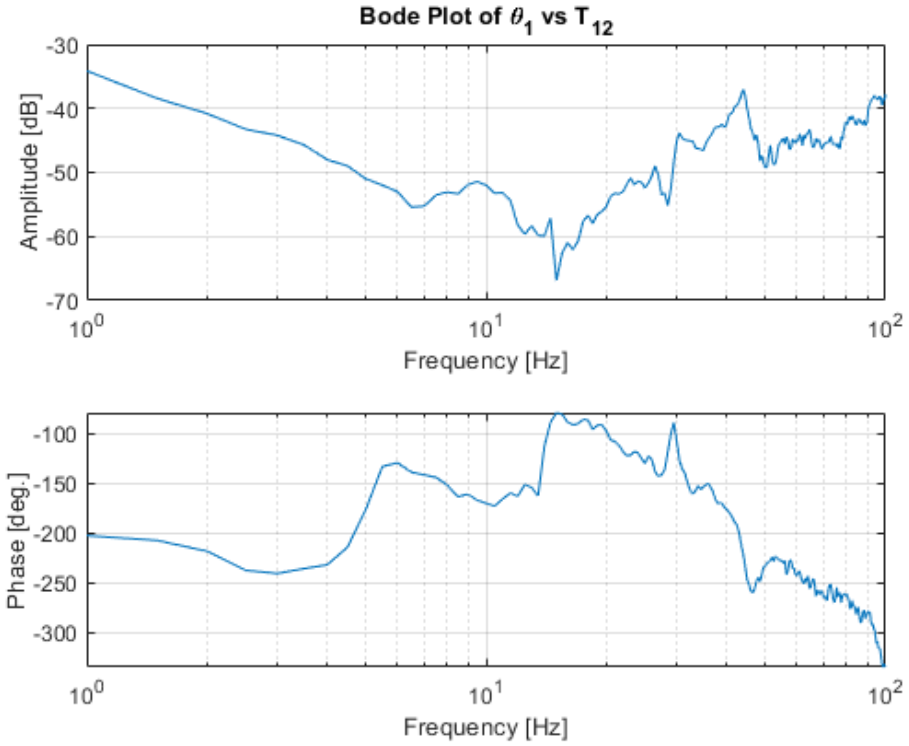

Figure 20: Bode plot of the measured real system between θ_1 vs T_{12}

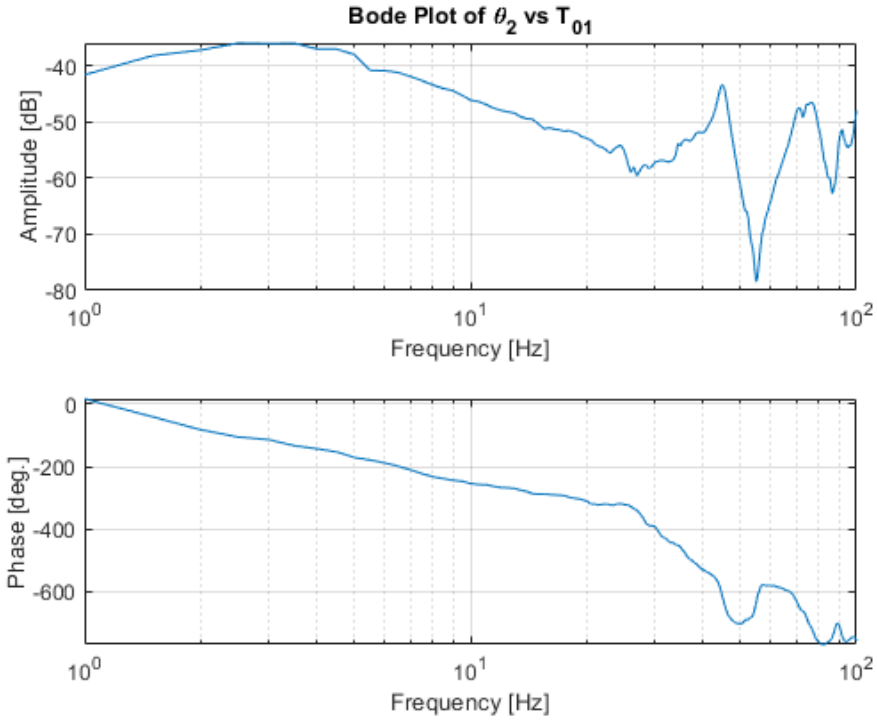

Figure 21: Bode plot of the measured real system between θ_2 vs T_{01}

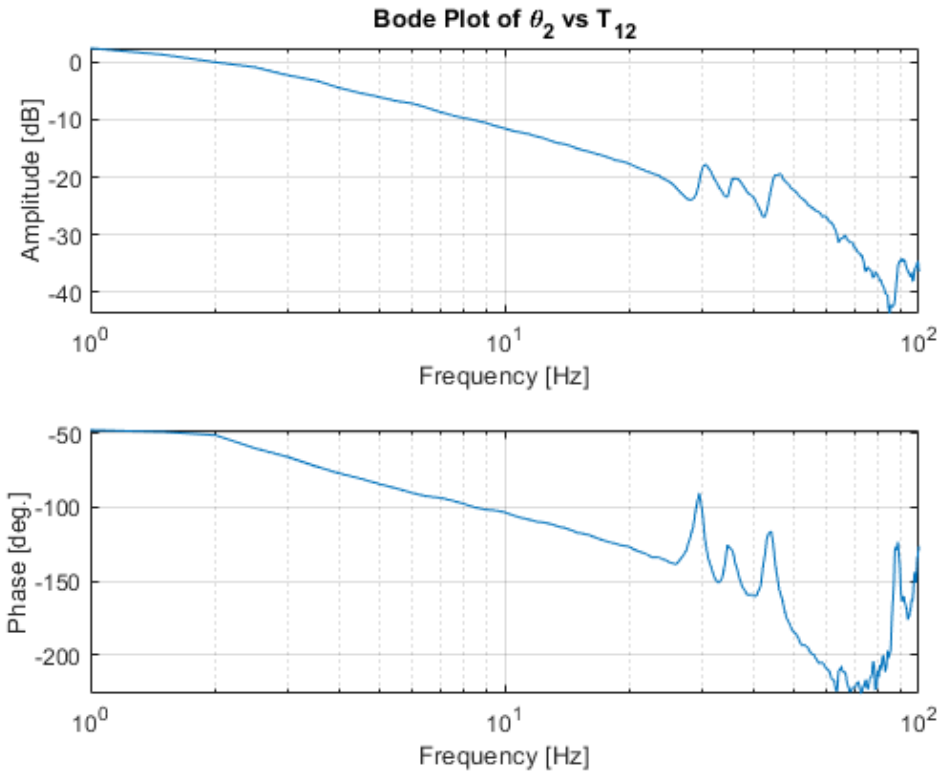

Figure 22: Bode plot of the measured real system between θ_2 vs T_{12}

Figure 20 and Figure 21 show that cross-coupling between the gimbal axes is minimal. Although amplitudes change drastically around the resonance frequencies, amplitudes of the cross FRFs almost 30 dB to 40dB lower than the direct FRFs in the low and mid frequency regions where the system behaves like an ideal inertia system. The reason is that the gimbal system is designed to be statically and almost dynamically balanced. When the inertia matrices expressed in (2.43) and (2.44) are examined, it can be realized that elements of the diagonal and non-diagonal are quite different. Normalizing inertia matrices by dividing the largest inertia element and multiplying by 100 to express as percentage show that the largest non-diagonal inertia matrix is 8.21% and 3.57% for bodies 1 and 2, respectively.

$$\frac{\hat{J}_1^{(1)}}{\max\left(\hat{J}_1^{(1)}\right)}100 = \begin{bmatrix} 100 & 6.24 & -6.04 \\ 6.24 & 63.85 & -8.21 \\ -6.04 & -8.21 & 56.53 \end{bmatrix} kgm^2 \qquad (3.2)$$

$$\frac{\hat{J}_2^{(2)}}{\max\left(\hat{J}_2^{(2)}\right)} 100 = \begin{bmatrix} 85.32 & -3.57 & -1.14 \\ 3.57 & 100 & -2.48 \\ -1.14 & -2.48 & 70.97 \end{bmatrix} kgm^2 \quad (3.3)$$

In Figure 19 and Figure 22, bode plots of the direct FRFs show that velocity open loops of the control axes behave like a rigid body, ideal inertia, with $-20\ db/decade$ slope at frequencies lower than structural flexibilities dominate. However, mechanical resonances emerge around frequencies around $45\ Hz$ and $30\ Hz$. As observed in Figure 23, the linearized model starts not representing the real system after those frequencies. In addition, one of the highlighted points of the bode plot comparison Figure 23, is that phase information differs between velocity open loop responses, even in the low and mid frequency region. That indicates that the real system is non-minimum phase system and has delay most likely.

This thesis proposes the model reference adaptive control method to deal with discrepancies. In the controller design chapter, first, the classic full-state feedback control is to be designed for comparison and to be used for reference model selection purposes. Then, model reference adaptive control method is to be developed by using full-state feedback controller in the first section of the CONTROL DESIGN Chapter as the nominal controller. The effect of the model reference controller on the differences between real and linearized system dynamics is to be evaluated in the EXPERIMENTS AND RESULTS Chapter.

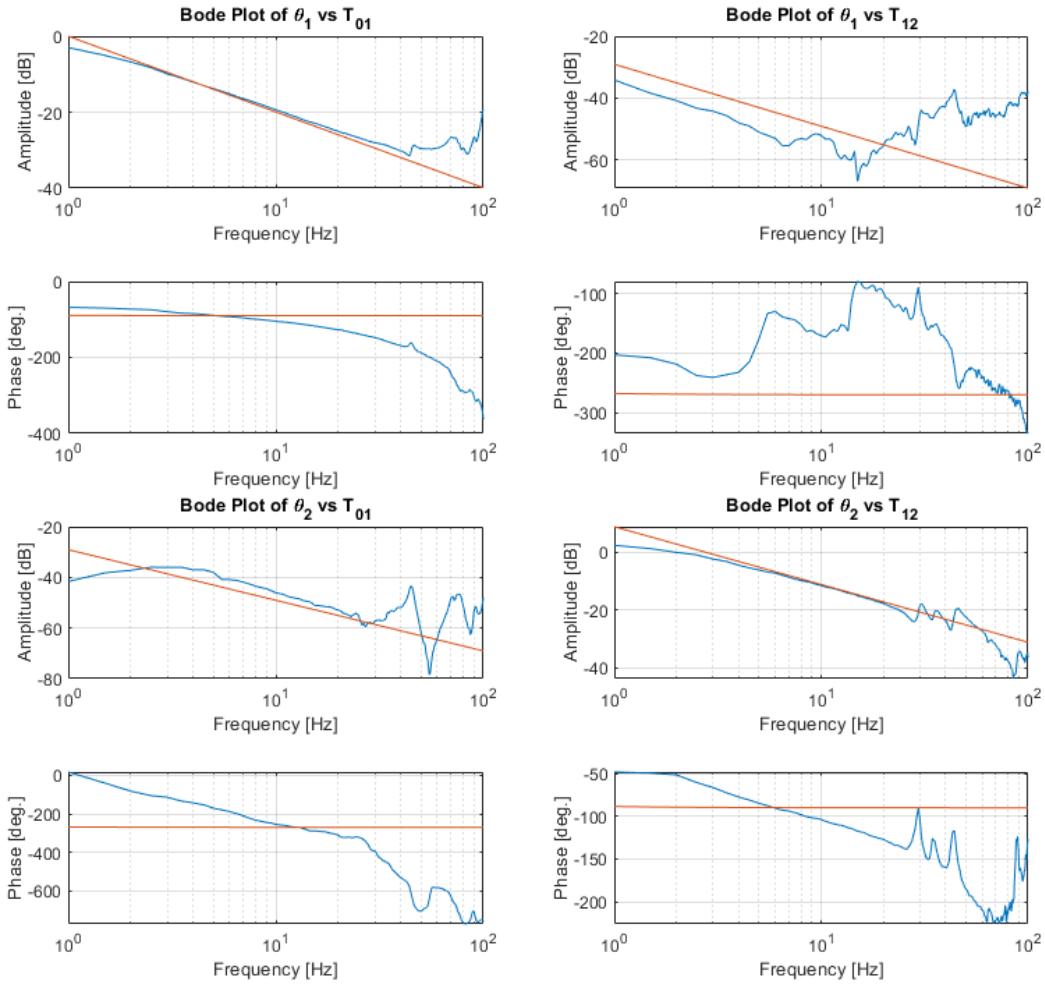

Figure 23: Bode plot of the velocity open loops. Blue and red lines indicate measured real system, linearized system, respectively

CHAPTER 4

CONTROL DESIGN

In this chapter, three different control methods were used to develop a control system for the gimbal system: full-state feedback control (FSFC), model reference adaptive control (MRAC) and cascade PI control. FSFC and MRAC were developed by considering the linearized coupled gimbal model, while the cascade PI control method uses the linear decoupled gimbal model. After those were designed according to the requirements, experiments and tests were made by applying them to the real gimbal system, and comparison were made accordingly in the following chapters.

4.1 Full-State Feedback Control

The full-state feedback control method is a state-space design method, and it provides a choice of placing the closed-loop poles of the system at desired locations. It is similar to root-locus method where it, however, places only the dominant closed-loop poles. The full-state feedback allows to place all the closed-poles of the system, if the linearized system is fully controllable and state observable. However, placing the poles of the system far away from the imaginary axis may result in saturation of the actuation due to high gain coefficients. Therefore, the location of the poles should be decided according to system requirements.

The state space representation of the gimbal system is expressed in the MATHEMATICAL MODELLING Chapter given by (2.90)-(2.93).

$$A = \begin{bmatrix} 0 & 1 & 0 & 0 \\ 0 & -0.0636 & 0 & 0.0022 \\ 0 & 0 & 0 & 1 \\ 0 & 0.0022 & 0 & -0.1745 \end{bmatrix} \tag{4.1}$$

$$B = \begin{bmatrix} 0 & 0 \\ 6.35 & -0.22 \\ 0 & 0 \\ -0.22 & 17.45 \end{bmatrix} \tag{4.2}$$

$$C = \begin{bmatrix} 1 & 0 & 0 & 0 \\ 0 & 1 & 0 & 0 \\ 0 & 0 & 1 & 0 \\ 0 & 0 & 0 & 1 \end{bmatrix} \tag{4.3}$$

$$D = \begin{bmatrix} 0 & 0 \\ 0 & 0 \\ 0 & 0 \\ 0 & 0 \end{bmatrix} \tag{4.4}$$

Controllability of the system should be checked before using the control method. The controllability matrix is given by

$$M = [B\ AB\ A^2B\ A^3B] \Rightarrow$$

$$M = \begin{bmatrix} 0 & 0 & 6.356 & -0.222 & -0.405 & 0.053 & 0.026 & -0.010 \\ 6.356 & -0.222 & -0.405 & 0.053 & 0.026 & -0.010 & -0.002 & 0.002 \\ 0 & 0 & -0.222 & 17.454 & 0.053 & -3.047 & -0.010 & 0.532 \\ -0.222 & 17.454 & 0.053 & -3.057 & -0.010 & 0.532 & 0.002 & -0.093 \end{bmatrix} \tag{4.5}$$

The rank of the controllability matrix is found as

$$rank(M) = 4 \tag{4.6}$$

Therefore, the linearized gimbal system is fully state controllable.

The characteristic equation of the gimbal system is

$$|sI - A| = s^4 + 0.238s^3 + 0.011s^2 \Rightarrow$$

$$|sI - A| = s^2(s^2 + 0.238s^1 + 0.011) \tag{4.7}$$

Therefore, coefficients of the characteristic equation are

$$\begin{aligned} a_1 &= 0.238 \\ a_2 &= 0.011 \\ a_3 &= 0 \\ a_4 &= 0 \end{aligned} \tag{4.8}$$

It is observed that there are two free s terms in characteristic equation of the gimbal system; thus, the open loop system behaves as an integrator. Each free s terms correspond to azimuth and elevation control axis. That is because of the angular velocity states of the linearized gimbal system is independent of position variables.

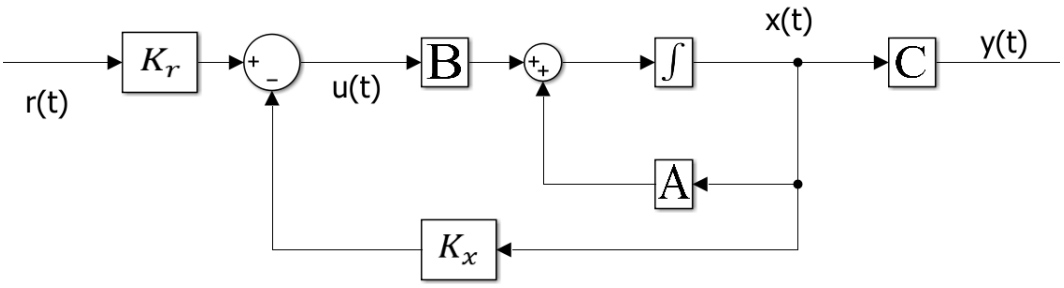

Figure 24: Structure of the control system for full-state feedback control method

The gimbal system needs to be stabilized against disturbances and track the reference signal. Thus, the control structure of the system is designed as shown in Figure 24. The reason for the selected control structure is that the system has free s terms; therefore, it behaves as an integrator for the position open loop. If the plant has no integrator, it was needed to convert reference signal path as closed loop by subtracting system output from reference input and inserting an integrator in the reference signal.

All states of the gimbal can be measurable, so they are available to use in K_x state feedback gain matrix. Besides, the reference input is to be followed via K_r reference feedforward gain matrix. Thus, the control signal applied to the gimbal system is chosen to be

$$u(t) = -K_x x(t) + K_r r(t) \tag{4.9}$$

where $x(t) \in \mathbb{R}^{4x1}$ is state vector, $r(t) \in \mathbb{R}^{4x1}$ is reference input vector, $K_x \in \mathbb{R}^{2x4}$ state feedback gain matrix, $K_r \in \mathbb{R}^{2x4}$ reference feedforward gain matrix.

In order for the position closed loop system to have 0.5 seconds settling time, dominant closed loop poles should be as follows.

$$t_s = \frac{4}{Re(s)} = 0.5 \Rightarrow Re(s) = 8 \tag{4.10}$$

(4.10) indicates that real part of the closed loop poles should be 8, and it is selected as 10 with safety factor. Imaginary part of the poles is selected as 0 considering the unit damping ratio $\zeta = 1$ so that the system has no oscillatory response. Therefore, two desired closed loop poles decided as following.

$$p_{1,2} = 10 \tag{4.11}$$

Two other poles belong to velocity loop of the control system, they should be far away from the dominant poles $\alpha_{1,2}$. They are selected as follows.

$$p_{3,4} = 40 \tag{4.12}$$

Dominant closed loops also describe bandwidth for $-3\ dB$ criteria of the closed loop of the control system,

$$\frac{\alpha_{1,2}}{2\pi} = 1.59\ Hz \tag{4.13}$$

Characteristic equation of the desired closed loop can be computed as follows.

$$(s - p_1)(s - p_2)(s - p_3)(s - p_4) = s^4 - 100s^3 + 3300s^2 - 40000s + 160000$$

Coefficients of the desired closed loop is, then,

$$\begin{gathered} \alpha_1 = -100 \\ \alpha_2 = 3300 \\ \alpha_3 = -40000 \\ \alpha_4 = 160000 \end{gathered} \tag{4.14}$$

According to [31], the state feedback gain matrix can be calculated as,

$$K_x = [\alpha_4 - a_4 \; \alpha_3 - a_3 \; \alpha_2 - a_2 \; \alpha_1 - a_1](MW)^{-1}$$

where M is controllability matrix computed in (4.5), and W is given by

$$W = \begin{bmatrix} a_3 & a_2 & a_1 & 1 \\ a_2 & a_1 & 1 & 0 \\ a_1 & 1 & 0 & 0 \\ 1 & 0 & 0 & 0 \end{bmatrix}$$

$$K_x = \begin{bmatrix} 62.96 & 7.86 & 0.80 & 0.10 \\ 0.80 & 0.1 & 22.93 & 2.86 \end{bmatrix} \tag{4.15}$$

Full-state feedback controller method manipulates the open loop control system, forms system matrix A_{cl} and the closed loop control system as followings.

$$A_{cl} = A - BK_x \tag{4.16}$$

$$G_{cl}(s) = C(sI - A_{cl})^{-1}B + D \Rightarrow$$

$$G_{cl}(s) = C(sI - A + BK_x)^{-1}B \tag{4.17}$$

Step responses of θ_1 and θ_2 for the unit step input to T_{01a}, T_{12a}, respectively, is shown in Figure 25 and Figure 26. As observed, K_r should be designed such that steady state value of the step responses converge to unit amplitude.

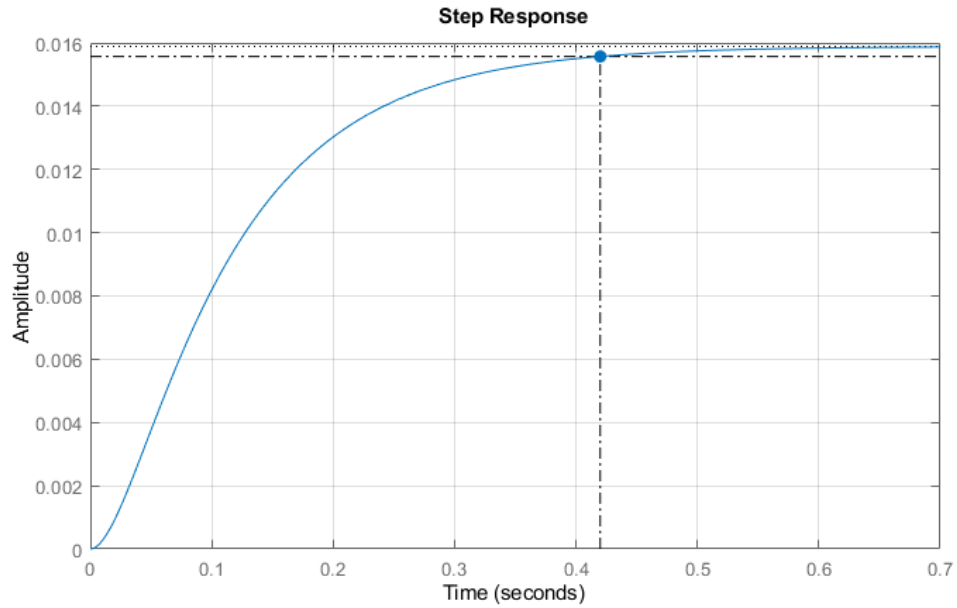

Figure 25: Step response of θ_1 without K_r adaptation

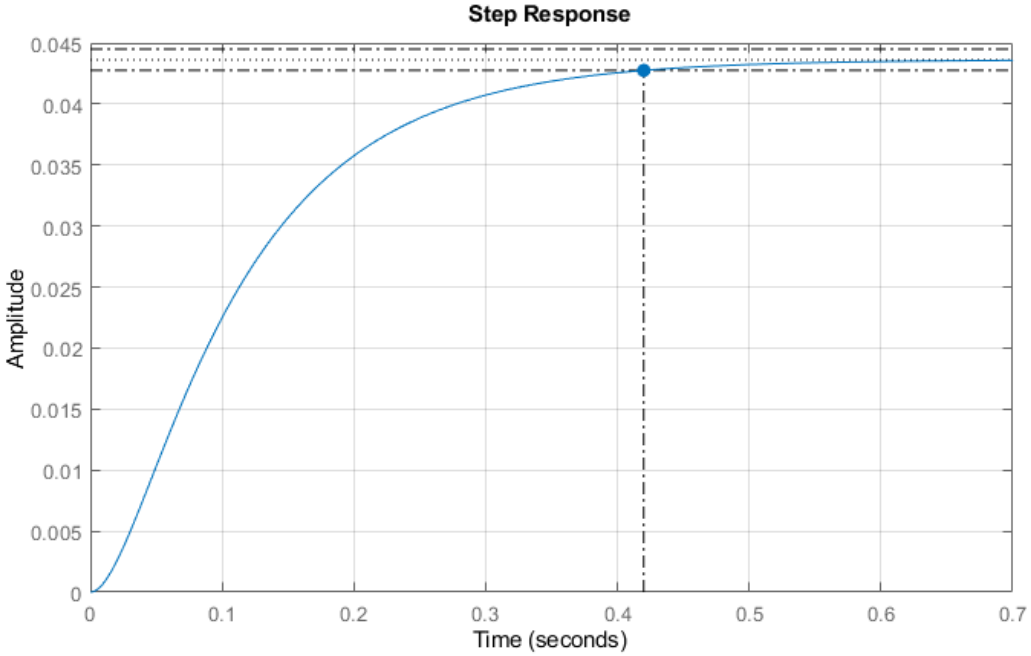

Figure 26: Step response of θ_2 without K_r adaptation

Reference feedforward gain matrix K_r should be equal to DC gain of the closed loop control system; therefore, the system can track the reference input with zero steady state error. K_r is calculated by the following relation.

$$G_{cl}(s) = \frac{Y}{RK_r} = C(sI - A + BK_x)^{-1}B \tag{4.18}$$

$$G(0) = -C(A - BK)^{-1}B \Rightarrow$$

$$K_r = G(0)^{-1} = -(C(A - BK)^{-1}B)^{-1} \tag{4.19}$$

Note that, pseudo inverse method should be used while calculating (4.19); since K_r is not square matrix. K_r is calculated as,

$$K_r = \begin{bmatrix} 62.96 & 0 & 0.80 & 0 \\ 0.80 & 0 & 22.93 & 0 \end{bmatrix} \tag{4.20}$$

Similarity of the K_x and K_r is predicted for the systems with free integrator. Reference gain matrix has the same coefficient that corresponds to position variable gain with the state feedback gain matrix.

Step responses with designed K_r gain is shown in Figure 26 and Figure 27.

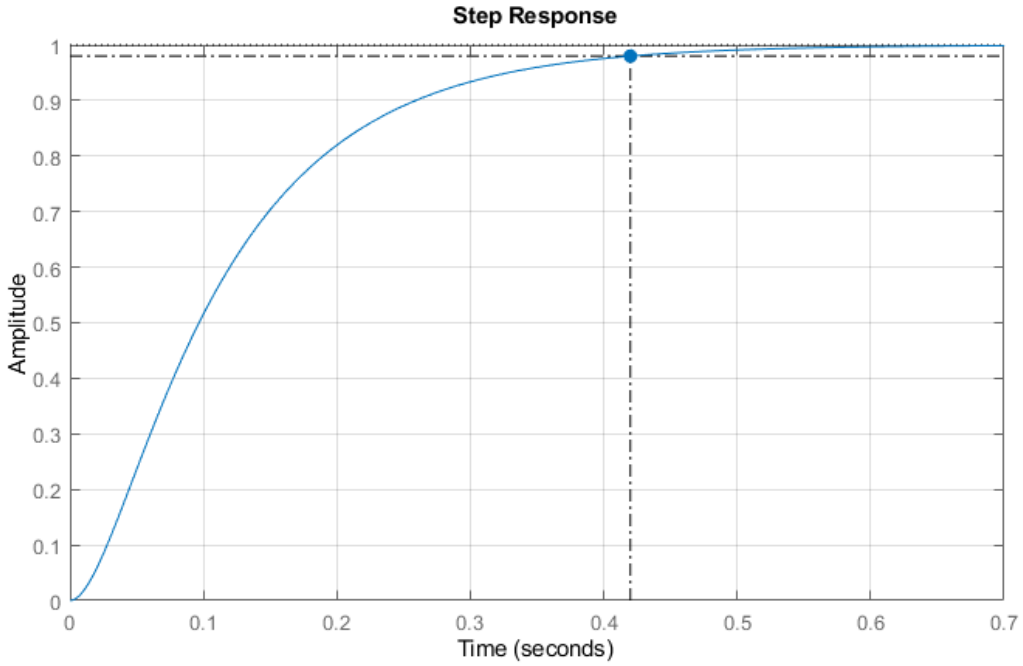

Figure 27: Step response of θ_1 with K_r adaptation

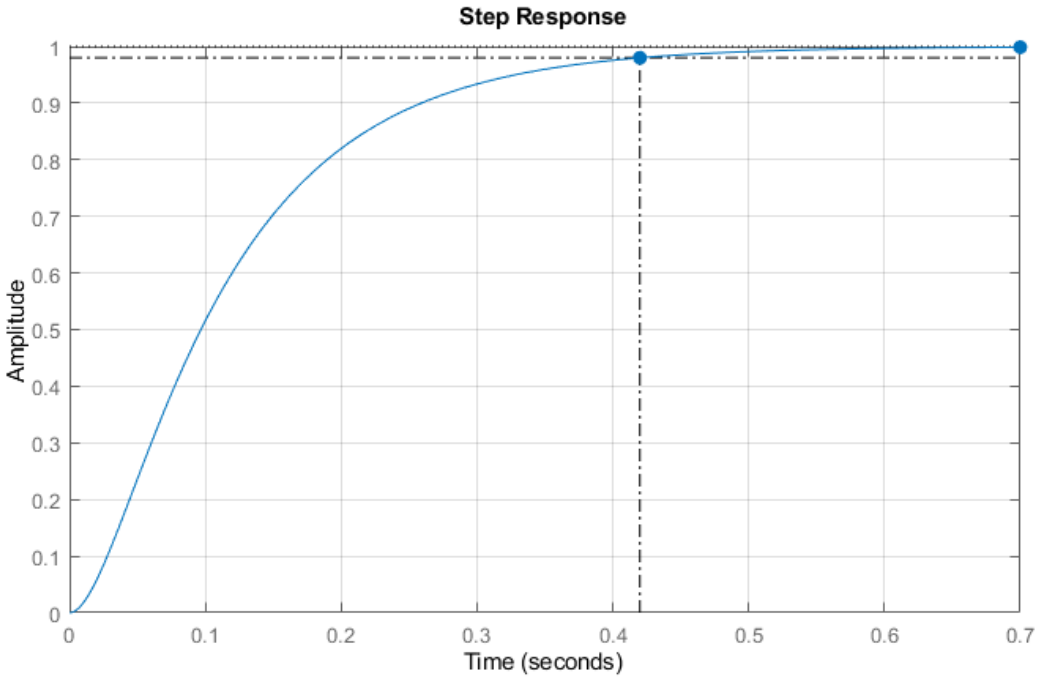

Figure 28: Step response of θ_2 with K_r adaptation

4.2 Model Reference Adaptive Control

Model reference adaptive control (MRAC) is an adaptive control method developed in the 1950s. The purpose of the MRAC is to adapt the control structure of the system so that the plant to be controlled behaves as the designed reference model. The MRAC adaptation law is driven by an error between the reference model output and the plant output. The method uses two control inputs; one of which is adaptive control input calculated by adaptation law; the latter is nominal control input of any kind. It combines those control inputs. MRAC structure can be divided into two parts. One of them is reference model that is design object and captures an ideal closed loop system performance. The real (nominal) system, however, does not behave like reference model only by using nominal controller in the presence of system uncertainties and disturbances. The other part, adaptive part (adjustment mechanism), applies a control signal to overcome those uncertainties and disturbances. The adaptive part calculates time-varying and nonlinear control input with changing parameters to nominal system. The adaptive part also composes two parts: the weight update law and the uncertainty parametrization which defines the uncertainties and disturbances as a multiplication of weights and basis functions. The weight update law forms the update law, relation, for the weights of the basis functions of the uncertainty parametrization. There are different techniques to define variables of the uncertainty parametrization. They can be defined as known state variables which is the most general method, or another frequently used neural network method. Radial basis functions are the most common neural network method used to define variable functions. Also, there are various methods for update law. Most commons are Lyapunov stability property and M.I.T. rules [32][33][34].

The structure of the MRAC method is shown in Figure 29.

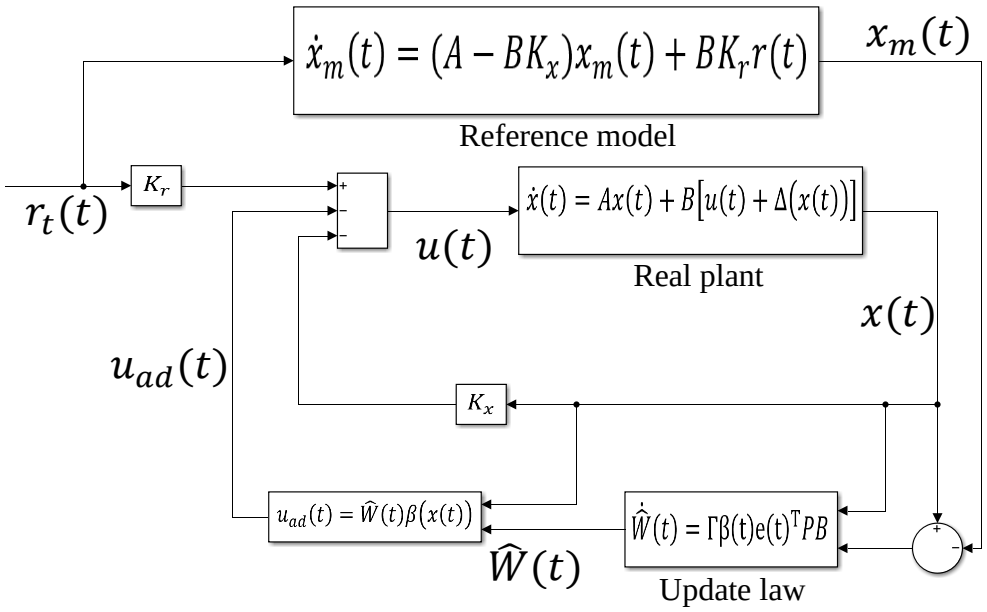

Figure 29: Structure of the control system for MRAC method

Nonlinear uncertain dynamical system can be represented with the following.

$$\dot{x}(t) = Ax(t) + B\big[u(t) + \Delta\big(x(t)\big)\big] \tag{4.21}$$

where $x(t) \in \mathbb{R}^n$ and $u(t) \in \mathbb{R}^m$ are state vector and input vector respectively, $A \in \mathbb{R}^{nxn}$ is state matrix, $B \in \mathbb{R}^{nxm}$ is input matrix, $\Delta: \mathbb{R}^n \rightarrow \mathbb{R}^m$ is system uncertainty and disturbance. The form of the uncertainty and disturbance of the system assumed as follows.

$$\Delta\big(x(t)\big) = W\beta\big(x(t)\big) \tag{4.22}$$

where $W \in \mathbb{R}^{mxn}$ is an ideal constant weighting matrix and $\beta \in \mathbb{R}^n$ is a basis function symbolizes the parametrization of the uncertainty and disturbances and is done as functions of the state of the system in this study.

$$\beta\big(x(t)\big) = x(t) = \begin{bmatrix} \theta_1 \\ \dot{\theta}_1 \\ \theta_2 \\ \dot{\theta}_2 \end{bmatrix} \tag{4.23}$$

The control input $u(t)$ is combined by adaptive control and nominal control inputs as following.

$$u(t) = u_n(t) - u_{ad}(t) \tag{4.24}$$

where nominal control law $u_n(t)$ is given by

$$u_n(t) = -K_x x(t) + K_r r(t) \tag{4.25}$$

where $K_x \in \mathbb{R}^{mxn}$ is state feedback gain, $K_r \in \mathbb{R}^{mxn}$ is reference feedforward gain, and $r(t) \in \mathbb{R}^n$ is reference input. Full-state feedback controller is used as a nominal controller as stated above. State equation of the nominal model becomes the following form with applied control input.

$$\dot{x}(t) = Ax(t) + B\left(-K_x x(t) + K_r r(t) - u_{ad}(t) + \Delta\big(x(t)\big)\right) \Rightarrow \tag{4.26}$$

$$\dot{x}(t) = (A - BK_x)x(t) + BK_r r(t) + B\left(-u_{ad}(t) + \Delta\big(x(t)\big)\right) \tag{4.27}$$

The reference model of MRAC structure can be represented as follows.

$$\dot{x}_m(t) = A_m x_m(t) + B_m r(t) \tag{4.28}$$

The reference model has the same dimensions with nominal model; where $x_m(t) \in \mathbb{R}^n$ is reference state vector, $A_m \in \mathbb{R}^{nxn}$, $B_m \in \mathbb{R}^{nxm}$.

The purpose of the MRAC control method is to equate nominal and reference model responses. Therefore, the full-state feedback controller can be designed such that closed loop response of the nominal controller results in the reference model response in the absence of uncertainties and disturbances. Those are to be compensated with adaptive control input. Thus, nominal controller gains are designed to satisfy the following.

$$A_m = A - BK_x \tag{4.29}$$

$$B_m = BK_r \tag{4.30}$$

Reference model can be expressed as,

$$\dot{x}_m(t) = (A - BK_x)x_m(t) + BK_r r(t) \tag{4.31}$$

Adaptive control input should have same form with the assumed uncertainty and disturbance of the system to cancel those out. Therefore, the structure of (4.22) represents adaptive control input as well. However, the ideal constant weightings W is not known by the controller; therefore, an estimate of weightings is used in the adaptive control input $u_{ad}(t)$ as following.

$$u_{ad}(t) = \widehat{W}(t)\beta\big(x(t)\big)^T \tag{4.32}$$

where $\widehat{W}(t)$ is an estimate of W with the same dimension satisfying the update law. It is updated, recalculated in every time step by adaptive controller. The update law for the MRAC is given as:

$$\dot{\widehat{W}}(t) = \Gamma\beta(t)e(t)^T PB \tag{4.33}$$

where $\Gamma \in \mathbb{R}^{nxn}$ is a positive-definite learning rate matrix and it increases the sensitivity of the update law to error between referenced and nominal systems, $P \in \mathbb{R}^{nxn}$ is positive-definite solution of the Lyapunov equation which is

$$A_m^T P + PA_m + R = 0 \tag{4.34}$$

where $R \in \mathbb{R}^{nxn}$ is a positive-definite design selection matrix. Any positive-definite matrix can be selected to manipulate MRAC update law. The error function can be stated as,

$$e(t) = x(t) - x_m(t) \tag{4.35}$$

where $e(t) \in \mathbb{R}^n$. As stated, the aim of the MRAC method is that the error signal converges to zero; following relation express the statement mathematically. The MRAC method is said to be successful if the zero-error condition satisfies. On the contrary, increasing error signal drives adaptation mechanism to change weightings faster.

$$\lim_{t\to\infty} e(t) = 0 \tag{4.36}$$

Another critical point for the MRAC method, as in all control problems, is that stability condition of generated control input. The Lyapunov stability analysis handles the stability condition; however, it is out of scope of this study.

Full-state feedback controller designed in the first section is to be used as nominal controller of the reference model of MRAC structure. Besides, nominal model is the real physical system. Thus, MRAC controller takes an action for parameter uncertainties and flexibility of the mechanical structure which are uncertainties and disturbances of the MRAC method in this study.

Design parameters of the MRAC method are selected mostly experimentally. An identity matrix of $R \in \mathbb{R}^{4x4}$ is selected for solution of Lyapunov equation (4.34).

$$R = \begin{bmatrix} 1 & 0 & 0 & 0 \\ 0 & 1 & 0 & 0 \\ 0 & 0 & 1 & 0 \\ 0 & 0 & 0 & 1 \end{bmatrix} \tag{4.37}$$

Coefficients of the learning rate Γ is selected as greater as that stability of the system preserved. It is observed that a larger learning rate might result in excitation of the high frequency signals for the closed loop system and increase high frequency error. Therefore, it is selected as follows.

$$\Gamma = \begin{bmatrix} 5000 & 0 & 0 & 0 \\ 0 & 500 & 0 & 0 \\ 0 & 0 & 1000 & 0 \\ 0 & 0 & 0 & 200 \end{bmatrix} \tag{4.38}$$

4.3 Cascade PI Control

The PID control method is widely used in single-input single-output (SISO) systems in industry due to its simplicity and ability to provide satisfactory performance. The PID controller employs traditional control approaches, enabling control design directly on the system in the field. Tuning methods are used to achieve desired performance. However, as mentioned in the introduction chapter, tuning methods are

manual and can weaken the automation process. Therefore, this thesis focuses on an adaptive control method, the model reference adaptive control (MRAC) method. Nevertheless, in order to make a comparison, a cascaded PI control method was also developed and tested in this study as it is frequently used in industry.

The PID controller comprises three components: proportional (P), integral (I), and derivative (D) of the errors. The derivative term is typically avoided due to its tendency to amplify high-frequency noise. In multi-variable control systems, cascaded control loops are preferred due to their disturbance rejection capability. In this study, as shown in the figure, the PI control method was used to control the angular velocity variable in the inner control loop (rate loop) and the P control method was used to control the angular position variable in the outer control loop (position loop). The reason for using the PI control method in the inner loop is to eliminate disturbance effects on the system in the speed control loop before they appear in the position variable. The integral term (I) in the inner loop is used to eliminate steady-state error. The proportional term (P) is adjusted to provide system stability and meet transient requirements. Since the requirements for both the inner and outer gimbal control axes are the same, the control system was designed for each control axis using similar steps.

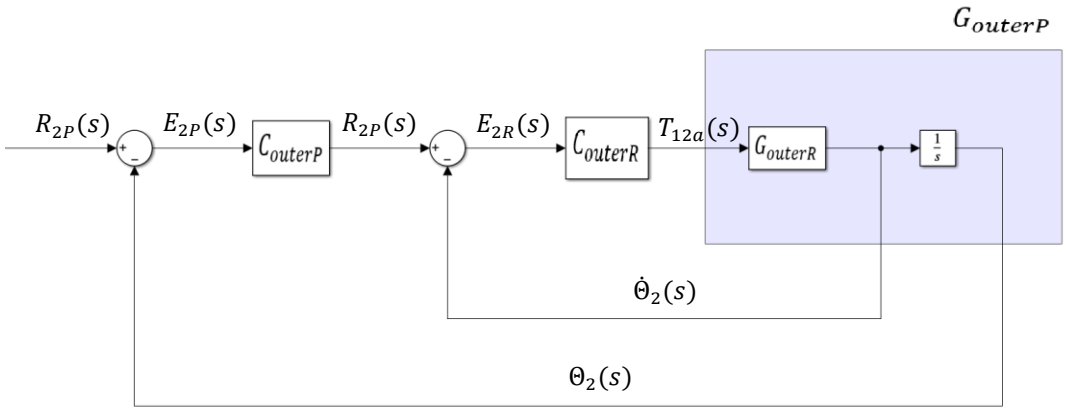

Figure 30: Block diagram of cascaded P and PI control system of the outer gimbal

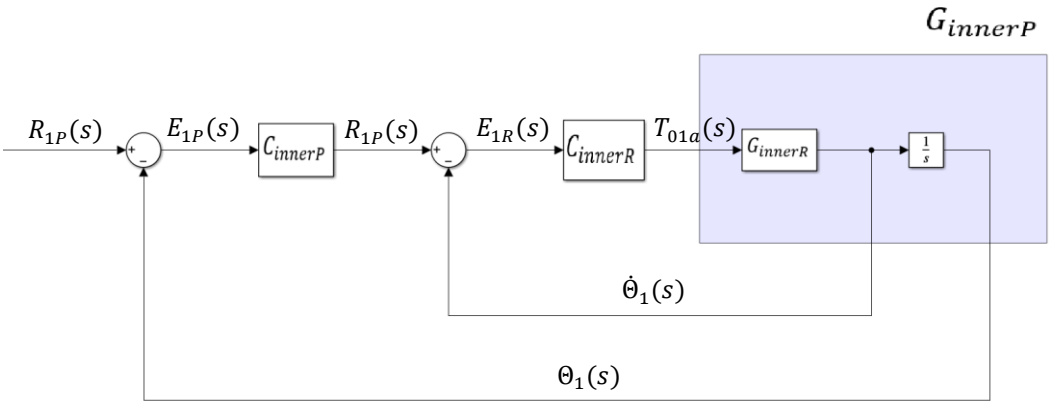

Figure 31: Block diagram of cascaded P and PI control system of the inner gimbal

In the block diagrams Figure 30 and Figure 31, transfer functions and signals denote as follows.

- C_{outerP} is position controller of the outer gimbal
- C_{outerR} is rate controller of the outer gimbal
- $R_{1P}(s)$ is reference position of the outer gimbal
- $R_{1R}(s)$ is reference velocity of the outer gimbal
- $E_{1P}(s)$ is position error of the outer gimbal
- $E_{1R}(s)$ is velocity error of the outer gimbal
- C_{innerP} is position controller of the inner gimbal
- C_{innerR} is rate controller of the inner gimbal
- $R_{2P}(s)$ is reference position of the inner gimbal
- $R_{2R}(s)$ is reference velocity of the inner gimbal
- $E_{2P}(s)$ is position error of the inner gimbal
- $E_{2R}(s)$ is velocity error of the inner gimbal

For both gimbal axis, the continuous transfer function of the P type position controller and the PI type velocity controller are in the form of,

$$C_P = K_P \tag{4.39}$$

$$C_R = K_P + \frac{K_i}{s} \tag{4.40}$$

where K_p and K_i represents the proportional and derivative term of the controller respectively. PI controller can also be expressed in the form of real zero as follows.

$$C_R = K_P \frac{(s+z)}{s} \tag{4.41}$$

where the zero $z = \frac{K_i}{K_p}$.

As seen in the PI controller expression, the controller adds an integrator which is the pole at the origin and a real zero at the point $-z = -\frac{K_i}{K_p}$ to the control system. If the zero of the PI controller is quite small and very close to the integrator, the controller does not change the shape of the root locus. Yet, the steady state error drastically improved because of the increase of the system type by one with the integrator. The zero of the PI controller was set as $z = 0.1$. The proportional gain K_p adjusted to meet the requirements of each gimbal control axis via root locus approach. After the rate loop was designed, the proportional gain of the position controller was adjusted according to the transient response requirements. In the following, the controller design procedure was carried out for both outer and inner gimbals.

The controller requirements are such that the dominant poles are on negative real axis and selected as -10 and -40 specified in (4.11) and (4.12), for position and rate control loops, respectively.

4.3.1 Outer gimbal velocity loop

The rate plant for the outer gimbal, G_{outerR}, has the transfer function given in the (2.74), and its poles are located at:

$$p = -\frac{c_{01d}}{J_{outer}} = -0.654 \tag{4.42}$$

The root locus of the G_{outerR} is shown in the Figure 32.

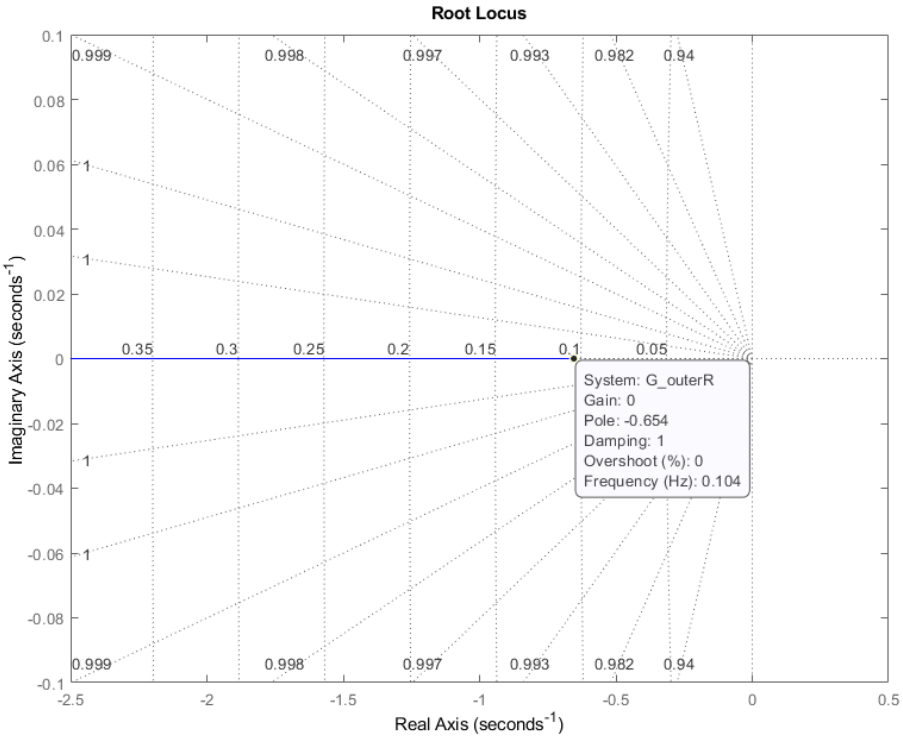

Figure 32: Root locus of the rate plant for the outer gimbal

As mentioned, addition of the zero and the integrator of the PI controller does not change the shape of the root locus while it provides zero steady state error. After applying PI controller, the root locus of the rate loop became as shown in the Figure 33 and Figure 34.

Zoomed region of the zero location of the PI controller shows that one of the closed loop poles is almost identical with to the zero; therefore, they cancelled each outer and the resultant shape of the root locus is same.

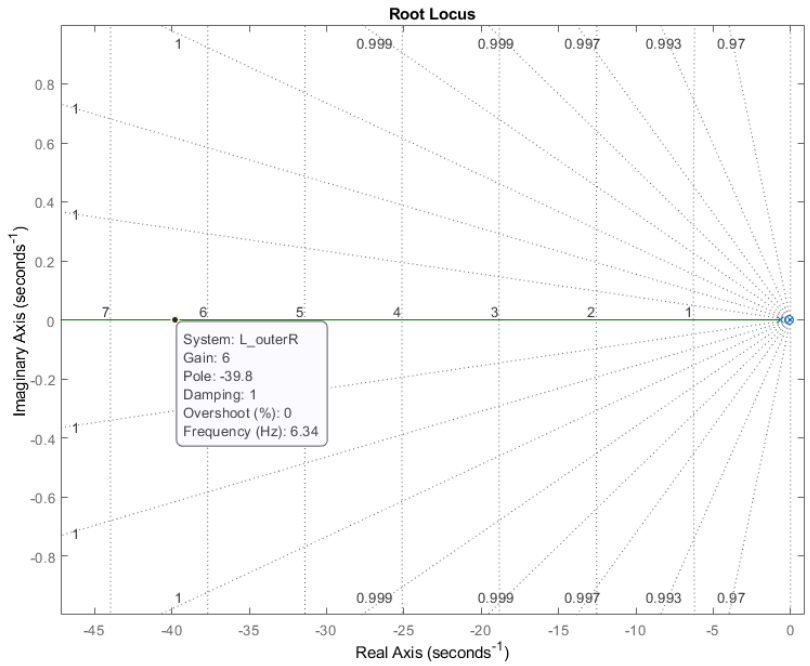

Figure 33: Root locus of the outer gimbal rate control loop with PI controller

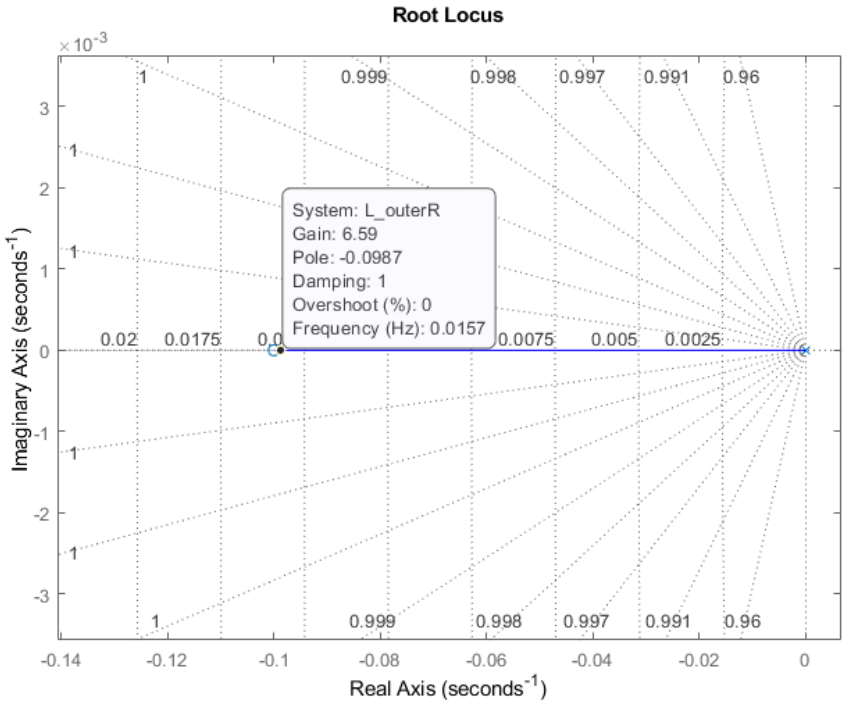

Figure 34: Root locus of the outer gimbal rate control loop with PI controller zoomed in

Adjusting proportional gain of the PI controller as $K_p = 6$ locates the pole of the rate loop at almost the desired location $p = -39.8 \approx -40$. Therefore, rate loop PI controller and the closed loop transfer function of the outer gimbal are as follows.

$$C_{outerR} = 6\frac{(s + 0.1)}{s} \tag{4.43}$$

$$G_{cl,outerR} = \frac{C_{outerR}G_{outerR}}{1 + C_{outerR}G_{outerR}} \Rightarrow \tag{4.44}$$

$$G_{cl,outerR} = \frac{6s + 0.6}{0.153s^2 + 6.1s^2 + 0.6} \tag{4.45}$$

The step response of the outer gimbal velocity loop can be observed in the Figure 35.

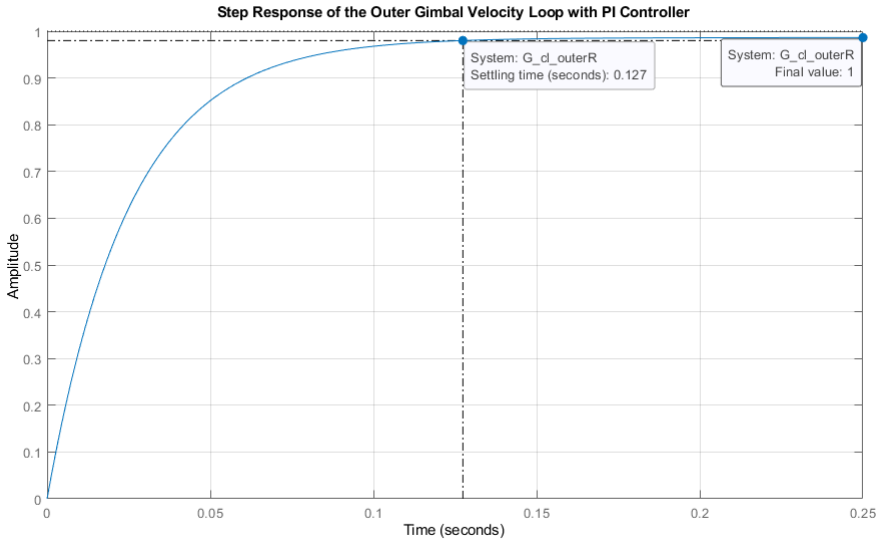

Figure 35: Step response of the outer gimbal rate loop with PI controller

After closed the rate loop, open loop transfer function between the position input and output, L_{outerP}, has the following transfer function and root locus shown in the Figure 36.

$$L_{outerP} = C_{outerP}G_{cl,outerR}\frac{1}{s} \tag{4.46}$$

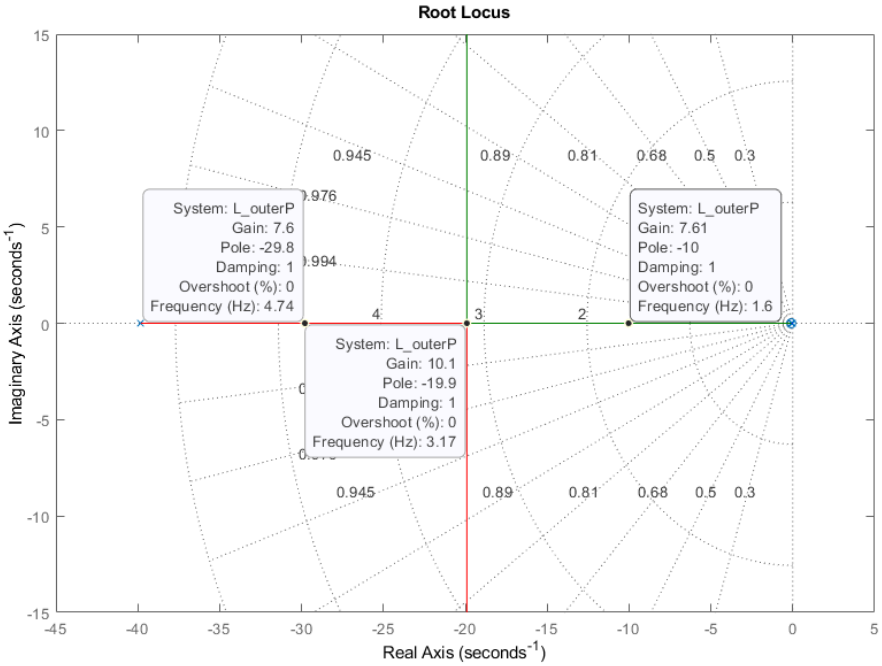

Figure 36: Root locus of the outer gimbal position control loop with P controller

As shown in the root locus, the closed loop response represents the oscillatory behavior for the gain higher than $K_P = 10.1$. Also, very zoomed region of the zero location of the PI controller shows that one of the closed loop poles is almost identical to the zero; therefore, they cancelled each outer. Setting the proportional gain of the position controller as $C_{outerP} = 7.6$ satisfies the requirements and the closed loop poles of the position loop and the transfer function are as follows.

$$p_1 = -10, \qquad p_2 = -29.8 \tag{4.47}$$

$$G_{cl,outerP} = \frac{45.6s + 4.56}{0.153s^3 + 6.1s^2 + 46.2s + 4.56} \tag{4.48}$$

The step response of the outer gimbal position loop can be observed in the Figure 37.

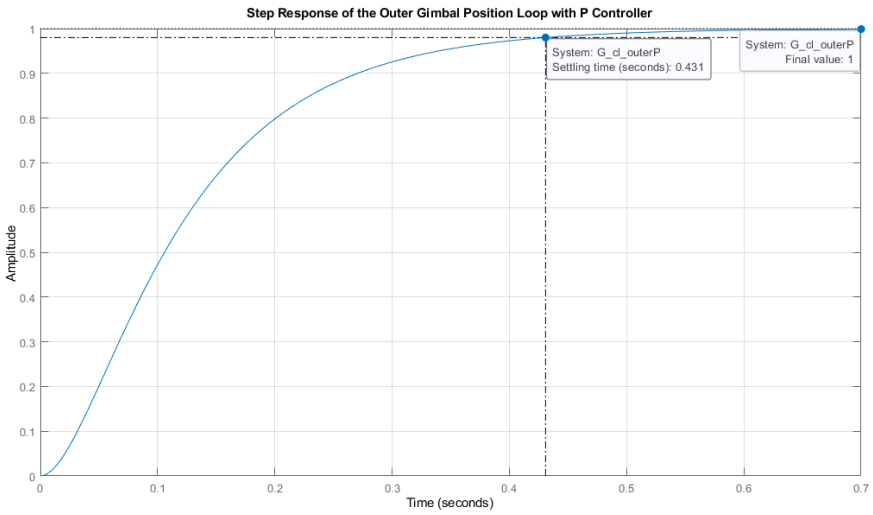

Figure 37: Step response of the outer gimbal position loop with P controller

4.3.2 Inner gimbal velocity loop

The rate plant for the inner gimbal, G_{innerR}, has the transfer function given in the (2.78), and poles located at:

$$p = -\frac{c_{12d}}{J_{inner}} = -1.745 \tag{4.49}$$

The root locus of the G_{innerR} is shown in the Figure 38.

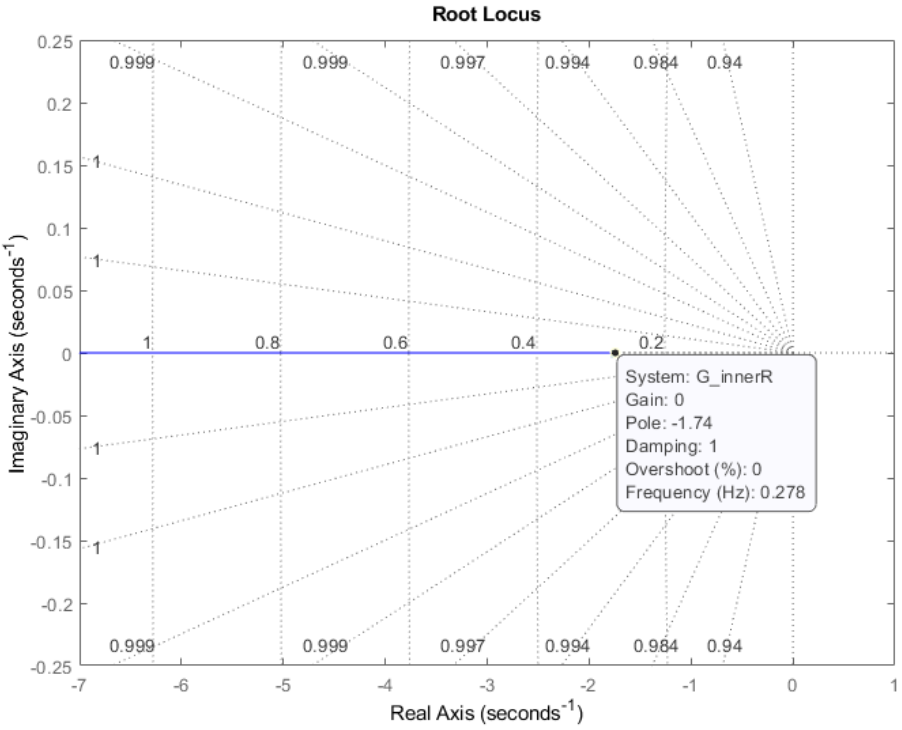

Figure 38: Root locus of the rate plant for the inner gimbal

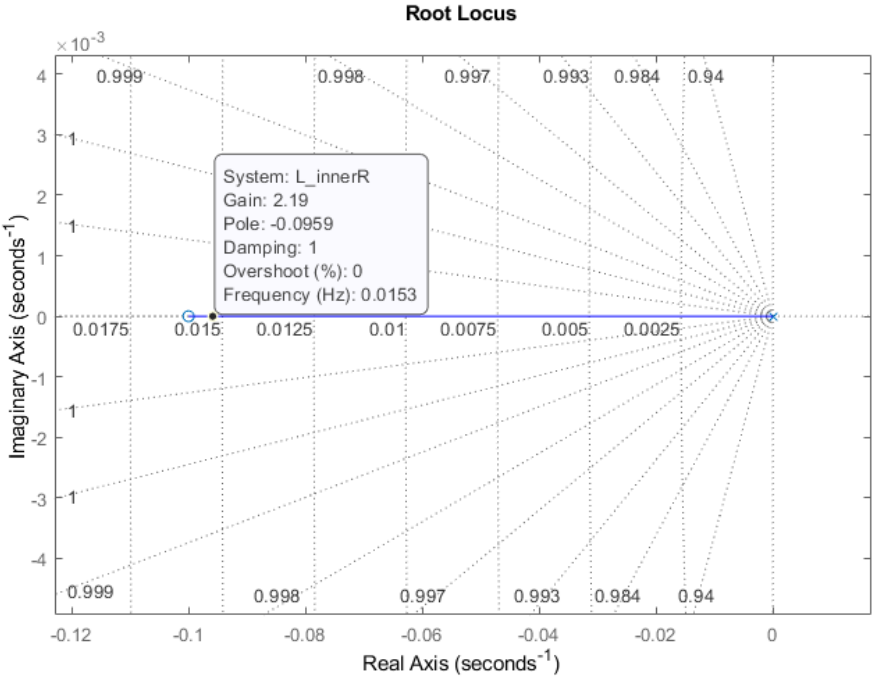

Figure 39: Root locus of the inner gimbal rate control loop with PI controller

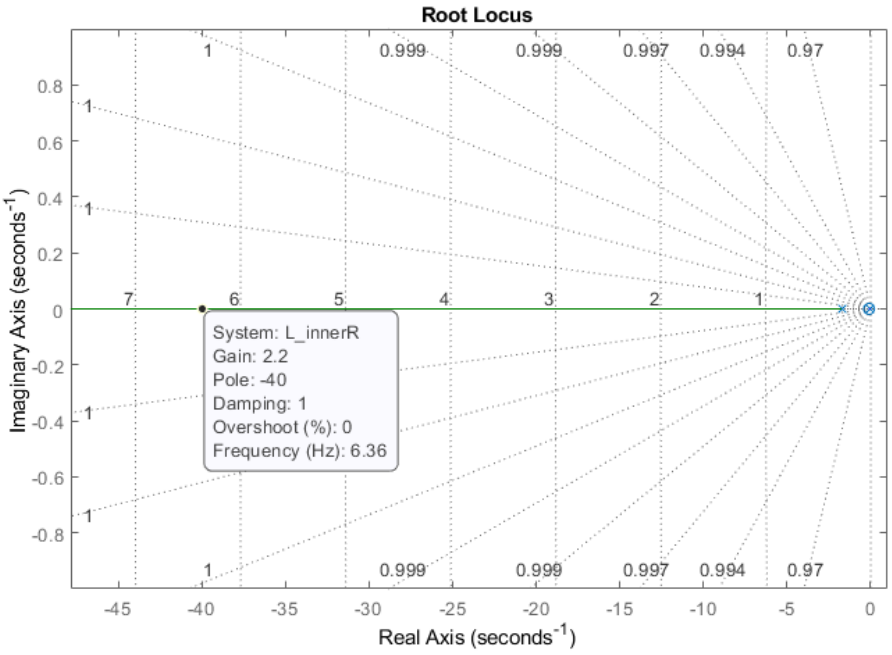

Figure 40: Root locus of the inner gimbal rate control loop with PI controller zoomed in

Zoomed region of the zero location of the PI controller shows that one of the closed loop poles is almost identical with to the zero; therefore, they cancelled each outer and the resultant shape of the root locus is same.

Adjusting proportional gain of the PI controller as $K_p = 2.2$ locates the pole of the rate loop at desired location $p = -40$. Therefore, rate loop PI controller and the closed loop transfer function of the outer gimbal are as follows.

$$C_{innerR} = 2.2\frac{(s+0.1)}{s} \tag{4.50}$$

$$G_{cl,innerR} = \frac{C_{innerR}G_{innerR}}{1 + C_{innerR}G_{innerR}} \Rightarrow \tag{4.51}$$

$$G_{cl,innerR} = \frac{s+0.1}{0.057s^2 + 1.1s^2 + 0.1} \tag{4.52}$$

The step response of the inner gimbal velocity loop can be observed in the Figure 41.

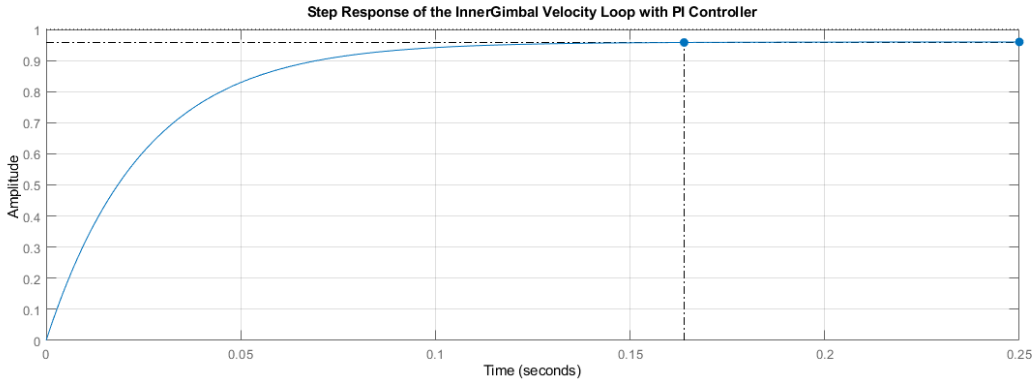

Figure 41: Step response of the inner gimbal rate loop with PI controller

After closed the rate loop, open loop transfer function between the position input and output, L_{innerP}, has the following transfer function and root locus shown in the Figure 42.

$$L_{innerP} = C_{innerP} G_{cl,innerR} \frac{1}{s} \tag{4.53}$$

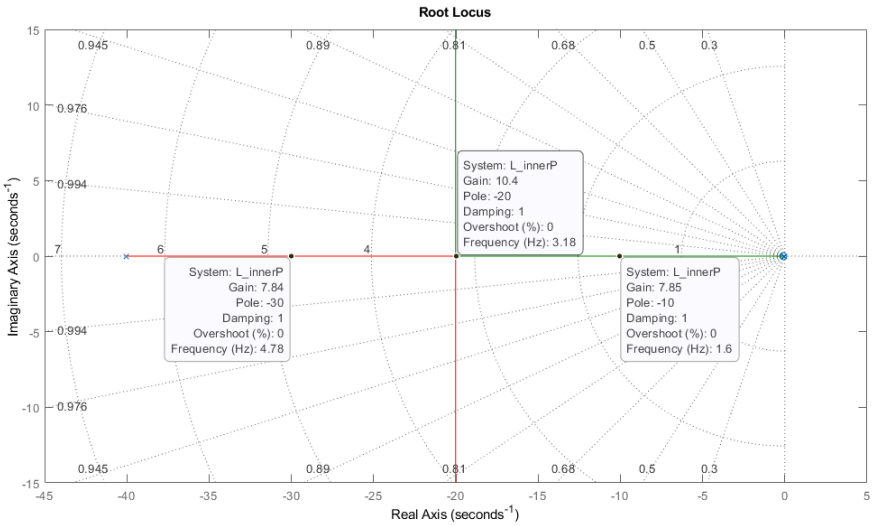

Figure 42: Root locus of the inner gimbal position control loop with P controller

As shown in the root locus, the closed loop response represents the oscillatory behavior for the gain higher than $K_P = 10.4$. Also, very zoomed region of the zero location of the PI controller shows that one of the closed loop poles is almost identical to the zero; therefore, they cancelled each outer. Setting the proportional

gain of the position controller as $C_{innerP} = 7.85$ satisfies the requirements and the closed loop poles of the position loop and the transfer function are as follows.

$$p_1 = -10, \qquad p_2 = -30 \tag{4.54}$$

$$G_{cl,outerP} = \frac{17.27s + 1.727}{0.057s^3 + 2.3s^2 + 17.49s + 1.727} \tag{4.55}$$

The step response of the outer gimbal position loop can be observed in the Figure 43.

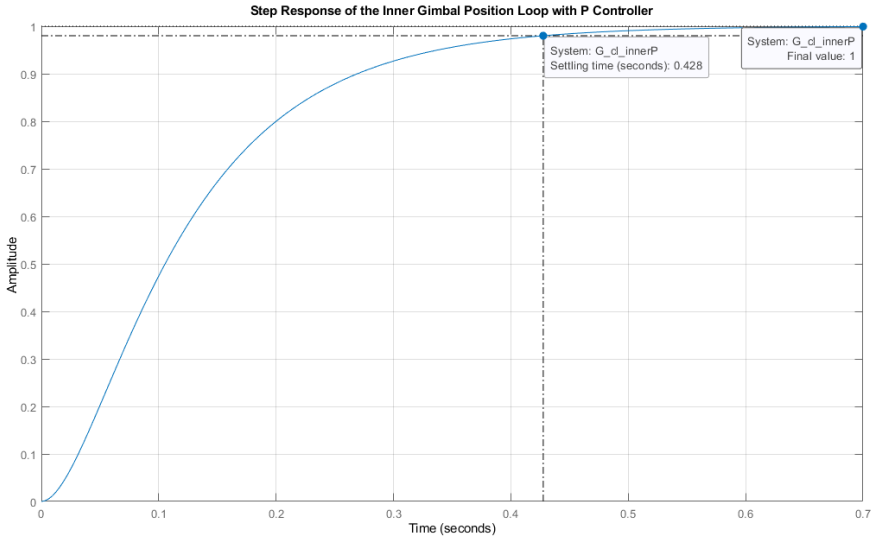

Figure 43: Step response of the inner gimbal position loop with P controller

CHAPTER 5

EXPERIMENTS AND RESULTS

In this chapter, the control methods designed in the CONTROL DESIGN were verified and evaluated with tests performed on the real system. Two types of tests were carried out. These were for reference tracking and disturbance rejection purposes. In the tracking test, the performance of the gimbal system to direct to the desired position angles was tested, while in the disturbance test, the maintaining the orientation of the gimbal system against the disturbance effects caused by the movement of the platform on which the gimbal system was mounted was tested. Apart from the tests performed directly on the physical gimbal system, the same test was also carried out on both the 3D coupled nonlinear and linear gimbal models, and the validity of the model was observed. In the tracking tests, a chirp signal as a position reference input shown in Figure 44 and step responses were applied. Besides, periodical platform position movement tests were carried out according to the requirement mentioned in the section 1.2 and the movement were shown in the Figure 91.

5.1 Reference Tracking

The reference input signals shown in Figure 44, were designed to excite frequencies from $0.1\ Hz$ to $5\ Hz$; however, they exceed the desired range as a property of the chirp signal. In addition, the response occurs at frequencies other than the applied input signal in nonlinear systems. Therefore, even if the tracking signal is as shown, the spectrum of the system's response will be such that it includes the natural frequency of the gimbal system.

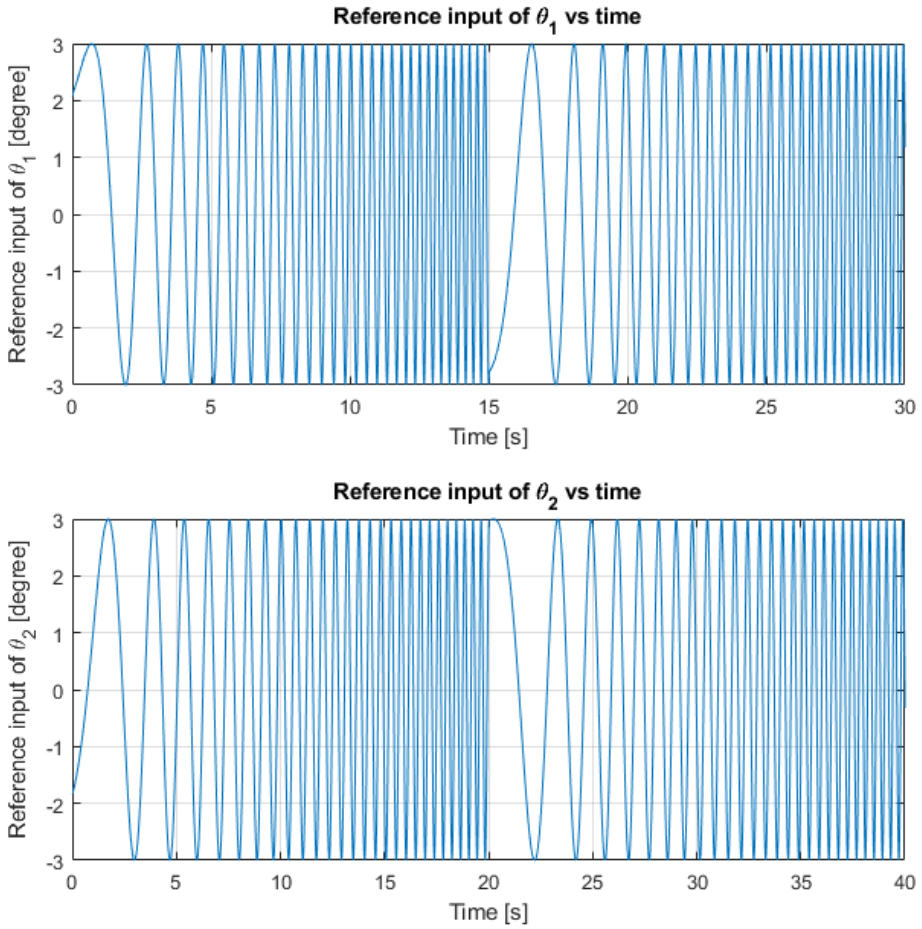

Figure 44: Swept sine type reference input for gimbal angular positions

First, tracking experiments were carried out on the linear and nonlinear coupled gimbal models to represent validity of the linearization. Then, for the developed full-state feedback control system, the chirp reference input and step input were applied. The gimbal position variables obtained as a result of the experiment were recorded, and these experimental data were compared with the simulation results. Likewise, the same reference input and step inputs were applied to the control system developed by MRAC method. As stated in the controller design chapter, in this study, the reference model in the MRAC method is considered as the control system developed by full-state feedback method. Therefore, in the tests performed for the MRAC system, the control system before the adaptation process is the same as the

full-state feedback control system. Accordingly, response to swept sine reference input and step response were obtained for the MRAC method. In addition, the change of the estimated constant weight matrix in accordance with the MRAC update law is presented in Figure 60 and Figure 61. The error signal before and after the MRAC adaptation process is given by Figure 66 and Figure 67 to verify the achievement of the MRAC method. As stated in the first chapter, the motivation of this study was to increase the performance of the gimbal control axes by converging the reference model of the gimbal system determined in the MRAC method. For this reason, frequency response functions are presented in Figure 86-Figure 89. Apart from those two control methods, the cascade PI control system were tested for the same inputs to compare the performance of the gimbal control system using the decoupled gimbal approach.

Both FSFC and MRAC control systems were tested in the tracking experiment of the nonlinear gimbal model. However, only the FSFC control system was used in the tracking experiments of the linear gimbal model. Because the MRAC method uses the FSFC control system in its structure as a reference model, it does not produce a different result. The MRAC method resulted in a slightly different response on the nonlinear gimbal model due to nonlinearity differences. As observed in the figures from Figure 45 to Figure 48, all the responses were pretty close to each other and differed only by about %1 from each other. Although the responses were almost identical; the MRAC control system converged the response of the FSFC control system applied on the nonlinear model to the FSFC control system applied on the linear model, which is the primary objective of the MRAC method. Besides, the step responses were very close to each other, as shown in the figures Figure 49 Figure 50. Therefore, it can be said that the control systems have the same performance on both the linear and nonlinear gimbal models.

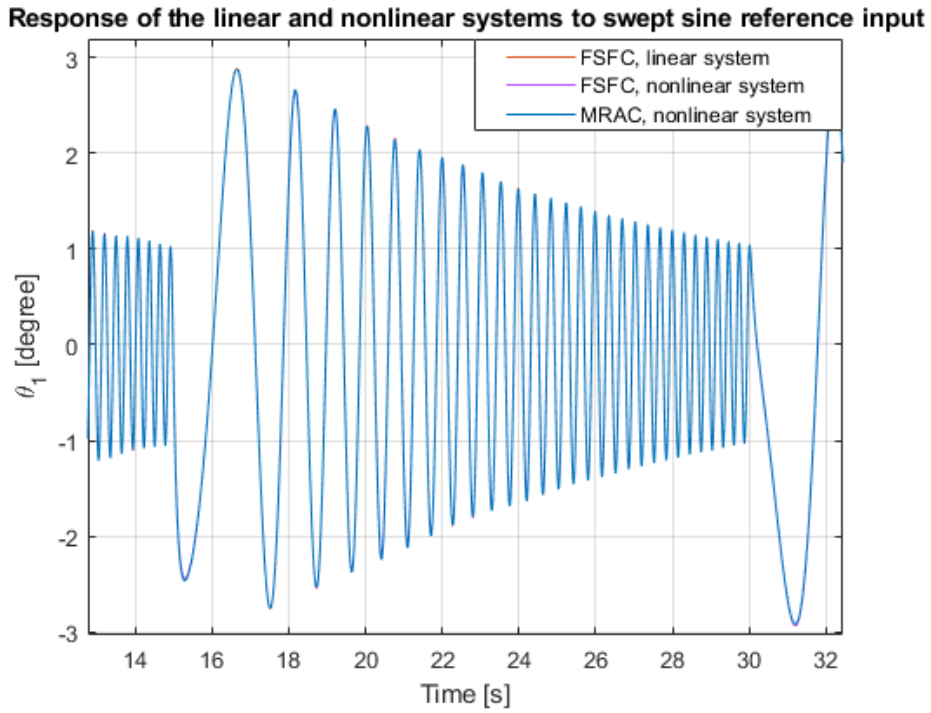

Figure 45: Response θ_1 of the linear and nonlinear coupled gimbal model with FSFC and MRAC controller to swept sine reference input

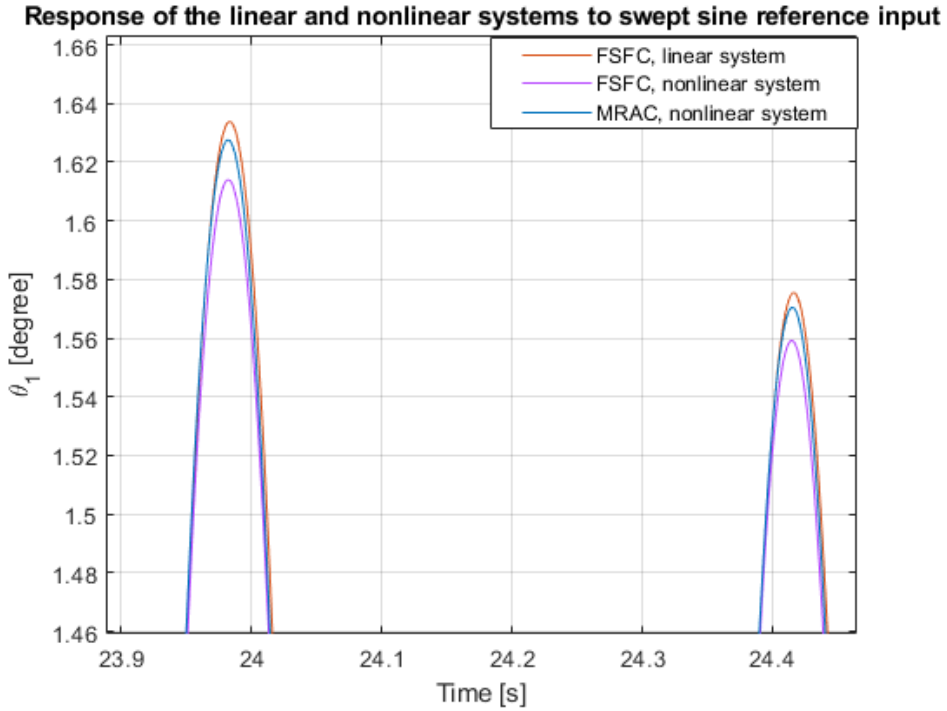

Figure 46: Response θ_1 of the linear and nonlinear coupled gimbal model with FSFC and MRAC controller to swept sine reference input zoomed in

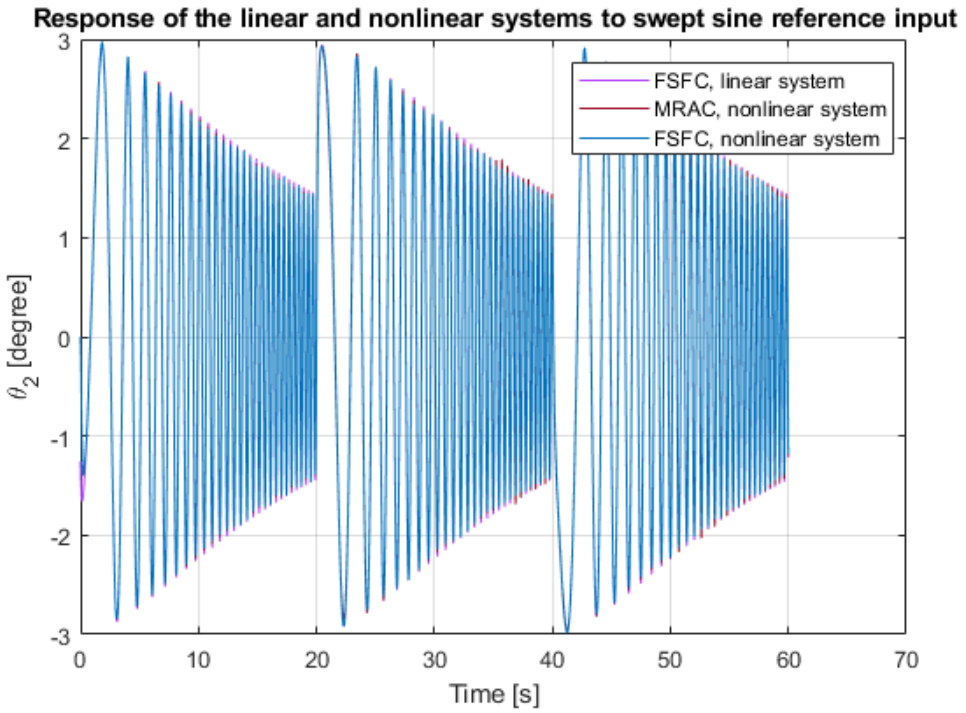

Figure 47: Response θ_2 of the linear and nonlinear coupled gimbal model with FSFC and MRAC controller to swept sine reference input

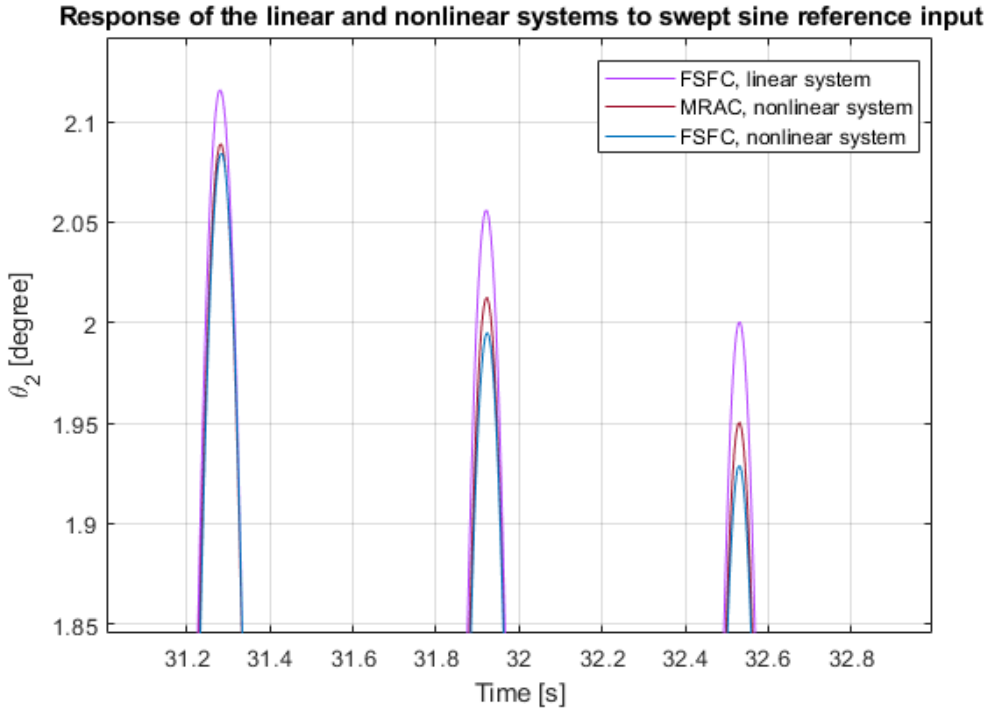

Figure 48: Response θ_2 of the linear and nonlinear coupled gimbal model with FSFC and MRAC controller to swept sine reference input zoomed in

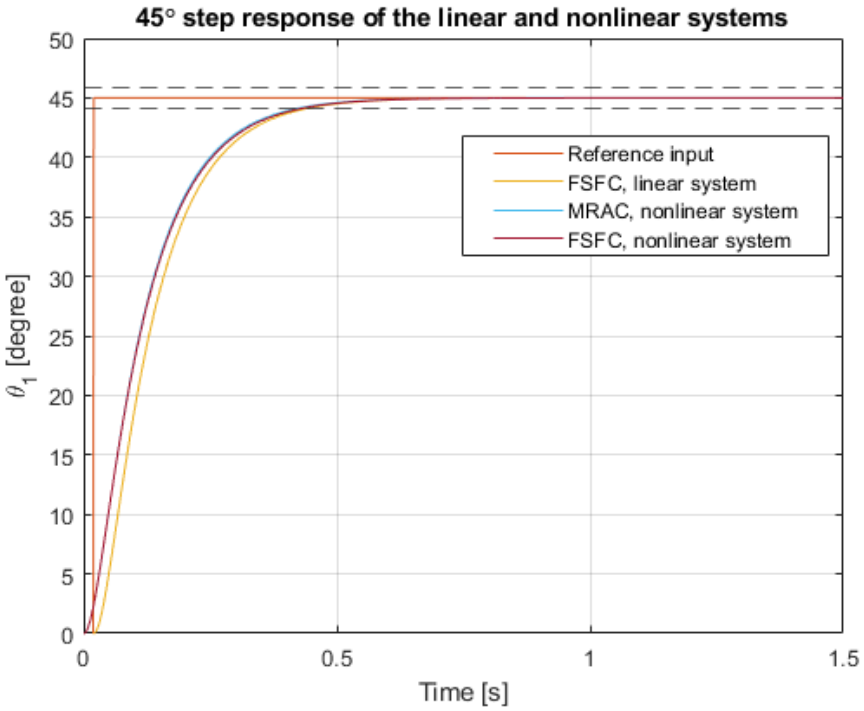

Figure 49: 45° step response θ_1 of the linear and nonlinear coupled gimbal model with FSFC and MRAC controller

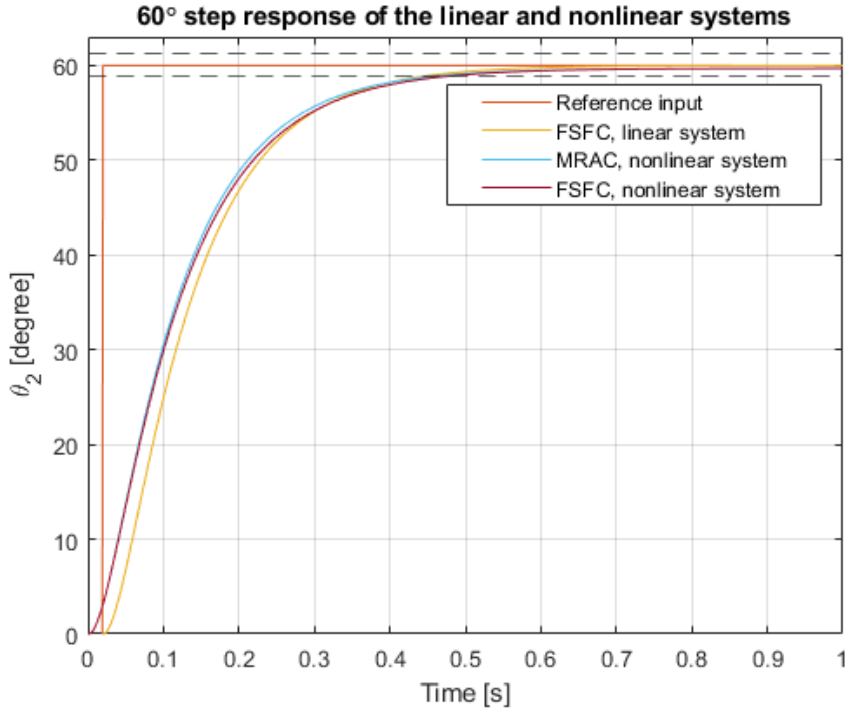

Figure 50: 60° step response θ_1 of the linear and nonlinear coupled gimbal model with FSFC and MRAC controller

As a result of the tests performed on the control system developed with the FSFC method, the response of the reference tracking signal applied to the azimuth control axis is seen in Figure 51 and Figure 52. Likewise, the response of the reference tracking signal for the elevation control axis is shown in Figure 53 and Figure 54. As observed in the azimuth control axis, the actual system response is quite close to the simulation response but lower in value. When the elevation control axis is examined, it is observed that there is a large difference between the systems. It was seen that the real system generates a higher response than it should in low frequency regions, and it has a very low response as the frequency increases.

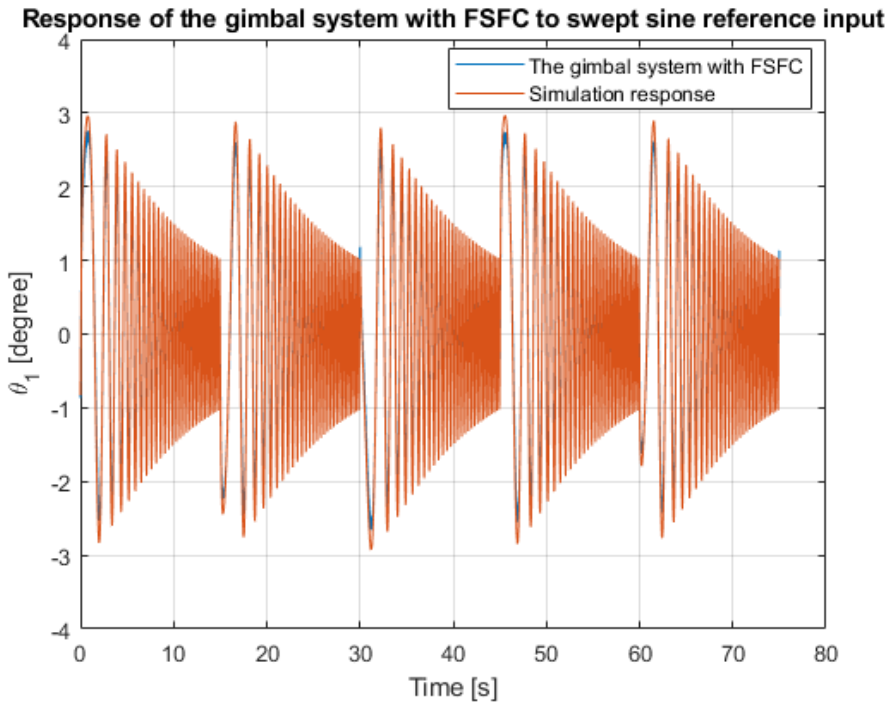

Figure 51: Response of θ_1 of the gimbal system with full-state feedback control to swept sine reference input

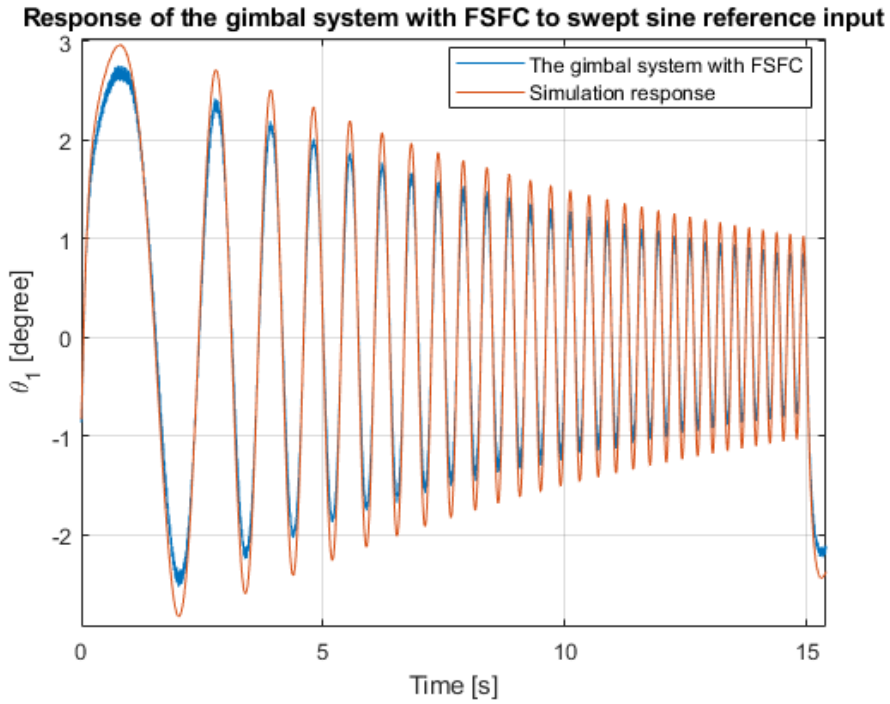

Figure 52: Response of θ_1 the gimbal system with full-state feedback control to swept sine reference input zoomed in

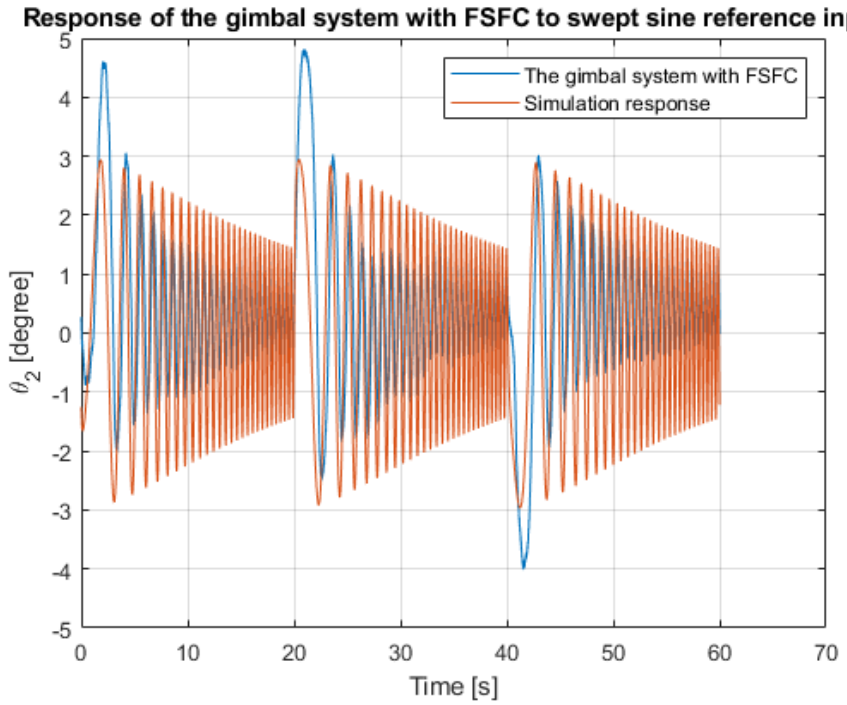

Figure 53: Response of θ_2 of the gimbal system with full-state feedback control to swept sine reference input

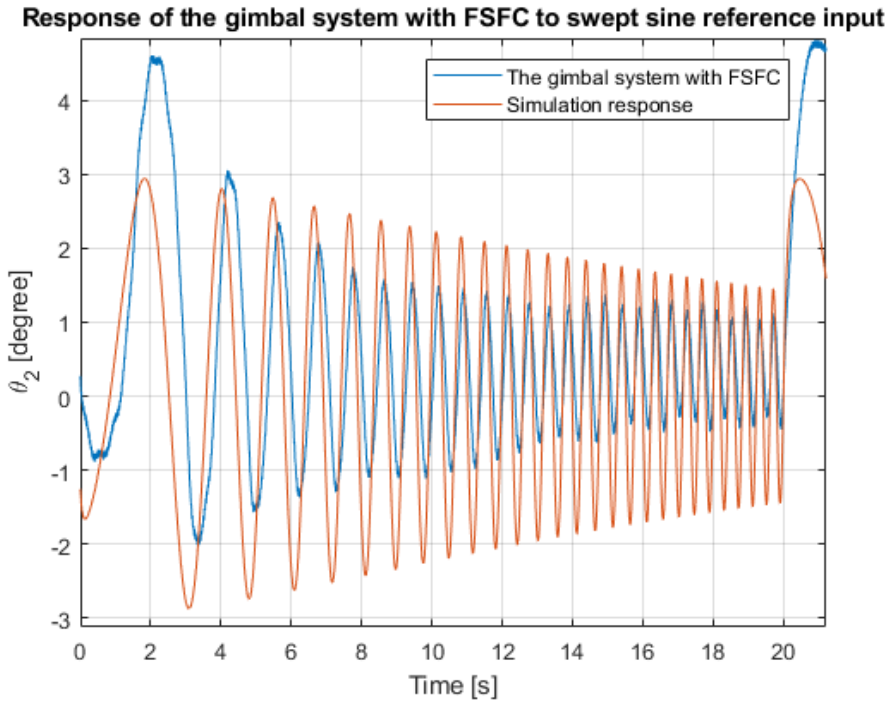

Figure 54: Response of θ_2 of the gimbal system with full-state feedback control to swept sine reference input zoomed in

In Figure 55-Figure 59, different step inputs were applied on control system developed with FSFC method. The system behaves differently for the amplitude of the step input because of the actuator saturation. As a result of the 3° step input applied to the azimuth axis, an angular position error of about 0.11° was observed without any overshoot behavior, and when a 45° step input was applied, it was observed that it had a positional error of more than 1°, and the system showed an overshoot behavior. The reason for the overshoot behavior is that the motor torque signal produced against the high amplitude step input is saturated. Also, it is observed that transient characteristics were not sufficient in both step inputs. Besides, when a 3° step input is applied to the elevation control axis, it is observed that the position error is close to 0.5° which is a large tracking error. Due to the high steady state error, the initial position is different than 0° as seen in the Figure 59. In addition, it seems that the transient response of the system is far from the requirements.

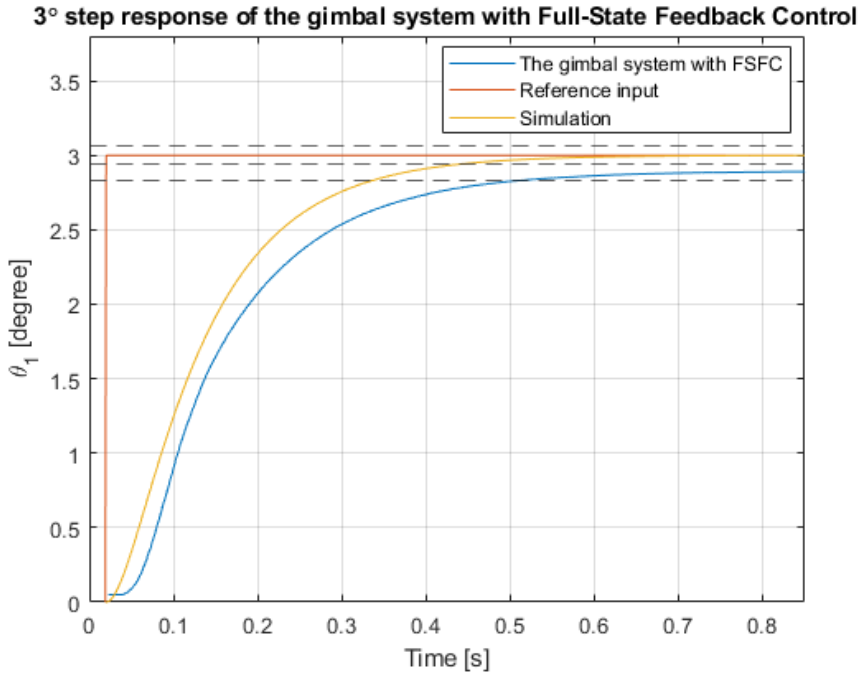

Figure 55: 3° Step response of θ_1 of the gimbal system with full-state feedback control

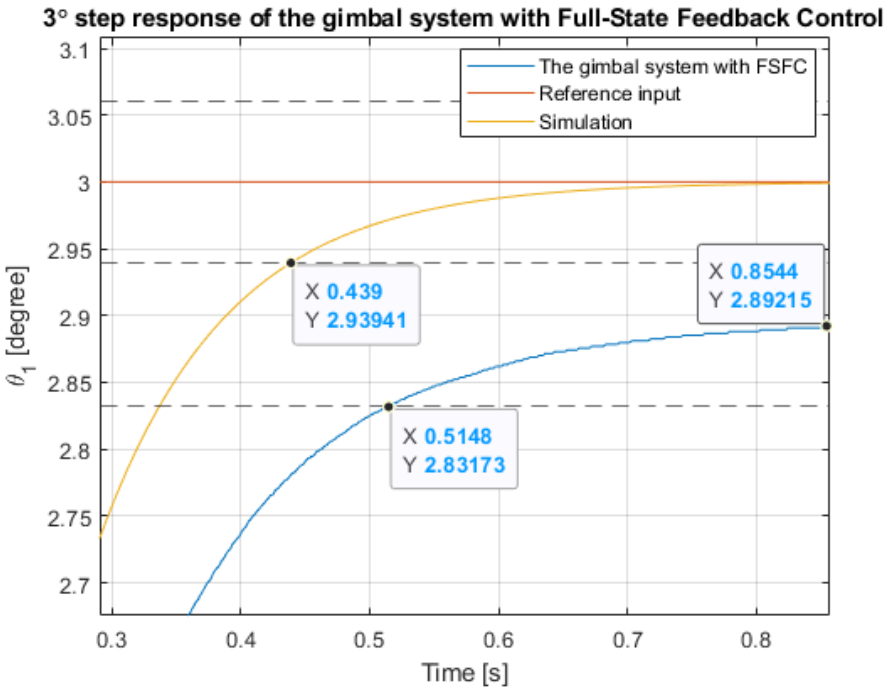

Figure 56: 3° Step response of θ_1 of the gimbal system with full-state feedback control zoomed in

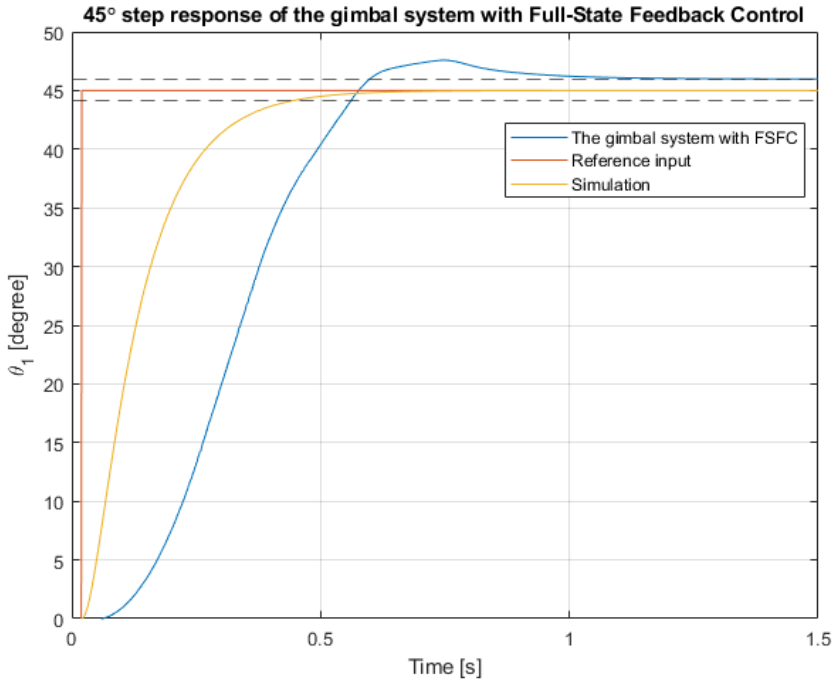

Figure 57: 45° Step response of θ_1 of the gimbal system with full-state feedback control

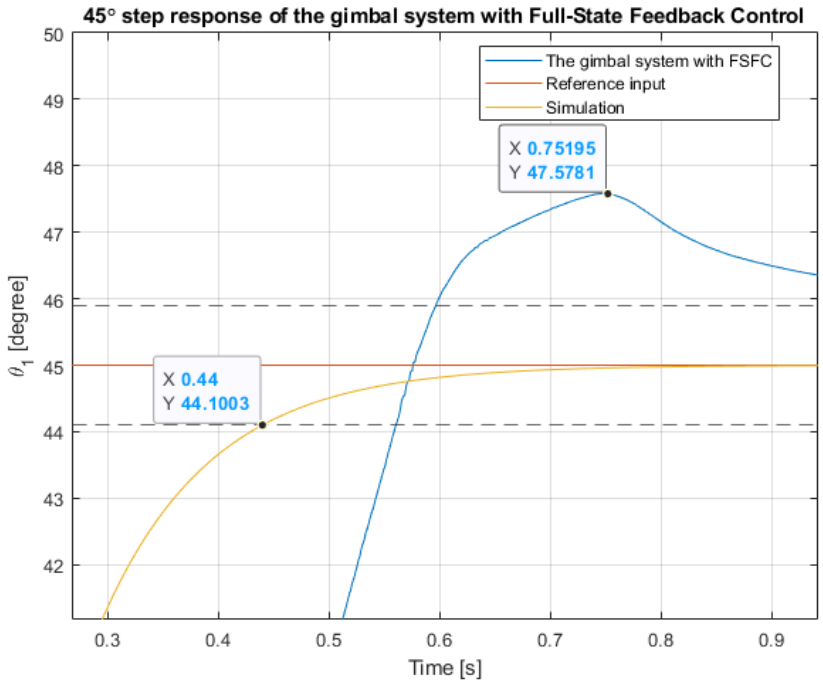

Figure 58: 45° Step response of θ_1 of the gimbal system with full-state feedback control zoomed in

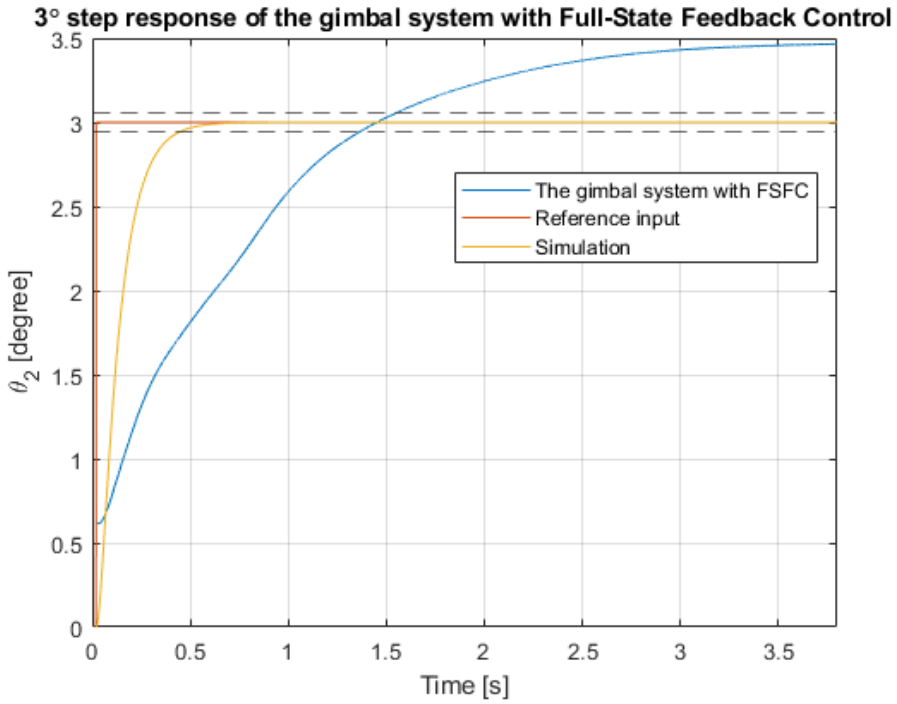

Figure 59: 3° Step response of θ_2 of the gimbal system with full-state feedback control

After the gimbal system with FSFC method tested, MRAC method was applied with the same reference inputs. As shown in Figure 60 and Figure 61, adaptation process took times $80 - 100\ seconds$ nearly for the swept sine signal. Also, elements of the weighting matrix change periodically due to periodic swept sine signal. As mentioned in section 4.2, learning rates of the MRAC update law selected such that the gimbal system responds quickly but not overshoot or loose stability due to high gain change. Besides, it is observed that $\widehat{W}_{11}$ and $\widehat{W}_{23}$ are greater in magnitude than the other coefficients of the constant weighting matrix that oscillate around 0 to 1.

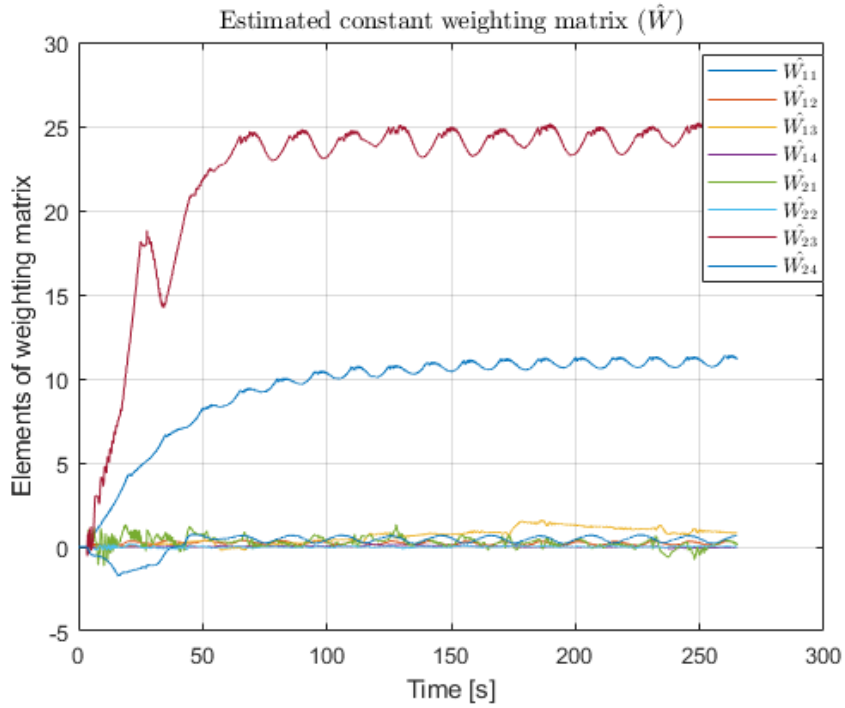

Figure 60: Estimated constant weighting matrix elements vs time

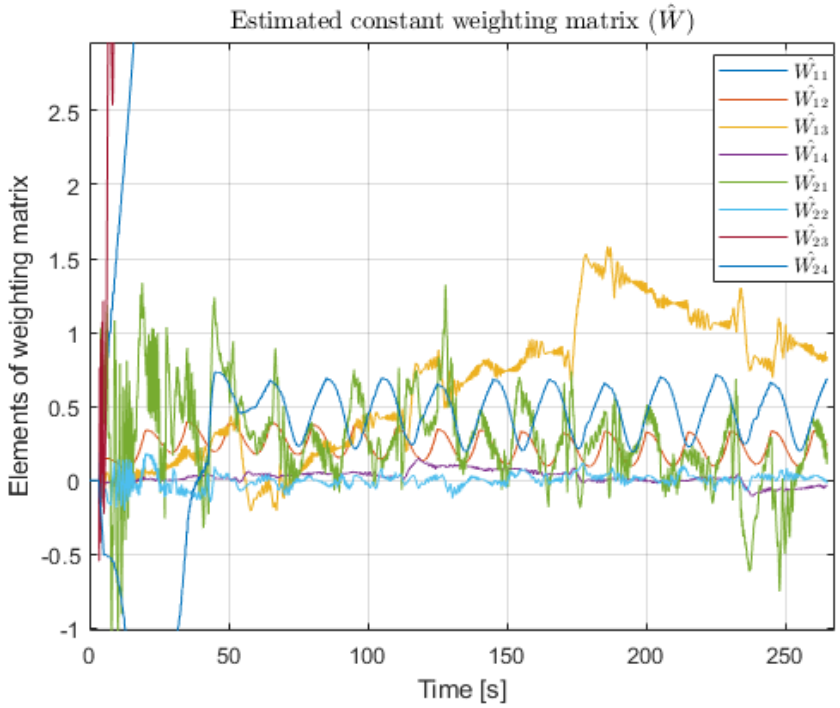

Figure 61: Estimated constant weighting matrix elements vs time zoomed in

Responses of the gimbal system with MRAC after the system adapted were provided in Figure 62-Figure 74. The system responds very close to the reference system for the swept sine tracking input. The response for the azimuth axis was a little smaller in low frequency region (early stage of the periodical swept sine signal) and little greater in high frequency region of the signal than reference model as shown in Figure 62 and Figure 63. Besides, the response for the elevation axis is smaller in low and high frequency region and greater in mid frequency region as shown in Figure 64 and Figure 65. However, it is observed that both the responses were quite improved compared to the control system with FSFC method shown in Figure 51-Figure 54. In addition, the phase quantity of the elevation angle was quite enhanced. Although, it is not obvious in time domain responses shown in Figure 54 and Figure 65; frequency response function present the phase relation directly given in Figure 88. For the azimuth control axis, the difference was not such noticeable as in the elevation axis as shown in the Figure 86.

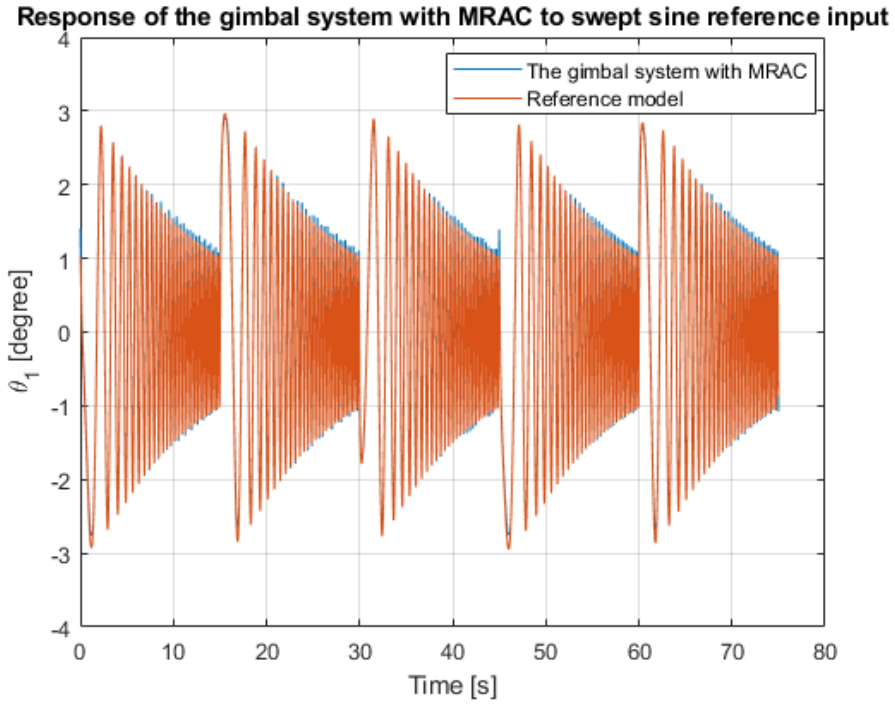

Figure 62: Response of θ_1 of the gimbal system with MRAC to swept sine reference input

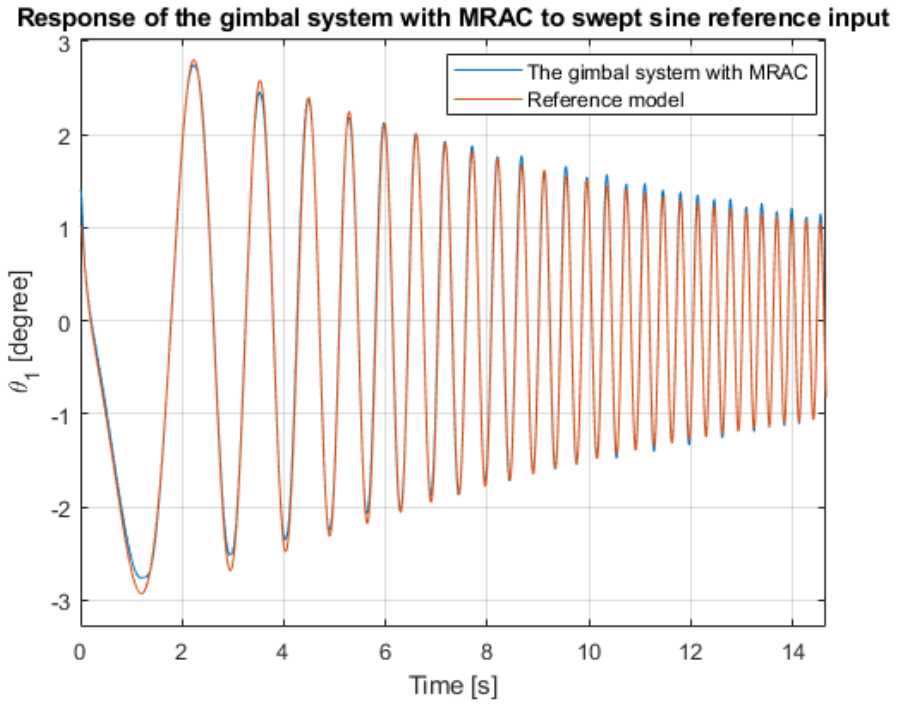

Figure 63: Response of θ_1 of the gimbal system with MRAC to swept sine reference input zoomed in

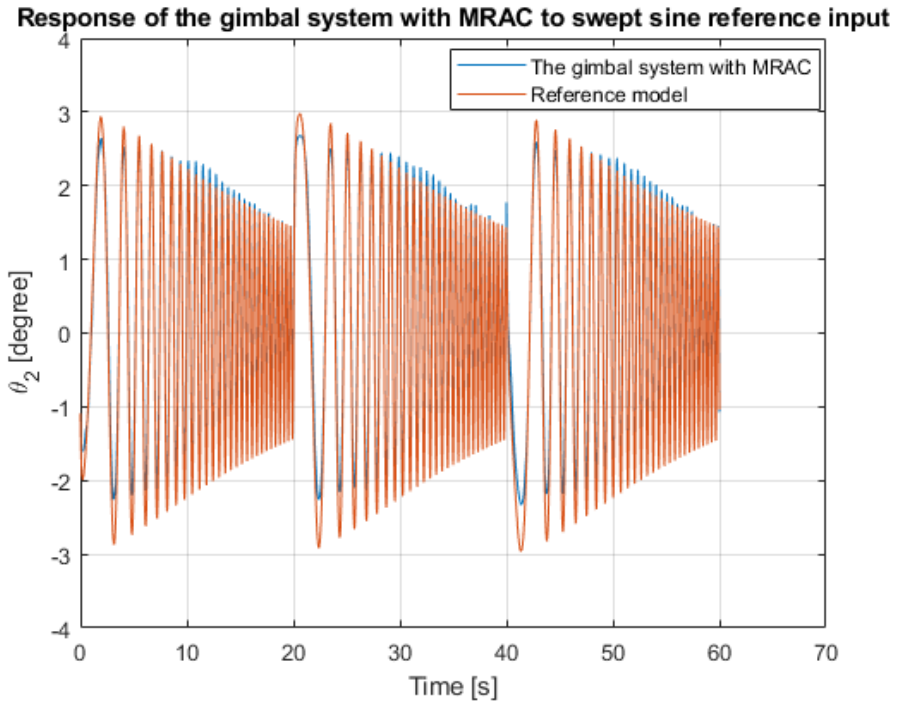

Figure 64: Response of θ_2 of the gimbal system with MRAC to swept sine reference input

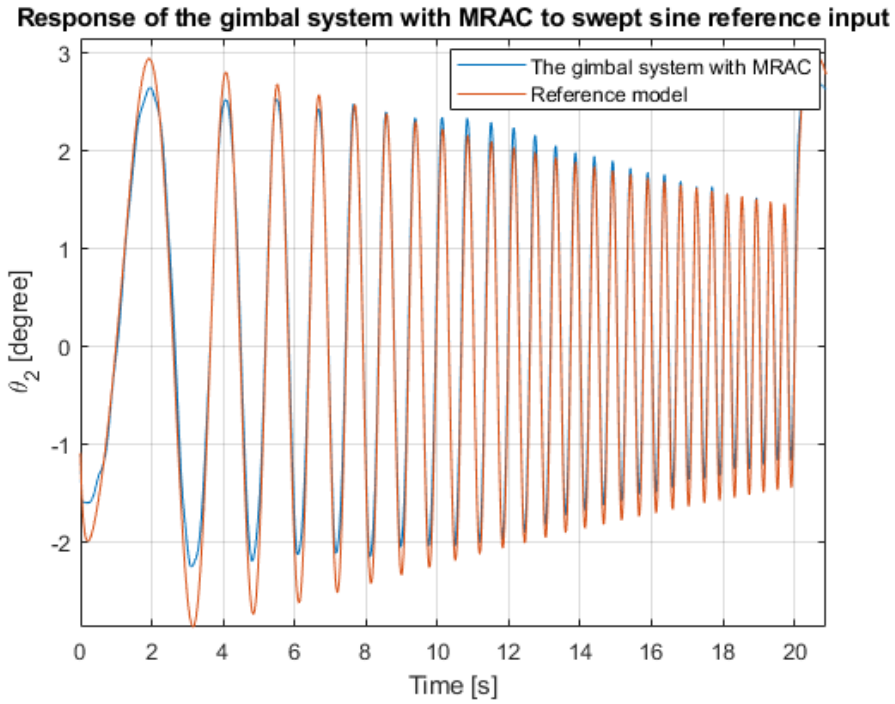

Figure 65: Response of θ_2 of the gimbal system with MRAC to swept sine reference input zoomed in

Error of the angular position variables of the gimbal system between the real system response and reference model response for both the control systems with FSFC and MRAC methods were provided in Figure 66 and Figure 67. The error in azimuth position angle, θ_1, were decreased from $\pm 0.4°$ to $\pm 0.1°$ approximately as shown in Figure 66. The difference or improvement is quite larger in elevation position angle, θ_2 which was changed from $2° - 4°$ depending on the frequency to $\pm 0.2°$ at most as shown in Figure 67.

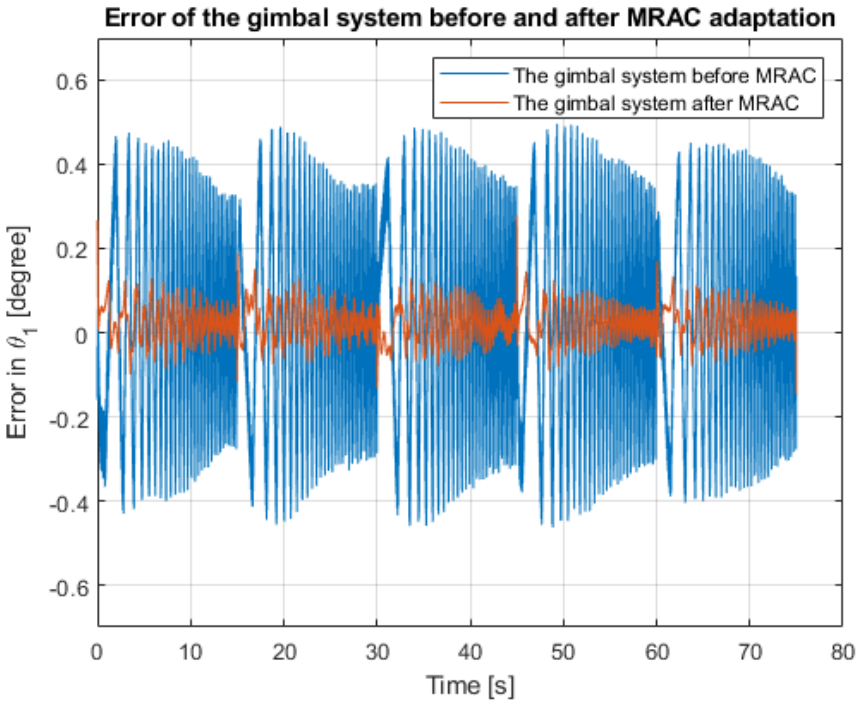

Figure 66: Error of θ_1 of the gimbal system before and after MRAC adaptation

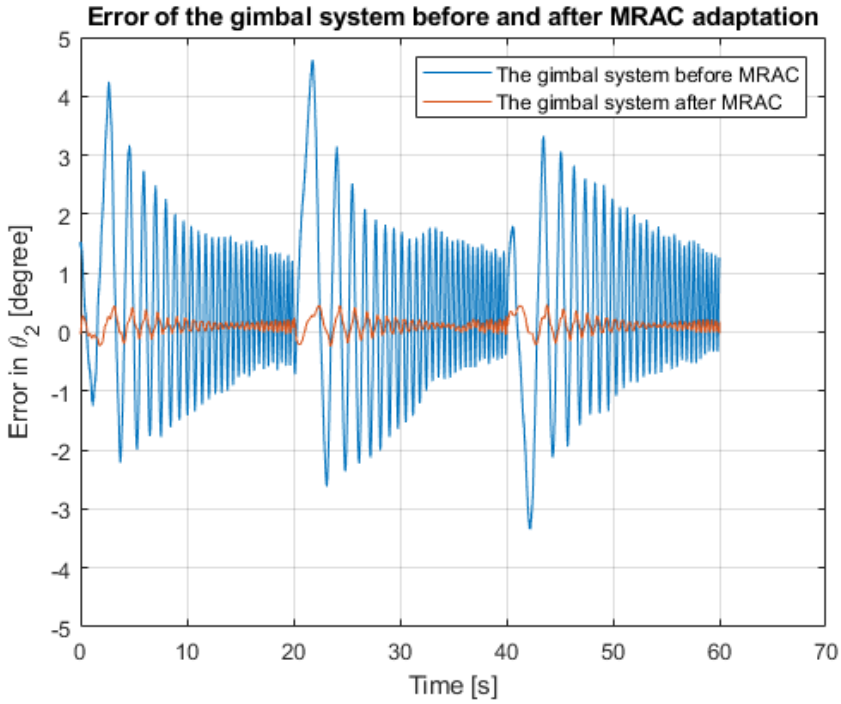

Figure 67: Error of θ_2 of the gimbal system before and after MRAC adaptation

The step response of the gimbal system with MRAC method is provided in Figure 68-Figure 74. As stated in the results of the FSFC method, amplitude of the step input resulted in different response characteristic due to actuator saturation, is also shown in MRAC method. The transient response of the step function differs for the 3° and 45° step amplitude. The gimbal system presented lag behavior for the larger step input. However, setling time for the azimuth axis was very close to the reference model in both step responses. For the elevation axis, settling time was much smaller than the reference model and close to the reference model in high step input amplitude. Therefore, it was observed that both the steady state and transient behavior of the gimbal system improved, especially for the elevation control axis. Besides, the steady state response of the gimbal system was improved in both control axis where it achieves position error smaller than $\pm 0.1°$. As provided in Figure 59, steady state error of the elevation axis was far from the requirements, while, it was satisfied in the MRAC method as shown in Figure 72-Figure 74.

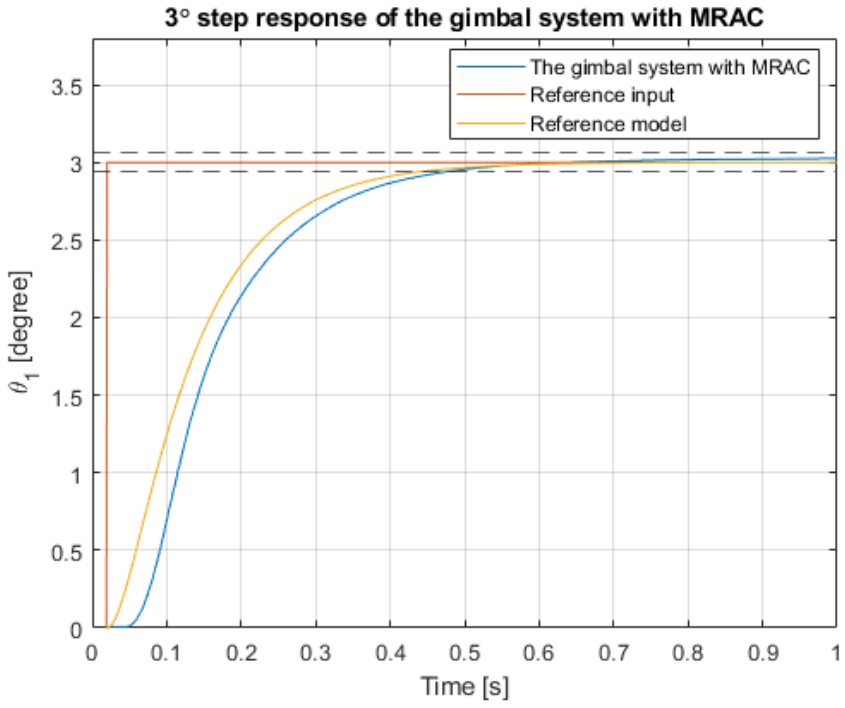

Figure 68: 3° Step response of θ_1 of the gimbal system with MRAC

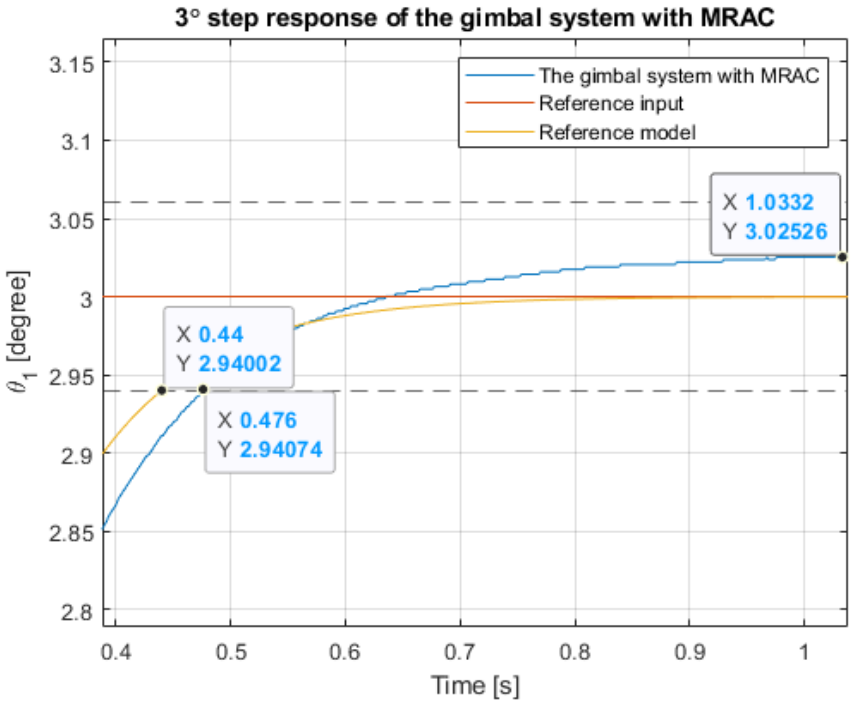

Figure 69: 3° Step response of θ_1 of the gimbal system with MRAC zoomed in

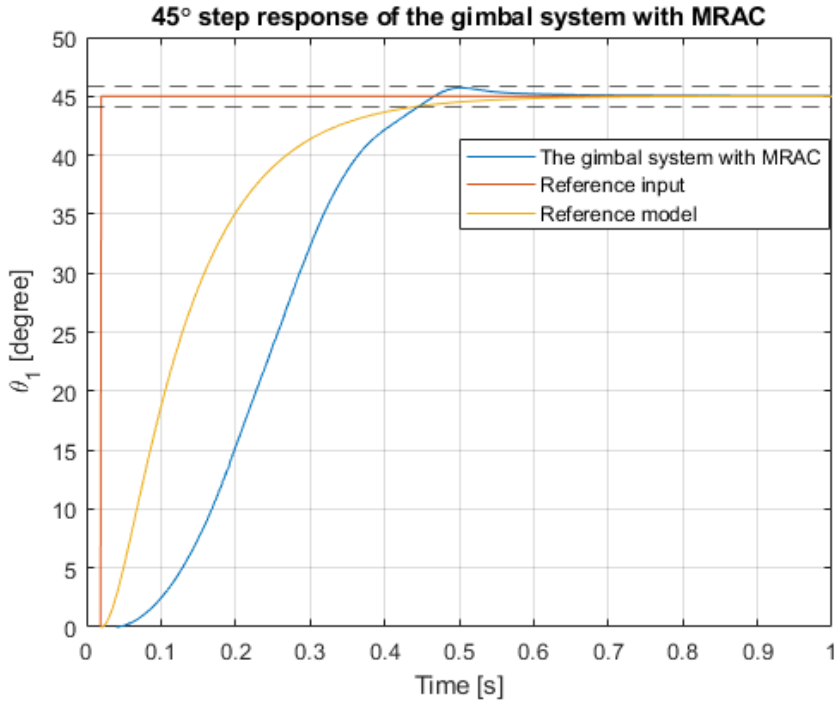

Figure 70: 45° Step response of θ_1 of the gimbal system with MRAC

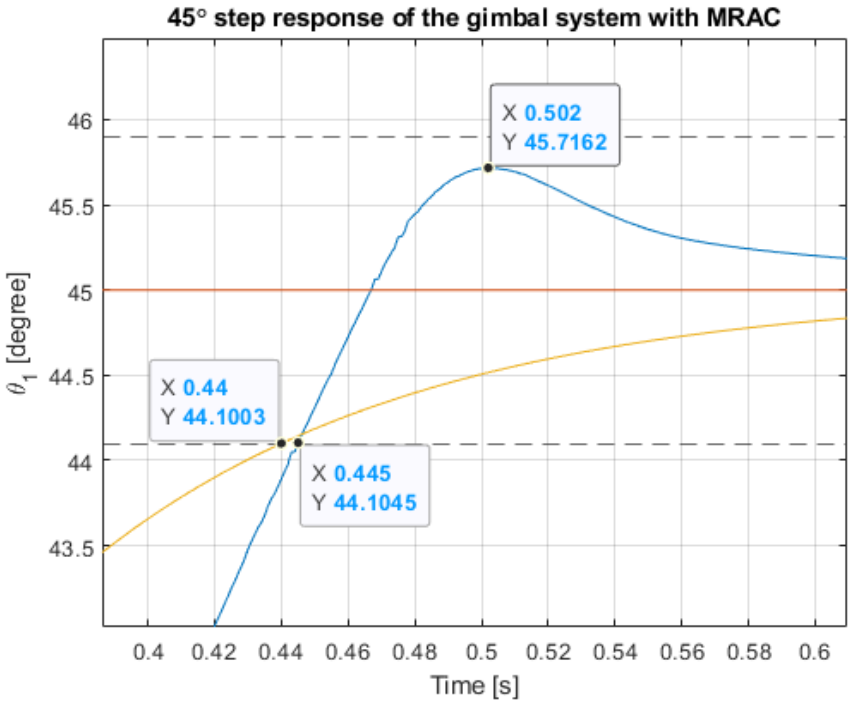

Figure 71: 45° Step response of θ_1 of the gimbal system with MRAC zoomed in

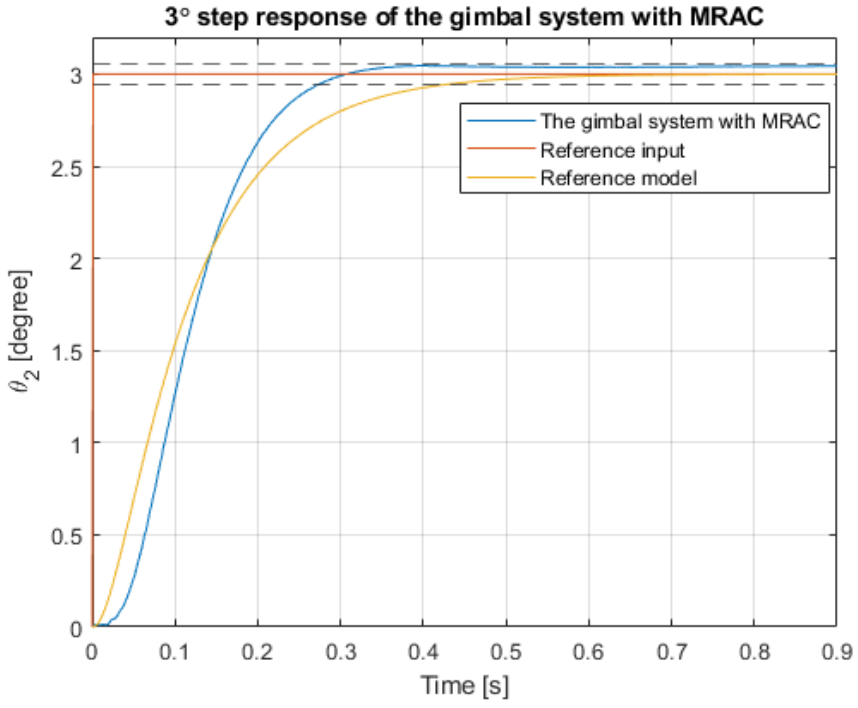

Figure 72: 3° Step response of θ_2 of the gimbal system with MRAC

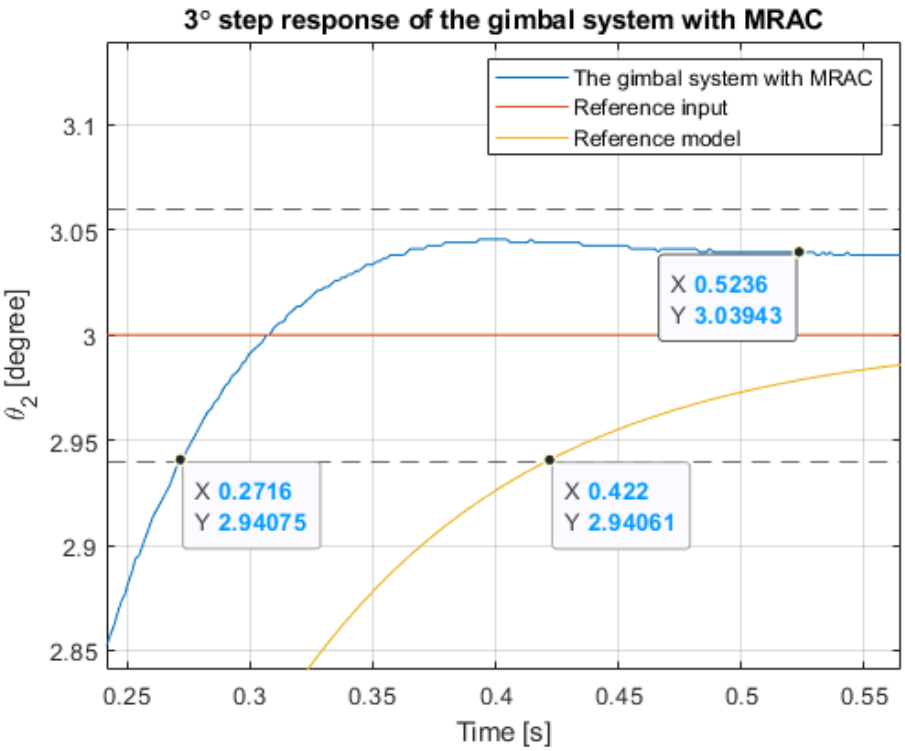

Figure 73: 3° Step response of θ_2 of the gimbal system with MRAC zoomed in

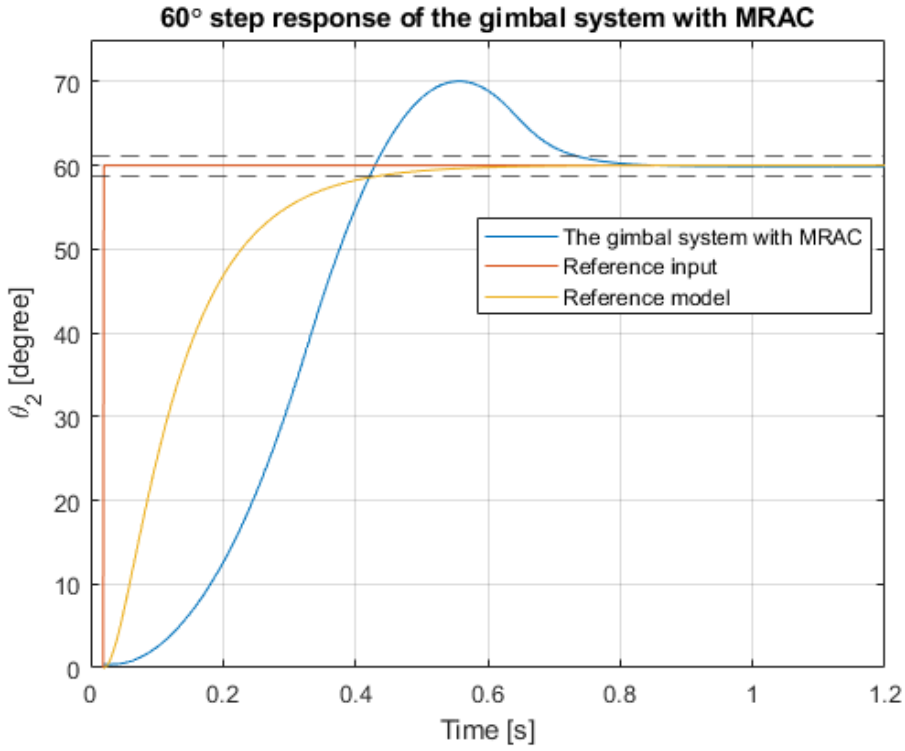

Figure 74: 60° Step response of θ_2 of the gimbal system with MRAC

As a result of the tests performed on the cascade PI control system developed based on decoupled gimbal model, the response of the reference tracking signal applied to the azimuth control axis is seen in Figure 75 and Figure 76. Likewise, the response of the reference tracking signal for the elevation control axis is shown in Figure 77 and Figure 78. As observed in the azimuth control axis, the actual system response is close to the simulation response but lower in value over the frequency region. A similar situation is observed in the elevation control axis, system response is lower in value all over the frequency region; however, the difference is larger than the azimuth axis. Therefore, it can be concluded that increasing the gain of the controller might improve the error, but it might result in stability problems because of that increasing gain also alters the high frequency response.

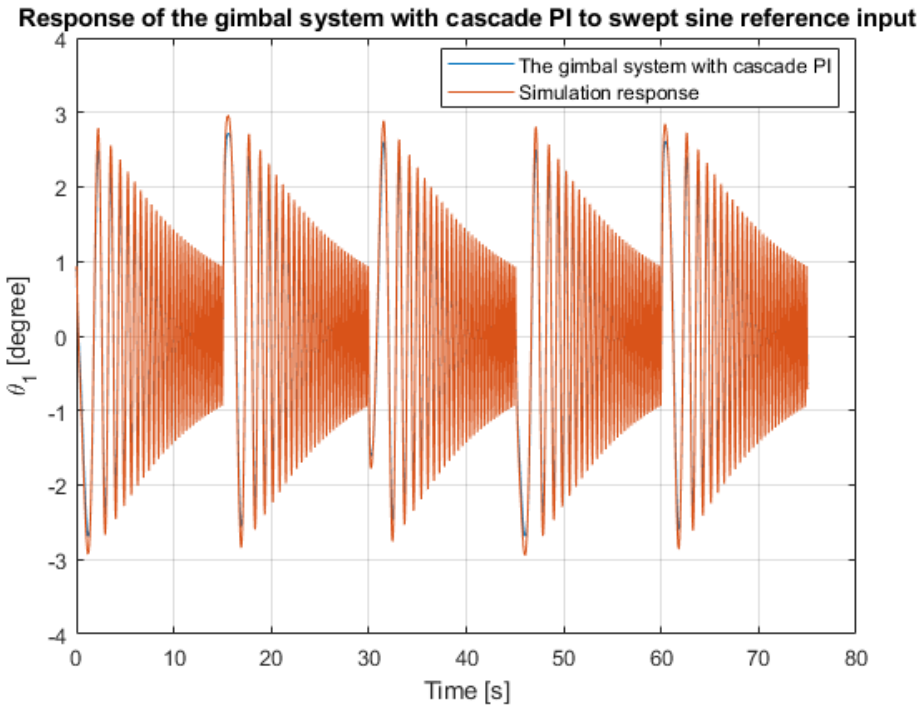

Figure 75: Response of θ_1 of the gimbal system with Cascade PI to swept sine reference input

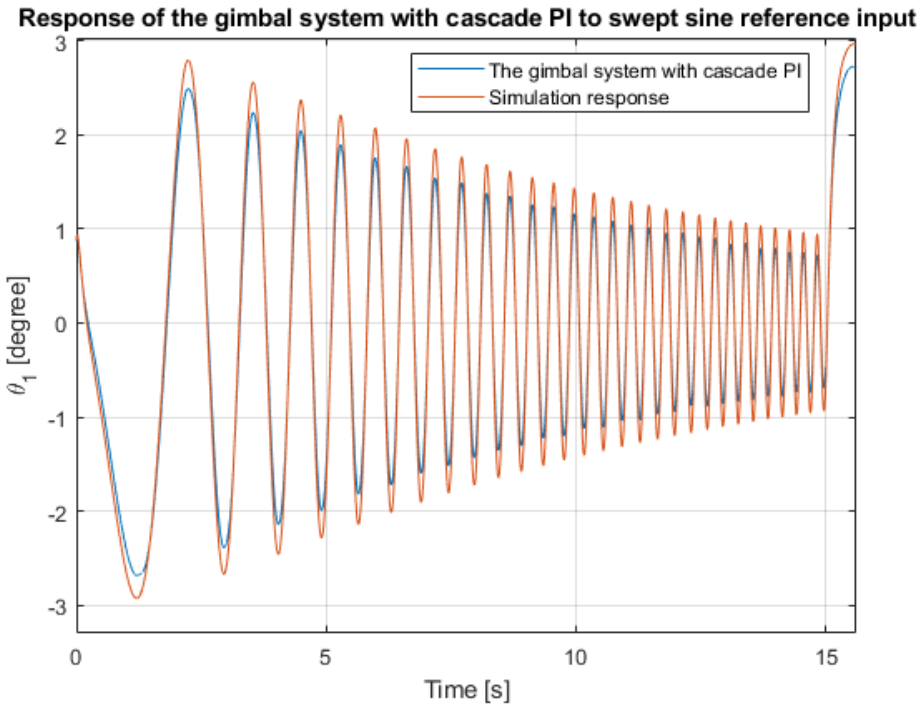

Figure 76: Response of θ_1 of the gimbal system with Cascade PI to swept sine reference input zoomed in

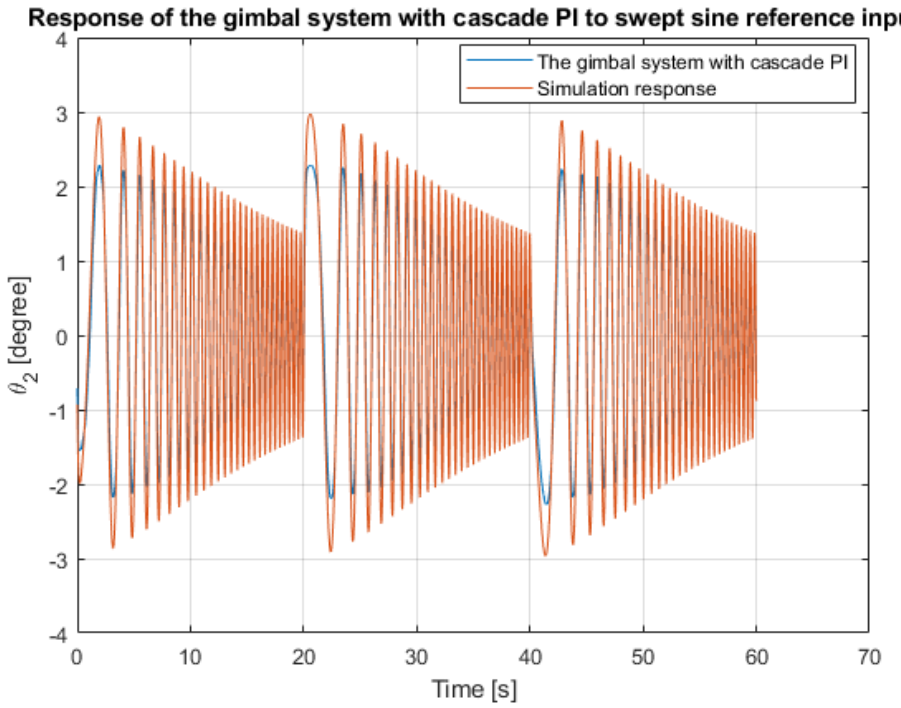

Figure 77: Response of θ_2 of the gimbal system with Cascade PI to swept sine reference input

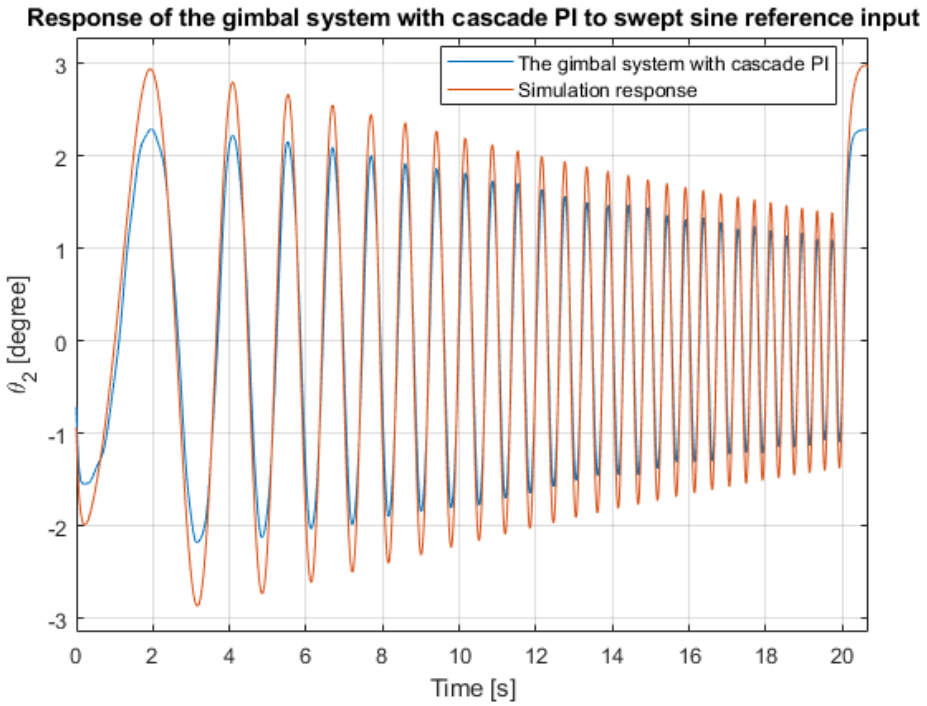

Figure 78: Response of θ_2 of the gimbal system with Cascade PI to swept sine reference input zoomed in

The step response of the gimbal system with cascade PI method provided from Figure 79 to Figure 85. It was observed that using integral term improves the steady state performance, however settling time was significantly deteriorated compared to the MRAC. That was clearer in the response of the elevation axis. Overall, the transient response was not sufficient. Although overshoot behavior was not shown in the azimuth axis, it was seen in the elevation axis when the high amplitude step response applied. This time, accumulation of the error signal due to the integral term resulted in overshoot as well as actuator saturation which was common to all methods. Accumulation of the error due to the integral term can be improved by a technique known as anti windup, which was not involved in this study to focus the scope of the thesis.

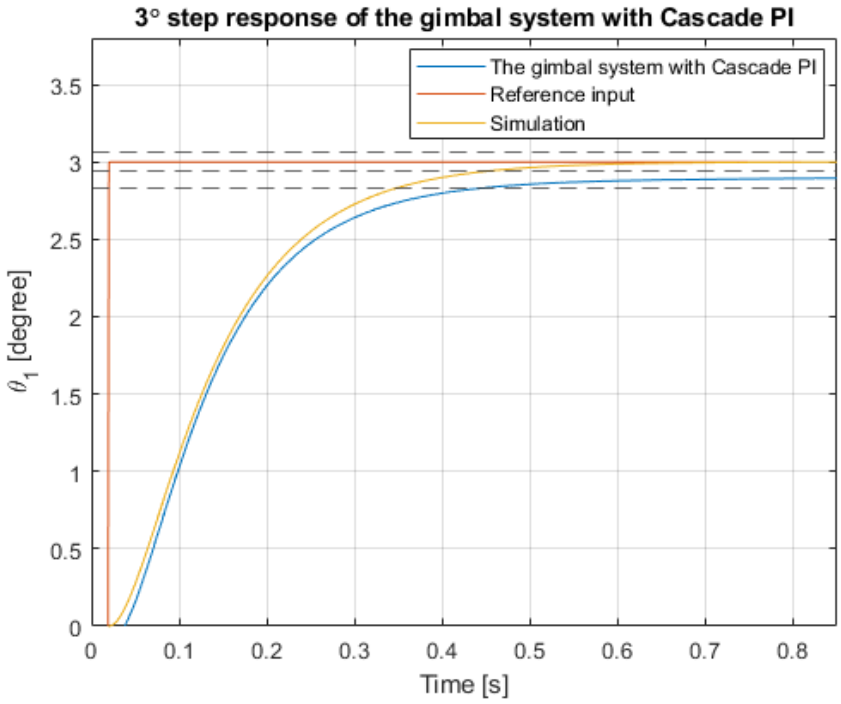

Figure 79: 3° Step response of θ_1 of the gimbal system with Cascade PI

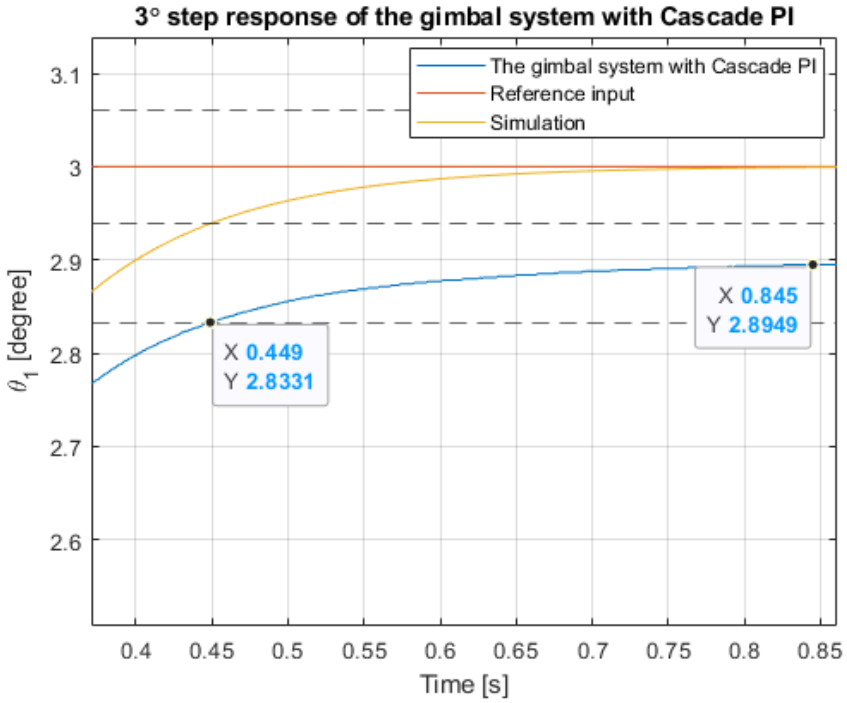

Figure 80: 3° Step response of θ_1 of the gimbal system with Cascade PI zoomed in

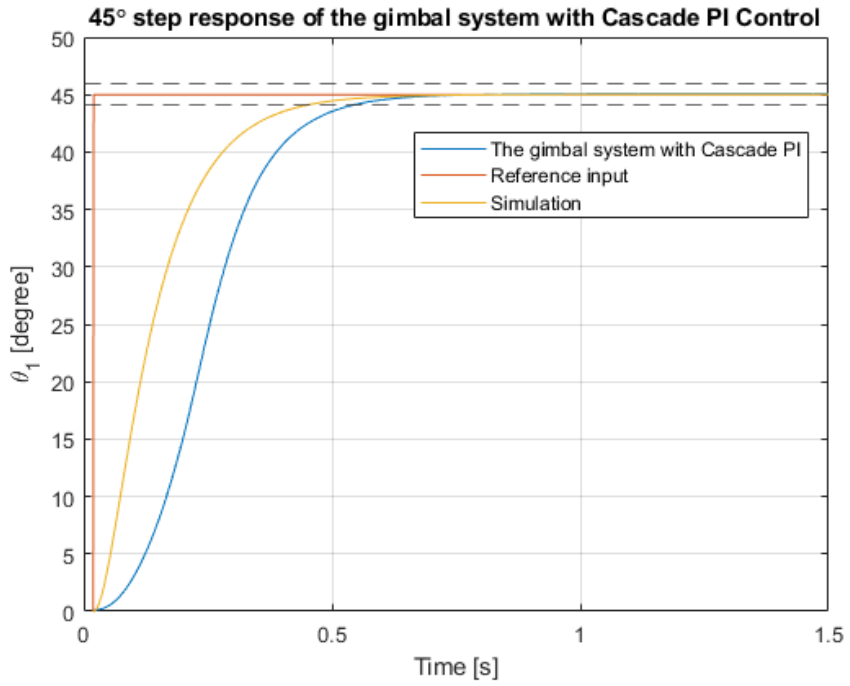

Figure 81: 45° Step response of θ_1 of the gimbal system with Cascade PI

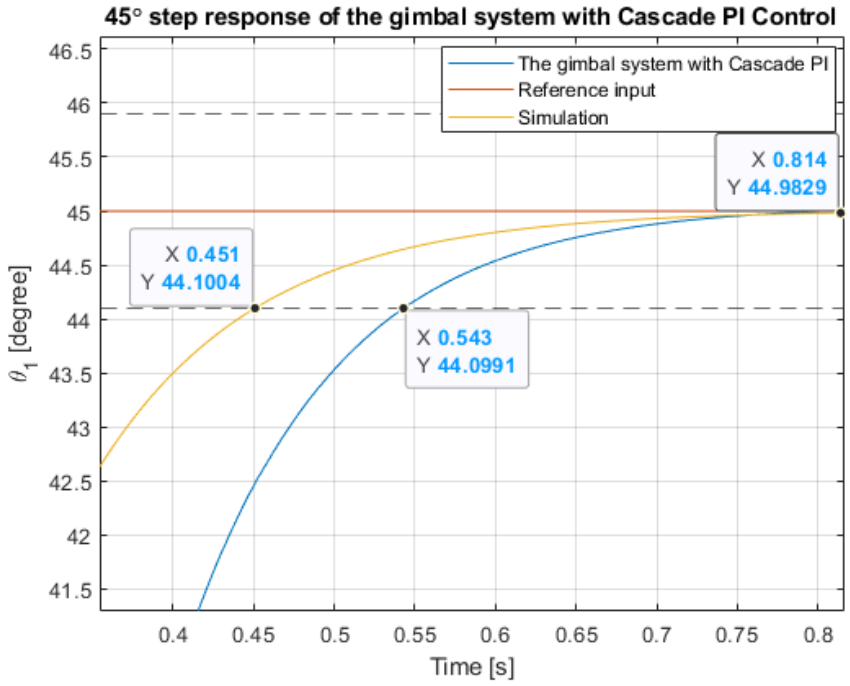

Figure 82: 45° Step response of θ_1 of the gimbal system with Cascade PI zoomed in

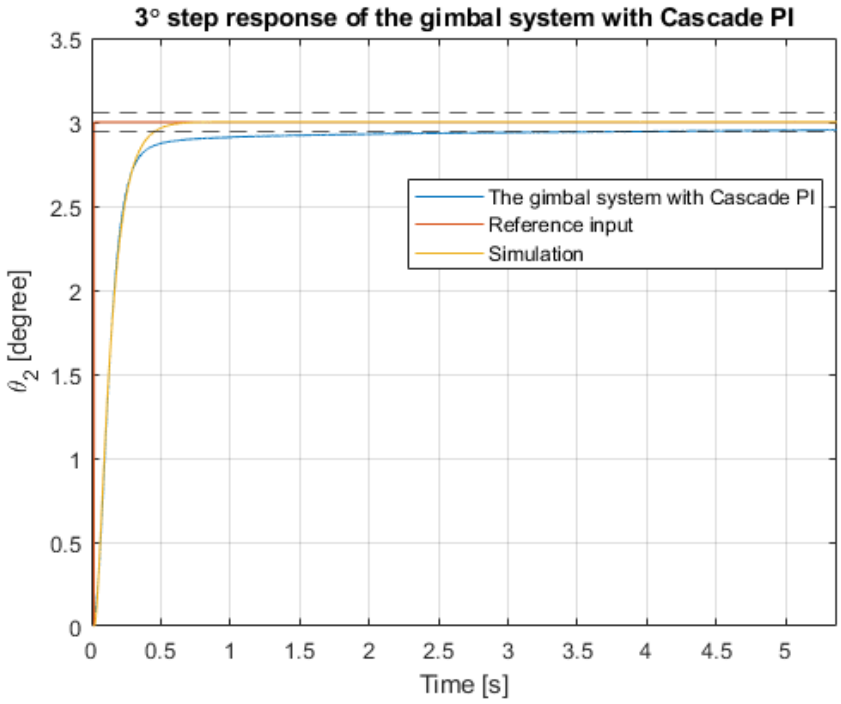

Figure 83: 3° Step response of θ_2 of the gimbal system with Cascade PI

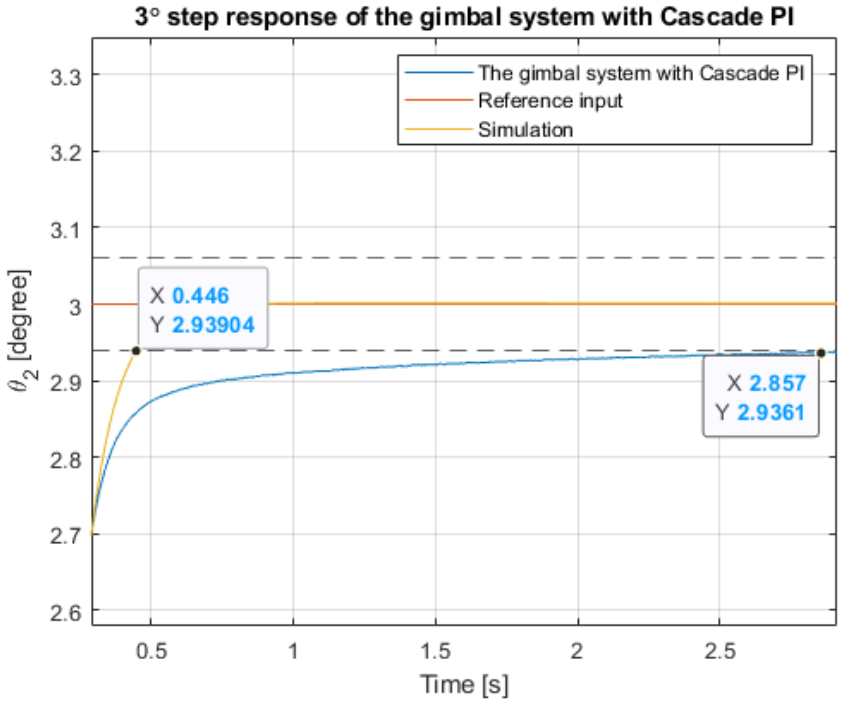

Figure 84: 3° Step response of θ_2 of the gimbal system with Cascade PI zoomed in

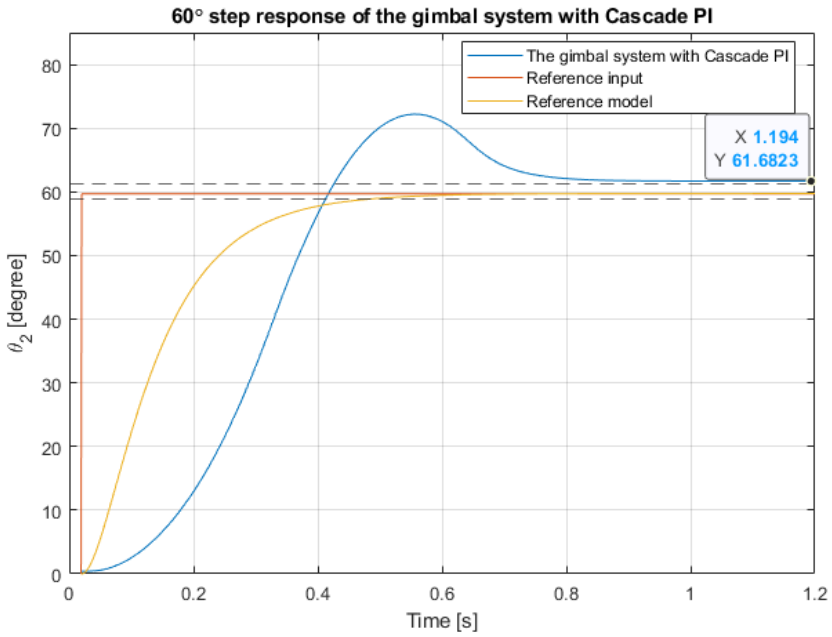

Figure 85: 60° Step response of θ_2 of the gimbal system with Cascade PI

Frequency response functions of the closed loop control system of the gimbal were provided in Figure 86-Figure 89. The closed loop frequency response of the azimuth axis shown in Figure 86 indicated that MRAC method converges the frequency response of the control system before MRAC adaptation which is also identical to FSFC method to the reference model. Although the phase relations overlapped for all the models, amplitudes overlapped after the MRAC method for them. As observed in Figure 87, the closed loop bandwidth of the gimbal system increased from 1.9 Hz to 2.5 Hz which was almost identical with the reference model. For the elevation control axis, both the amplitude and phase relations of the control system differ from each other before the MRAC adaptation. The effect of the MRAC method was noticeable; even though the closed loop response after the MRAC method was not overlapped compared to the azimuth control axis, the change was quite greater. Also, it was observed that contributed phase is more significant in the mid frequency region, 1 Hz, around $+40°$ than low and high frequency regions, 0.1 Hz and 5 Hz, around $+20°$. In addition, closed loop bandwidth of the elevation axis improved from 1.1 Hz to 2.8 where the reference model has 3.5 Hz as shown in Figure 89. Therefore, it can be stated that MRAC method contributed more for the elevation

axis due to high change in system response, although the azimuth axis presented closer behavior to the reference model. Frequency response of the cascade PI control system were almost identical to FSFC (before MRAC adaptation) in azimuth axis. That is, both the FSFC method and the cascade PI control method exhibited similar frequency response performance, where the responses were observed without adaptation or fine-tuning process. However, the cascade PI method had better frequency response performance than FSFC in the elevation axis, while it had a lower magnitude than MRAC.

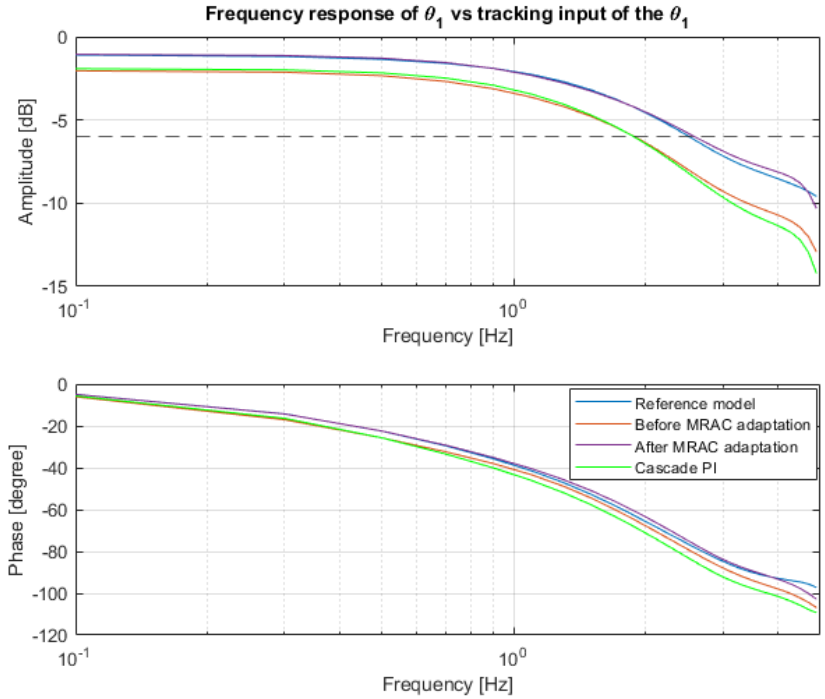

Figure 86: Frequency response of θ_1 vs reference input of θ_1

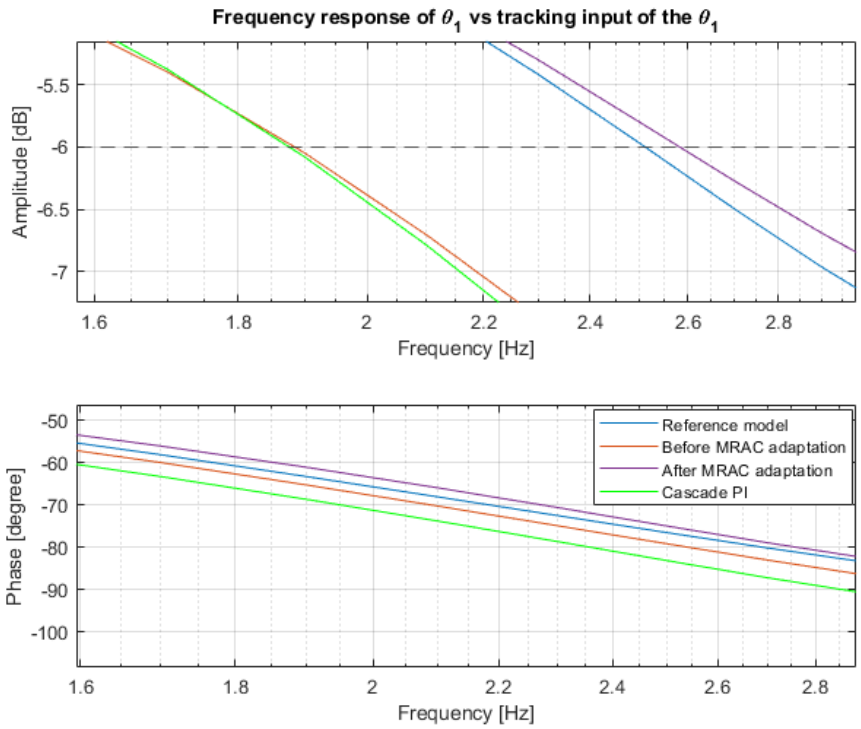

Figure 87: Frequency response of θ_1 vs reference input of θ_1 zoomed in

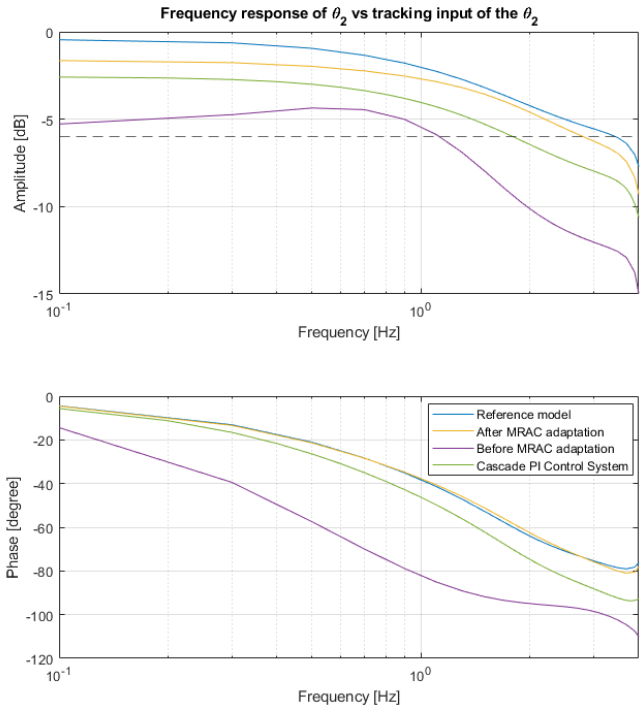

Figure 88: Frequency response of θ_2 vs reference input of θ_2

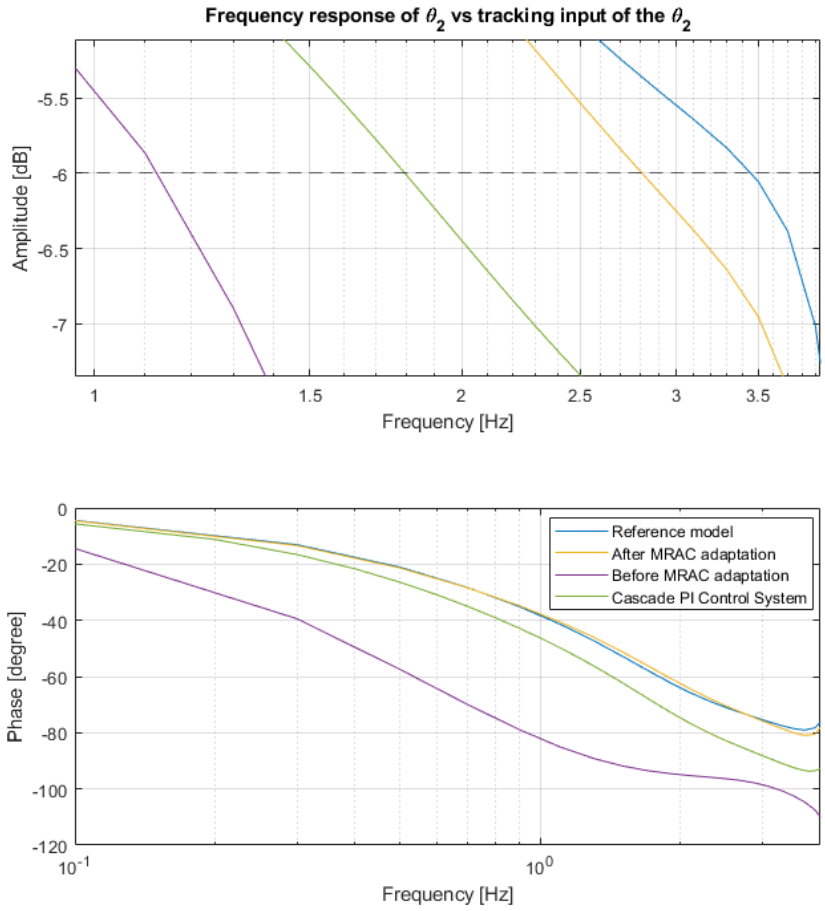

Figure 89: Frequency response of θ_2 vs reference input of θ_2 zoomed in

5.2 Disturbance Rejection

In addition to directing the gimbal system to the desired position (tracking), another requirement (stabilization) of the gimbal system is to maintain its position in response to the movements of the platform to which it was assembled. Although the main objective of the gimbal system studied in this thesis is tracking, the disturbance rejection performance of the control system is the second concern, while it might be the primary objective for other gimbal systems. Therefore, the performance criteria of the disturbance rejection property were limited to bound the gimbal orientation error to $\pm 0.5°$ as specified in the section 1.2. As stated before, experiments were

carried out on each of the platform axes shown in Figure 1 to demonstrate the robustness of the control system against unmodelled disturbances. Stewart platform was used to simulate platform movements during these experiments. The gimbal system is mounted to a stewart test platform similar to the one in the Figure 90. The placement of the gimbal system on the stewart platform was made in such a way that the yaw axis and the azimuth axis were parallel, and the elevation axis was randomly positioned. In order to simulate desired platform movements, the periodic signal was applied to all three axes sequentially as in the Figure 91. This experiment was repeated for each FSFC, MRAC, the cascade PI control systems and, therefore, was performed three times in total. During the experiment performed for the MRAC control system, the estimated constant weighting matrix was recorded and presented in the Figure 92. The figure was divided into three regions on the time axis. The disturbance signal was applied periodically in the pitch axis until the $210\ seconds$, in the roll axis between $210 - 355\ seconds$, and then in the yaw axis. In the regions where the MRAC estimated weighting matrix change reached equilibrium, the response of the gimbal system shown in the Figure 93-Figure 95 along with the responses obtained in the FSFC control system.

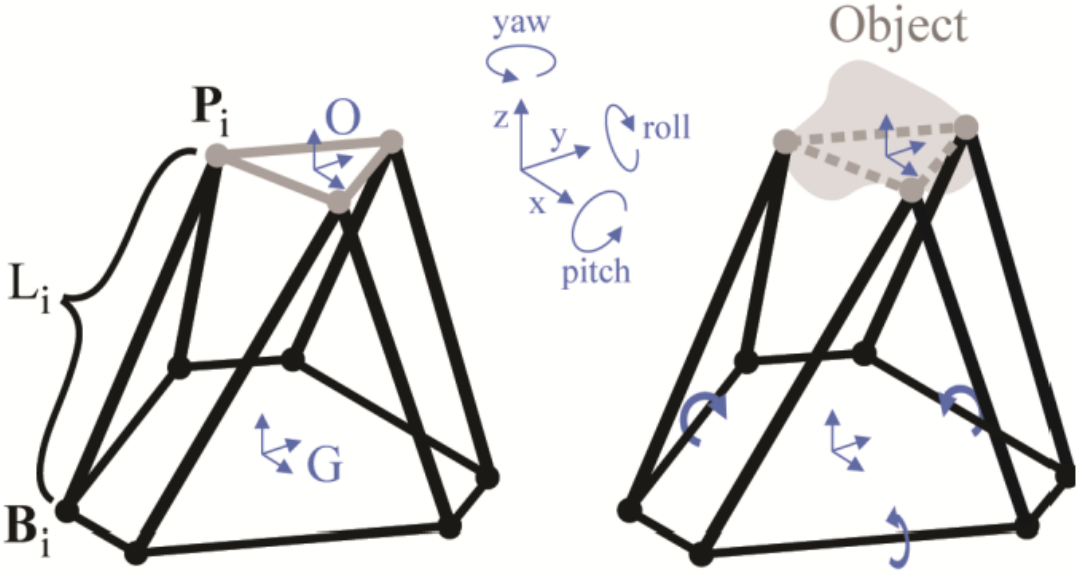

Figure 90: Stewart platform representation [35]

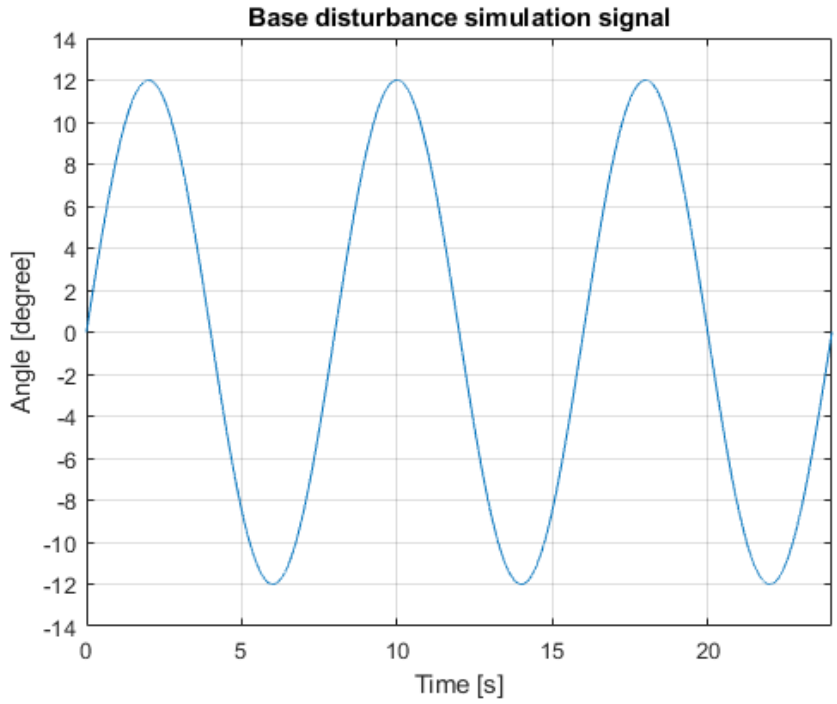

Figure 91: Base disturbance simulation signal for all pitch, roll, and yaw axes

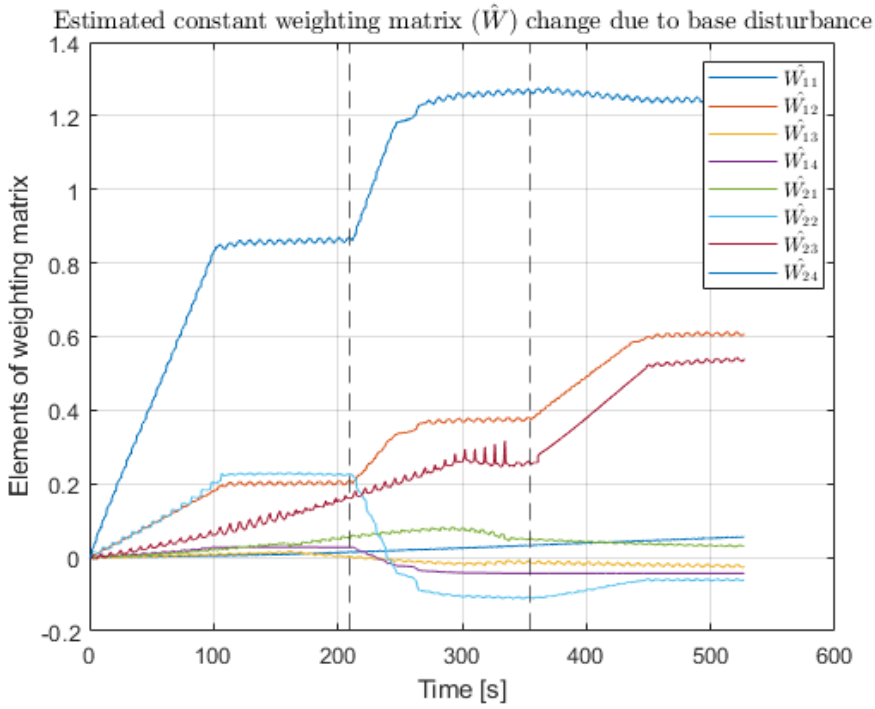

Figure 92: Estimated constant weighting matrix change due to base disturbance

In Figure 93, the responses of the gimbal control systems excited in the direction of the pitch axis are shown. According to that, the MRAC control system had an error of $\pm 0.2°$ in the azimuth axis and $\pm 0.4°$ in the elevation axis, while the FSFC control system had an error of $-0.4°, +0°$ in the azimuth axis and $-0.2°, +0.6°$ in the elevation axis; also, the cascade PI control system had an error of lower than $\pm 0.2°$ in azimuth axis and nearly $\pm 0.4°$ in elevation axis . While the position deviation of the gimbal system was comparable in all control systems, in the FSFC control system, the gimbal system oscillated around a different position than 0°, that is it had steady state error. The control system, adapted with the MRAC method, eliminated the position error as experienced in the tracking case and provided the system oscillate around 0°, that is it eliminated steady state error. According to the gimbal system excited in the roll axis shown in Figure 94, responses similar to those in the pitch axis are observed. Position deviations are similar for both control methods and steady state error is eliminated by MRAC control system. As mentioned above, the assembly of the gimbal system to the stewart platform is made in a way that the azimuth axis and the yaw axis are parallel. Therefore, the disturbance movements in the yaw axis were directly observed in the azimuth axis, the effect on the elevation axis was due to the cross-coupling between the gimbal axes. When Figure 95 was examined, it was observed that the majority of the response in the gimbal system occurs in the azimuth axis, and its motion in the elevation axis is incomparably small. While the position error in the azimuth axis was $\pm 0.3°$ in the FSFC control system, this value increased to ± 0.4 in the MRAC control system. On the other hand, while the error in the elevation axis in the FSFC control system increased gradually with time, this error was reduced throughout time in the MRAC control system. The reason for this was to improve the cross-coupling effect between gimbal systems with the MRAC control method. The cascade PI control system handled the disturbance effect due to cross-coupling phenomena because of the integral term, it was taught.

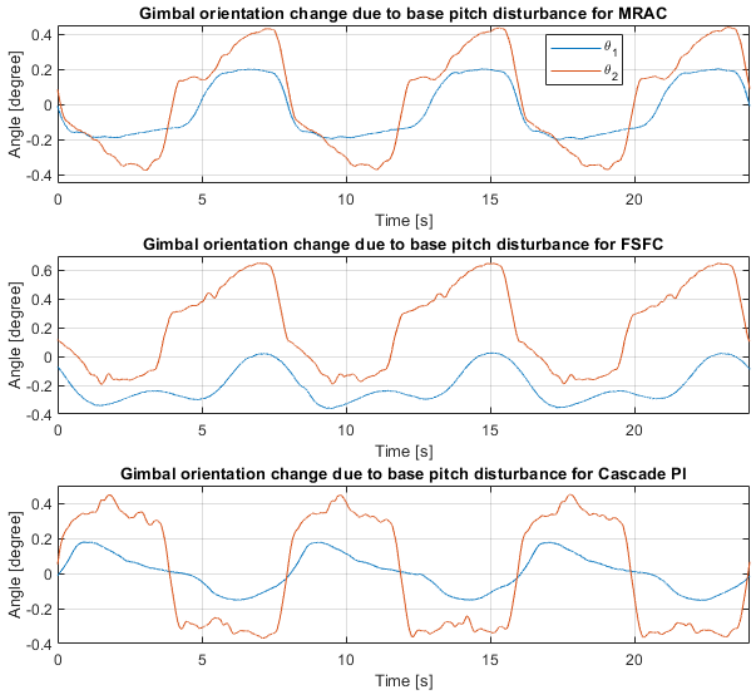

Figure 93: Gimbal orientation change due to base pitch disturbance

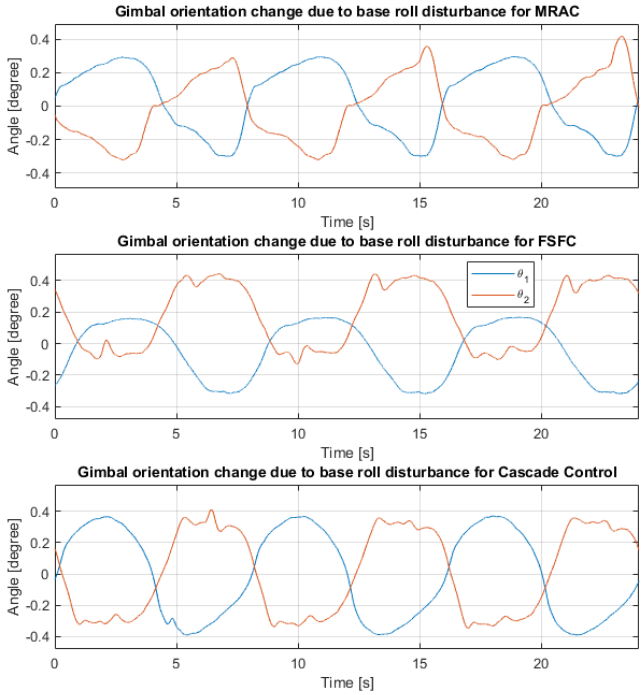

Figure 94: Gimbal orientation change due to base roll disturbance

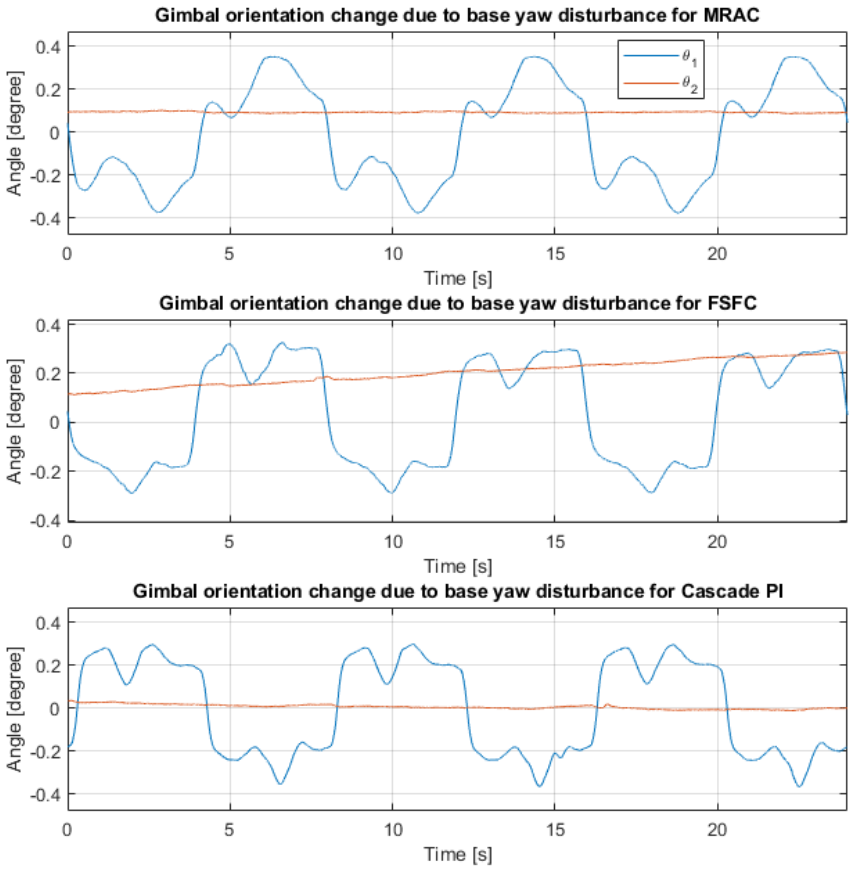

Figure 95: Gimbal orientation change due to base yaw disturbance

CHAPTER 6

DISCUSSION AND CONCLUSION

In the MATHEMATICAL MODELLING chapter, first the 3D coupled nonlinear statically balanced but dynamically unbalanced gimbal system was modelled. Then, with the decoupled gimbal axis approach, the gimbal system was modelled as two dependent gimbal control axis. These models were validated by comparison with tests performed on a physical gimbal system. As expected, the coupled nonlinear gimbal model better represented the system behavior, while the decoupled gimbal model, although obtained with a very simple approach, had a response that was not far from the real system. The nonlinear coupled gimbal model was linearized to be used in the designing of the control systems discussed in this thesis.

Frequency domain based system identification tests were performed to observe the differences between the real system, and the gimbal system assumed as rigid masses in this study. As a result of the mechanical gimbal system being composed of flexible masses contrary to the assumption, it was figured out that the differences in frequency responses caused the real system to behave differently from the modeled ones.

Three control methods:full-state feedback control, model reference adaptive control and the cascade PI control methods were developed in CONTROL DESIGN Chapter, implemented on real system, and experiments were carried out to verify and compare the control methods. It was concluded that the full-state feedback control method did not provide sufficient performance as designed and shown in simulations. Implementing the MRAC method used for the purpose of unmodeled uncertainties and nonlinearities emerged from friction and structural flexibility provided quite improvement in the real gimbal system. It enabled the gimbal system to both lower steady state error and higher closed loop control bandwidth, which also

presented in improved transient response of the system. In addition, it was stated that the effectiveness of the MRAC method was more noticeable in the elevation axis as provided in EXPERIMENTS AND RESULTS Chapter. The reason behind it was thought that nonlinear effects and uncertainties were more dominant in the elevation axis compared to the azimuth axis. One of the performance criteria of the gimbal system was to have $0.5\ seconds$ settling time and satisfied with MRAC method, whereas the FSFC method did not meet the requirement. In addition, it was observed that high amplitude position demand resulted in a worsening in the transient behavior of the gimbal system due to actuator saturation; yet the transient requirement could have been provided for the large position demands as well. Besides, the cascade PI control method using the decoupled gimbal models was tested. It was observed that it had improved steady state behavior due to integral term, whereas the transient performance of it was not sufficient. It was commented that fine-tuning methods might improve the transient characteristics, yet the stability of the gimbal system should be noticed. Therefore, the straightforward cascade PI control method can be an alternative with fine tuning methods.

As another design requirement, this study also included the disturbances from the platform where the gimbal system was assembled and intended to present performance of the control system, which evaluated as the robustness of it against these disturbances. Experiments were carried out by assembling the gimbal system on the stewart platform in order to simulate the marine vehicle. According to the experimental results, MRAC method reduced the steady state error in the tracking working condition. Although it did not provide an overall improvement in the error amplitude, it was observed that the cross-coupling effect of the MRAC method was improved, especially during the tests performed on the yaw axis. For the disturbance rejection performance of the cascade PI control system, it satisfied the requirements as in the other methods It was observed all control systems developed were robust enough against disturbances, and the gimbal system was stabilized within an angle error of less than $0.5°$.

To conclude, the MRAC method provided the desired performance on the two-axis gimbal system. In this method, nonlinear effects and uncertainties were assumed to be in terms of system states, and adaptive control signal were derived accordingly. However, this seems to be a very general and poor estimate for a very complex gimbal system. This work, it was leading the use of radial basis functions being neural network method, which are often used in the MRAC method, to estimate such nonlinear effects. In future studies, this method can be used to predict nonlinear behavior in the gimbal system. In addition, throughout this study, it was noticed that a prominent nonlinear and dominant effect in the gimbal system, other than the mechanical structural flexibility, was friction. It was thought that by defining the friction in more detail, its contribution to the performance would be noticeable. Therefore, the friction feature of the gimbal system will be examined in detail in the future.

REFERENCES

[1] V. Weerackody and E. G. Cuevas, “Technical Challenges and Performance of Satellite Communications on-the-Move Systems,” *Johns Hopkins APL Tech Dig*, vol. 30, no. 2, pp. 113–121, 2011.

[2] J. M. Hilkert, “Inertially Stabilized Platform Technology Concepts and Principles,” *IEEE Control Syst*, vol. 28, no. 1, pp. 26–46, 2008, doi: 10.1109/MCS.2007.910256.

[3] R. Jia, V. K. Nandikolla, G. Haggart, C. Volk, and D. Tazartes, “System Performance of an Inertially Stabilized Gimbal Platform with Friction, Resonance, and Vibration Effects,” 2017, doi: 10.1155/2017/6594861.

[4] N. S. Norman, *Control Systems Engineering*. John Wiley & Sons, 2020.

[5] D. E. Miller, “A new approach to model reference adaptive control; A new approach to model reference adaptive control,” *IEEE Trans Automat Contr*, vol. 48, no. 5, p. 743, 2003, doi: 10.1109/TAC.2003.811251.

[6] B. Ekstrand, “Equations of motion for a two-axes gimbal system,” *IEEE Trans Aerosp Electron Syst*, vol. 37, no. 3, pp. 1083–1091, Jul. 2001, doi: 10.1109/7.953259.

[7] B. E. Birinci and B. Özkan, “Görüntüleme Sistemlerinde Kullanılan Çeşitli Kardanlı Yönlendirme Mekanizmalarının Başarım Özelliklerinin Karşılaştırılması,” in *Uluslararası Katılımlı 17. Makina Teorisi Sempozyumu*, İzmir, Jun. 2015, pp. 114–123.

[8] R. J. Rajesh, “Camera gimbal stabilization using conventional PID controller and evolutionary algorithms; Camera gimbal stabilization using conventional PID controller and evolutionary algorithms,” *2015 International Conference on Computer, Communication and Control (IC4)*, 2015, doi: 10.1109/IC4.2015.7375580.

[9] A. Greco, “Developement of the SmartGimbal control system of the SmartBay platform,” MSc Degree Thesis, POLITECNICO DI TORINO, 2019.

[10] M. Abdo, A. R. Toloei, A. R. Vali, and M. R. Arvan, “Cascade Control System for Two Axes Gimbal System with Mass Unbalance,” *Int J Sci Eng Res*, vol. 4, no. 9, p. 2013, 2013.

[11] I. E. Şener, “Stabilization of an Image Based Tracking System,” MSc Degree Thesis, Middle East Technical University, 2015.

[12] C. Knospe, “PID control,” *IEEE Control Systems Magazine*, vol. 26, no. 1, pp. 30–31, 2006.

[13] Y. Han, Y. Lu, and H. Qiu, “An Improved Control Scheme of Gyro Stabilization Electro-Optical Platform,” *IEEE International Conference on Control and Automation*, pp. 346–351, 2007.

[14] W. Ji, Q. Li, B. Xu, J.-J. Tu, and D.-A. Zhao, “Cascade servo control for LOS stabilization of opto-electronic tracking platform - design and self-tuning,” *2009 International Conference on Information and Automation*, 2009, doi: 10.1109/ICINFA.2009.5205070.

[15] B. Özkan, E. N. Yıldız, and B. Dönmez, “Precise Position Control of a Gimbaled Camera System,” in *AIAA Guidance, Navigation and Control Conference and Exhibit*, Honolulu, Hawaii, Jun. 2008, pp. 1–18.

[16] B. Özkan, “Görüntüleme Sistemlerinin Yönlendirilmesinde Kullanılan Kardanlı Yapıların Denetiminde Uygulanabilecek Başlıca Yöntemlerin Karşılaştırılması,” in *9. Ulusal Havacılık ve Uzay Konferansı*, İzmir, Sep. 2022, pp. 1–8.

[17] K.-J. Seong’, H.-G. Kang’, B.-Y. Yeol, and H.-P. Lee2, “The Stabilization Loop Design for a Two-Axis Gimbal System Using LQG/LTR Controller,” 2006, doi: 10.1109/SICE.2006.315268.

[18] J. A. R. K. Moorty, R. Marathe, and H. B. Srivastava, “Fuzzy controller for line-of-sight stabilization systems,” *https://doi.org/10.1117/1.1737371*, vol. 43, no. 6, pp. 1394–1400, Jun. 2004, doi: 10.1117/1.1737371.

[19] Z. Zhou, B. Zhang, and D. Mao, “MIMO Fuzzy Sliding Mode Control for Three-Axis Inertially Stabilized Platform,” 2019, doi: 10.3390/s19071658.

[20] B. Xiang and Q. Mu, “Gimbal control of inertially stabilized platform for airborne remote sensing system based on adaptive RBFNN feedback model,” *IFAC Journal of Systems and Control*, vol. 16, Jun. 2021, doi: 10.1016/J.IFACSC.2021.100148.

[21] X. Zhou, C. Yang, and T. Cai, “A Model Reference Adaptive Control/PID Compound Scheme on Disturbance Rejection for an Aerial Inertially Stabilized Platform,” 2016, doi: 10.1155/2016/7964727.

[22] K. Szabat and T. Orlowska-Kowalska, “Vibration Suppression in a Two-Mass Drive System Using PI Speed Controller and Additional Feedbacks-Comparative Study,” *IEEE TRANSACTIONS ON INDUSTRIAL ELECTRONICS*, vol. 54, no. 2, p. 1193, 2007, doi: 10.1109/TIE.2007.892608.

[23] T. Sasaki, T. Shimomura, S. Pullen, and H. Schaub, “Attitude and vibration control with double-gimbal variable-speed control moment gyros,” *Acta Astronaut*, 2018, doi: 10.1016/j.actaastro.2018.08.047.

[24] S. Jia and J. Shan, “Flexible Structure Vibration Control Using Double-Gimbal Variable-Speed Control Moment Gyros,” *JOURNAL OF GUIDANCE, CONTROL, AND DYNAMICS*, vol. 44, no. 5, pp. 954–966, May 2021, doi: 10.2514/1.G005684.

[25] Z. Tao, J. Yang, S. Li, and C. Chen, “On Disturbance Rejection for Gimbal Servo System of Flexible Mounting Control Moment Gyroscope,” 2021, doi: 10.23919/CCC52363.2021.9550476.

[26] Y. Cui, Y. Yang, Y. Zhu, J. Qiao, and L. Guo, “Composite Velocity-Tracking Control for Flexible Gimbal System With Multi-Frequency-Band Disturbances,” *IEEE TRANSACTIONS ON CIRCUITS AND SYSTEMS-I: REGULAR PAPERS*, vol. 68, no. 10, 2021, doi: 10.1109/TCSI.2021.3095527.

[27] R. Shaffer, M. Karpenko, and Q. Gong, “Robust Control of a Flexible Double Gimbal Mechanism; Robust Control of a Flexible Double Gimbal Mechanism,” 2018, doi: 10.23919/ACC.2018.8430958.

[28] D. Kaiser and P. Compumotor, “Fundamentals of Servo Motion Control,” *Motion System Design*, vol. 43, no. 9, p. 22, 2001.

[29] J. M. Varela and C. G. Soares, “Interactive Simulation of Ship Motions in Random Seas based on Real Wave Spectra,” in *GRAPP*, Mar. 2011.

[30] M. K. Ozgoren, *Kinematics of General Spatial Mechanical Systems*. Wiley, 2020. doi: 10.1002/9781119195740.

[31] K. Ogata and Y. Yang, *Modern Control Engineering*, 5. Edition. Prentice-Hall EnglewoodCliffs, 2010.

[32] A. M. Lyapunov, “The general problem of the stability of motion,” *Int J Control*, vol. 55, no. 3, pp. 531–534, 1992, doi: 10.1080/00207179208934253.

[33] I. M. Y. Mareels, B. D. O. Anderson, R. R. Bitmead, M. Bodson, and S. S. Sastry, “Revisiting the Mit Rule for Adaptive Control,” *IFAC Proceedings Volumes*, vol. 20, no. 2, pp. 161–166, Jul. 1987, doi: 10.1016/S1474-6670(17)55954-6.

[34] P. C. Parks and P. C. Parks, “Liapunov Redesign of Model Reference Adaptive Control Systems,” *IEEE Trans Automat Contr*, vol. 11, no. 3, pp. 362–367, 1966, doi: 10.1109/TAC.1966.1098361.

[35] C. M. McCann and A. M. Dollar, “Design of a stewart platform-inspired dexterous hand for 6-DOF within-hand manipulation,” *2017 IEEE/RSJ*

International Conference on Intelligent Robots and Systems (IROS), vol. 2017-September, pp. 1158–1163, Dec. 2017, doi: 10.1109/IROS.2017.8202287.

APPENDICES

A. Dynamic Relations

Moment equation for the body 1, (2.56), is rewritten.

$$\check{J}_1 \cdot \vec{\alpha}_1 + \vec{\omega}_1 \times \check{J}_1 \cdot \vec{\omega}_1 = \vec{M}_{01b} + \vec{T}_{01a} - \vec{T}_{12a} + \vec{T}_{01d} - \vec{T}_{12d} + \vec{r}_{C_{azi}O} \times \vec{F}_{01} + \vec{r}_{C_{azi}A} \times (-\vec{F}_{12A}) + \vec{r}_{C_{azi}C} \times (-\vec{F}_{12C})$$

Individual terms of the (2.56) can be expressed in matrix form in reference frame of body 1 as follows.

$$\hat{J}_1^{(1)} \bar{\alpha}_1^{(1)} = \hat{J}_1^{(1)} \hat{C}^{(1,0)} \bar{\alpha}_1^{(0)} = \begin{bmatrix} J_{111} & J_{112} & J_{113} \\ J_{112} & J_{122} & J_{123} \\ J_{113} & J_{123} & J_{133} \end{bmatrix} \begin{bmatrix} \cos\theta_1 & -\sin\theta_1 & 0 \\ \sin\theta_1 & \cos\theta_1 & 0 \\ 0 & 0 & 1 \end{bmatrix}^t \begin{bmatrix} 0 \\ 0 \\ \ddot{\theta}_1 \end{bmatrix} \Rightarrow$$

$$\hat{J}_1^{(1)} \bar{\alpha}_1^{(1)} = \begin{bmatrix} J_{113}\ddot{\theta}_1 \\ J_{123}\ddot{\theta}_1 \\ J_{133}\ddot{\theta}_1 \end{bmatrix} \tag{A.1}$$

Note that cross product operation is applied in matrix representation by using skew symmetric matrix property.

$$\tilde{\omega}_1{}^{(1)} \hat{J}_1 \bar{\omega}_1^{(1)} = skew\left(\begin{bmatrix} 0 \\ 0 \\ \dot{\theta}_1 \end{bmatrix}\right) \begin{bmatrix} J_{111} & J_{112} & J_{113} \\ J_{112} & J_{122} & J_{123} \\ J_{113} & J_{123} & J_{133} \end{bmatrix} \begin{bmatrix} 0 \\ 0 \\ \dot{\theta}_1 \end{bmatrix} \Rightarrow$$

$$\tilde{\omega}_1{}^{(1)} \hat{J}_1 \bar{\omega}_1^{(1)} = \begin{bmatrix} 0 & -\dot{\theta}_1 & 0 \\ \dot{\theta}_1 & 0 & 0 \\ 0 & 0 & 0 \end{bmatrix} \begin{bmatrix} J_{113}\dot{\theta}_1 \\ J_{123}\dot{\theta}_1 \\ J_{133}\dot{\theta}_1 \end{bmatrix} \Rightarrow$$

$$\tilde{\omega}_1{}^{(1)} \hat{J}_1 \bar{\omega}_1^{(1)} = \begin{bmatrix} -J_{123}\dot{\theta}_1^2 \\ -J_{113}\dot{\theta}_1^2 \\ 0 \end{bmatrix}, \qquad Eqn. \tag{A.2}$$

$$\left[\vec{r}_{C_{azi}O} \times \vec{F}_{01}\right]^{(1)} = skew\left(\bar{r}_{C_{azi}O}^{(1)}\right) \begin{bmatrix} F_{011} \\ F_{012} \\ F_{013} \end{bmatrix} \Rightarrow$$

$$\left[\vec{r}_{C_{azi}O} \times \vec{F}_{01}\right]^{(1)} = \begin{bmatrix} 0 & -c_{azi3} & c_{azi2} \\ c_{azi3} & 0 & 0 \\ -c_{azi2} & 0 & 0 \end{bmatrix} \begin{bmatrix} F_{011} \\ F_{012} \\ F_{013} \end{bmatrix} \Rightarrow$$

$$\left[\vec{r}_{C_{azi}O} \times \vec{F}_{01}\right]^{(1)} = \begin{bmatrix} c_{azi2}F_{013} - c_{azi3}F_{012} \\ c_{azi3}F_{011} \\ -c_{azi2}F_{011} \end{bmatrix} \tag{A.3}$$

$$\left[\vec{r}_{C_{azi}A} \times \left(-\vec{F}_{12A}\right)\right]^{(1)} = -skew\left(\bar{r}_{C_{azi}A}^{(1)}\right)\hat{C}^{(1,2)}\begin{bmatrix} F_{12A1} \\ F_{12A2} \\ F_{12A3} \end{bmatrix} \Rightarrow$$

$$\left[\vec{r}_{C_{azi}A} \times \left(-\vec{F}_{12A}\right)\right]^{(1)}$$

$$= -\begin{bmatrix} 0 & d_1 - c_{azi3} & -d_2 + c_{azi2} \\ c_{azi3} - d_1 & 0 & 0 \\ d_2 - c_{azi2} & 0 & 0 \end{bmatrix}\begin{bmatrix} \cos\theta_2 & -\sin\theta_2 & 0 \\ 0 & 0 & 1 \\ -\sin\theta_2 & -\cos\theta_2 & 0 \end{bmatrix}^t \begin{bmatrix} F_{12A1} \\ F_{12A2} \\ F_{12A3} \end{bmatrix} \Rightarrow$$

$$\left[\vec{r}_{C_{azi}A} \times \left(-\vec{F}_{12A}\right)\right]^{(1)} = \begin{bmatrix} F_{12A3}(d_1 - c_{azi3}) + (d_2 - c_{azi2})(F_{12A1}\sin\theta_2 + F_{12A2}\cos\theta_2) \\ (c_{azi3} - d_1)(F_{12A1}\cos\theta_2 - F_{12A2}\sin\theta_2) \\ (d_2 - c_{azi2})(F_{12A1}\cos\theta_2 - F_{12A2}\sin\theta_2) \end{bmatrix} \tag{A.4}$$

$$\left[\vec{r}_{C_{azi}C} \times \left(-\vec{F}_{12C}\right)\right]^{(1)} = -skew\left(\bar{r}_{C_{azi}C}^{(1)}\right)\hat{C}^{(1,2)}\begin{bmatrix} F_{12C1} \\ F_{12C2} \\ 0 \end{bmatrix} \Rightarrow$$

$$\left[\vec{r}_{C_{azi}C} \times \left(-\vec{F}_{12C}\right)\right]^{(1)}$$

$$= -\begin{bmatrix} 0 & d_1 - c_{azi3} & d_3 + c_{azi2} \\ c_{azi3} - d_1 & 0 & 0 \\ -(d_3 + c_{azi2}) & 0 & 0 \end{bmatrix}\begin{bmatrix} \cos\theta_2 & -\sin\theta_2 & 0 \\ 0 & 0 & 1 \\ -\sin\theta_2 & -\cos\theta_2 & 0 \end{bmatrix}^t \begin{bmatrix} F_{12C1} \\ F_{12C2} \\ 0 \end{bmatrix}$$

$\Rightarrow$

$$\left[\vec{r}_{C_{azi}C} \times \left(-\vec{F}_{12C}\right)\right]^{(1)} = \begin{bmatrix} -(d_3 + c_{azi2})(F_{24C1}\sin\theta_2 + F_{24C2}\cos\theta_2) \\ (c_{azi3} - d_1)(F_{12C1}\cos\theta_2 - F_{12C2}\sin\theta_2) \\ -(d_3 + c_{azi2})(F_{12C1}\cos\theta_2 - F_{12C2}\sin\theta_2) \end{bmatrix} \tag{A.5}$$

Moment equation for the body 2, (2.63), is rewritten.

$$\check{J}_2 \cdot \vec{\alpha}_2 + \vec{\omega}_2 \times \check{J}_2 \cdot \vec{\omega}_2 = \vec{T}_{12a} + \vec{T}_{12d} + \vec{r}_{C_{ele}A} \times \vec{F}_{12A} + \vec{r}_{C_{ele}C} \times \vec{F}_{12C}$$

Individual terms of the (2.63) can be expressed in matrix form in reference frame of body 2 as follows.

$$\hat{J}_2^{(2)}\bar{\alpha}_2^{(2)} = \begin{bmatrix} J_{211} & J_{212} & J_{213} \\ J_{212} & J_{222} & J_{223} \\ J_{213} & J_{223} & J_{233} \end{bmatrix}\hat{C}^{(2,0)}\bar{\alpha}_2^{(0)} \Rightarrow$$

$$\hat{J}_2^{(2)}\bar{\alpha}_2^{(2)}$$

$$= \begin{bmatrix} J_{211} & J_{212} & J_{213} \\ J_{212} & J_{222} & J_{223} \\ J_{213} & J_{223} & J_{233} \end{bmatrix} \begin{bmatrix} \cos\theta_1\cos\theta_2 & \sin\theta_1\cos\theta_2 & -\sin\theta_1 \\ -\cos\theta_1\sin\theta_2 & -\sin\theta_1\sin\theta_2 & -\cos\theta_1 \\ -\sin\theta_1 & \cos\theta_1 & 0 \end{bmatrix} \begin{bmatrix} -\dot{\theta}_1\dot{\theta}_2\cos\theta_1 - \ddot{\theta}_2\sin\theta_1 \\ -\dot{\theta}_1\dot{\theta}_2\sin\theta_1 + \ddot{\theta}_2\cos\theta_1 \\ \ddot{\theta}_1 \end{bmatrix}$$

$\Rightarrow$

$$\begin{matrix} \hat{J}_2^{(2)}\bar{\alpha}_2^{(2)} \\ = \begin{bmatrix} \ddot{\theta}_1(-J_{211}\sin\theta_2 - J_{212}\cos\theta_2) + \ddot{\theta}_2(J_{213}) + (-J_{211}\cos\theta_2\,\dot{\theta}_1\dot{\theta}_2 + J_{212}\sin\theta_2\,\dot{\theta}_1) \\ \ddot{\theta}_1(-J_{212}\sin\theta_2 - J_{222}\cos\theta_2) + \ddot{\theta}_2(J_{223}) + (-J_{212}\cos\theta_2\,\dot{\theta}_1\dot{\theta}_2 + J_{222}\sin\theta_2\,\dot{\theta}_1) \\ \ddot{\theta}_1(-J_{213}\sin\theta_2 - J_{223}\cos\theta_2) + \ddot{\theta}_2(J_{233}) + (-J_{213}\cos\theta_2\,\dot{\theta}_1\dot{\theta}_2 + J_{223}\sin\theta_2\,\dot{\theta}_1) \end{bmatrix} \end{matrix} \quad \text{(A.6)}$$

$$\tilde{\omega}_2{}^{(2)}\hat{J}_2\bar{\omega}_2^{(2)} = skew\left(\bar{\omega}_2^{(2)}\right)\begin{bmatrix} J_{211} & J_{212} & J_{213} \\ J_{212} & J_{222} & J_{223} \\ J_{213} & J_{223} & J_{233} \end{bmatrix}\bar{\omega}_2^{(2)} \Rightarrow$$

$$\tilde{\omega}_2{}^{(2)}\hat{J}_2\bar{\omega}_2^{(2)} = skew\left(\hat{C}^{(2,0)}\bar{\omega}_2{}^{(0)}\right)\begin{bmatrix} J_{211} & J_{212} & J_{213} \\ J_{212} & J_{222} & J_{223} \\ J_{213} & J_{223} & J_{233} \end{bmatrix}\hat{C}^{(2,0)}\bar{\omega}_2{}^{(0)} \Rightarrow$$

$$\tilde{\omega}_2{}^{(2)}\hat{J}_2\bar{\omega}_2^{(2)}$$

$$= skew\left(\begin{bmatrix} \cos\theta_1\cos\theta_2 & \sin\theta_1\cos\theta_2 & -\sin\theta_1 \\ -\cos\theta_1\sin\theta_2 & -\sin\theta_1\sin\theta_2 & -\cos\theta_1 \\ -\sin\theta_1 & \cos\theta_1 & 0 \end{bmatrix}\begin{bmatrix} -\dot{\theta}_2\sin\theta_1 \\ \dot{\theta}_2\cos\theta_1 \\ \dot{\theta}_1 \end{bmatrix}\right)\begin{bmatrix} J_{211} & J_{212} & J_{213} \\ J_{212} & J_{222} & J_{223} \\ J_{213} & J_{223} & J_{233} \end{bmatrix}\ldots$$

$$\begin{bmatrix} \cos\theta_1\cos\theta_2 & \sin\theta_1\cos\theta_2 & -\sin\theta_1 \\ -\cos\theta_1\sin\theta_2 & -\sin\theta_1\sin\theta_2 & -\cos\theta_1 \\ -\sin\theta_1 & \cos\theta_1 & 0 \end{bmatrix}\begin{bmatrix} -\dot{\theta}_2\sin\theta_1 \\ \dot{\theta}_2\cos\theta_1 \\ \dot{\theta}_1 \end{bmatrix} \Rightarrow$$

$$\tilde{\omega}_2{}^{(2)}\hat{J}_2\bar{\omega}_2^{(2)} = skew\left(\begin{bmatrix} -\dot{\theta}_1\sin\theta_2 \\ -\dot{\theta}_1\cos\theta_2 \\ \dot{\theta}_2 \end{bmatrix}\right)\begin{bmatrix} J_{211} & J_{212} & J_{213} \\ J_{212} & J_{222} & J_{223} \\ J_{213} & J_{223} & J_{233} \end{bmatrix}\begin{bmatrix} -\dot{\theta}_1\sin\theta_2 \\ -\dot{\theta}_1\cos\theta_2 \\ \dot{\theta}_2 \end{bmatrix} \Rightarrow$$

$$\tilde{\omega}_2{}^{(2)}\hat{J}_2\bar{\omega}_2^{(2)}$$

$$= \begin{bmatrix} 0 & -\dot{\theta}_2 & -\dot{\theta}_1\cos\theta_2 \\ \dot{\theta}_2 & 0 & \dot{\theta}_1\sin\theta_2 \\ \dot{\theta}_1\cos\theta_2 & -\dot{\theta}_1\sin\theta_2 & 0 \end{bmatrix}\begin{bmatrix} J_{211} & J_{212} & J_{213} \\ J_{212} & J_{222} & J_{223} \\ J_{213} & J_{223} & J_{233} \end{bmatrix}\begin{bmatrix} -\dot{\theta}_1\sin\theta_2 \\ -\dot{\theta}_1\cos\theta_2 \\ \dot{\theta}_2 \end{bmatrix} \Rightarrow$$

$$\begin{matrix} \tilde{\omega}_2{}^{(2)}\hat{J}_2\bar{\omega}_2^{(2)} \\ = \begin{bmatrix} J_{223}\left(\dot{\theta}_1^2\cos^2\theta_2 - \dot{\theta}_2^2\right) + J_{212}\dot{\theta}_1\dot{\theta}_2\sin\theta_2 + J_{213}\dot{\theta}_1^2\sin\theta_2\cos\theta_2 - \dot{\theta}_1\dot{\theta}_2\cos\theta_2\,(J_{233} - J_{222}) \\ -J_{213}\left(\dot{\theta}_1^2\sin^2\theta_2 + \dot{\theta}_2^2\right) + \dot{\theta}_1\dot{\theta}_2\sin\theta_2\,(J_{211} + J_{233}) + J_{212}\dot{\theta}_1\dot{\theta}_2\cos\theta_2 - J_{223}\dot{\theta}_1^2\sin\theta_2\cos\theta_2 \\ J_{212}\left(\dot{\theta}_1^2\cos^2\theta_2 - \dot{\theta}_1^2\sin^2\theta_2\right) + \dot{\theta}_1^2\sin\theta_2\cos\theta_2\,(J_{211} - J_{222}) - J_{213}\dot{\theta}_1\dot{\theta}_2\cos\theta_2 + J_{223}\dot{\theta}_1\dot{\theta}_2\sin\theta_2 \end{bmatrix} \end{matrix} \quad \text{(A.7)}$$

$$\left[\vec{r}_{C_{ele}A} \times \vec{F}_{12A}\right]^{(2)} = skew\left(\bar{r}^{(2)}_{C_{ele}A}\right)\begin{bmatrix} F_{12A1} \\ F_{12A2} \\ F_{12A3} \end{bmatrix} \Rightarrow$$

$$\left[\vec{r}_{C_{ele}A} \times \vec{F}_{12A}\right]^{(2)} = \begin{bmatrix} 0 & c_2 + d_2 & 0 \\ -c_2 - d_2 & 0 & 0 \\ 0 & 0 & 0 \end{bmatrix}\begin{bmatrix} F_{12A1} \\ F_{12A2} \\ F_{12A3} \end{bmatrix} \Rightarrow$$

$$\left[\vec{r}_{C_{ele}A} \times \vec{F}_{12A}\right]^{(2)} = \begin{bmatrix} (c_2 + d_2)F_{12A2} \\ -(c_2 + d_2)F_{12A1} \\ 0 \end{bmatrix} \tag{A.8}$$

$$\left[\vec{r}_{C_{ele}C} \times \vec{F}_{12C}\right]^{(2)} = skew\left(\bar{r}^{(2)}_{C_{ele}C}\right)\begin{bmatrix} F_{12C1} \\ F_{12C2} \\ 0 \end{bmatrix}$$

$$\left[\vec{r}_{C_{ele}C} \times \vec{F}_{12C}\right]^{(2)} = \begin{bmatrix} 0 & c_2 - d_3 & 0 \\ d_3 - c_2 & 0 & 0 \\ 0 & 0 & 0 \end{bmatrix}\begin{bmatrix} F_{12C1} \\ F_{12C2} \\ 0 \end{bmatrix} \Rightarrow$$

$$\left[\vec{r}_{C_{ele}C} \times \vec{F}_{12C}\right]^{(2)} = \begin{bmatrix} (c_2 - d_3)F_{12C2} \\ (d_3 - c_2)F_{12C1} \\ 0 \end{bmatrix} \tag{A.9}$$

B. Equation of Motion

Solving (2.60) and (2.61) for F_{12C1} and F_{12C2},

$$F_{12C1} = -m_2 c_2 \cos\theta_2\, \ddot{\theta}_1 + m_2 g \sin\theta_2 - F_{12A1}$$

$$F_{12C2} = m_2 c_2 \sin\theta_2\, \ddot{\theta}_1 + m_2 g \cos\theta_2 - F_{12A2}$$

Substituting F_{12C1} and F_{12C2} into (2.65),

$$\begin{aligned}
&\ddot{\theta}_1(-J_{212}\sin\theta_2 - J_{222}\cos\theta_2) + \ddot{\theta}_2(J_{223}) + \left(-J_{212}\cos\theta_2\,\dot{\theta}_1\dot{\theta}_2 + J_{222}\sin\theta_2\,\dot{\theta}_1\right)\\
&\quad - J_{213}\left(\dot{\theta}_1^2\sin^2\theta_2 + \dot{\theta}_2^2\right) + \dot{\theta}_1\dot{\theta}_2\sin\theta_2\,(J_{211} + J_{233})\\
&\quad + J_{212}\dot{\theta}_1\dot{\theta}_2\cos\theta_2 - J_{223}\dot{\theta}_1^2\sin\theta_2\cos\theta_2\\
&\quad = -(c_2 + d_2)F_{12A1}\\
&\quad + (d_3 - c_2)\left(-m_2 c_2\cos\theta_2\,\ddot{\theta}_1 + m_2 g\sin\theta_2 - F_{12A1}\right) \Rightarrow\\
&\ddot{\theta}_1(-J_{212}\sin\theta_2 - J_{222}\cos\theta_2 + (d_3 - c_2)m_2 c_2\cos\theta_2) + \ddot{\theta}_2(J_{223})\\
&\quad + \left(-J_{212}\cos\theta_2\,\dot{\theta}_1\dot{\theta}_2 + J_{222}\sin\theta_2\,\dot{\theta}_1\right) - J_{213}\left(\dot{\theta}_1^2\sin^2\theta_2 + \dot{\theta}_2^2\right)\\
&\quad + \dot{\theta}_1\dot{\theta}_2\sin\theta_2\,(J_{211} + J_{233}) + J_{212}\dot{\theta}_1\dot{\theta}_2\cos\theta_2\\
&\quad - J_{223}\dot{\theta}_1^2\sin\theta_2\cos\theta_2 - (d_3 - c_2)m_2 g\sin\theta_2 = -(d_2 + d_3)F_{12A1}\\
&\quad \Rightarrow
\end{aligned}$$

Defining the dependent variables so that F_{12A1} can be expressed as follows.

$$CONS_{11} = \frac{-J_{212}\sin\theta_2 - J_{222}\cos\theta_2 + (d_3 - c_2)m_2 c_2\cos\theta_2}{-(d_2 + d_3)} \tag{B.1}$$

$$CONS_{12} = \frac{J_{223}}{-(d_2 + d_3)} \tag{B.2}$$

$$\begin{aligned}
&CONS_{13}\\
&= \frac{J_{222}\sin\theta_2\,\dot{\theta}_1 - J_{213}\left(\dot{\theta}_1^2\sin^2\theta_2 + \dot{\theta}_2^2\right) + \dot{\theta}_1\dot{\theta}_2\sin\theta_2\,(J_{211} + J_{233})}{-(d_2 + d_3)}\\
&+ \frac{-J_{223}\dot{\theta}_1^2\sin\theta_2\cos\theta_2 - (d_3 - c_2)m_2 g\sin\theta_2}{-(d_2 + d_3)}
\end{aligned} \tag{B.3}$$

$$F_{12A1} = \ddot{\theta}_1 CONS_{11} + \ddot{\theta}_2 CONS_{12} + CONS_{13} \tag{B.4}$$

Substituting F_{12C1} and F_{12C2} into, (2.64),

$$\ddot{\theta}_1(-J_{211}\sin\theta_2 - J_{212}\cos\theta_2 - (c_2 - d_3)m_2c_2\sin\theta_2) + \ddot{\theta}_2(J_{213})$$
$$+ \left(-J_{211}\cos\theta_2\,\dot{\theta}_1\dot{\theta}_2 + J_{212}\sin\theta_2\,\dot{\theta}_1\right) + J_{223}\left(\dot{\theta}_1^2\cos^2\theta_2 - \dot{\theta}_2^2\right)$$
$$+ J_{212}\dot{\theta}_1\dot{\theta}_2\sin\theta_2 + J_{213}\dot{\theta}_1^2\sin\theta_2\cos\theta_2$$
$$- \dot{\theta}_1\dot{\theta}_2\cos\theta_2\,(J_{233} - J_{222}) - (c_2 - d_3)m_2g\cos\theta_2$$
$$= (d_2 + d_3)F_{12A2} \Rightarrow$$

Defining the dependent variables so that F_{12A2} can be expressed as follows.

$$CONS_{21} = \frac{-J_{211}\sin\theta_2 - J_{212}\cos\theta_2 - (c_2 - d_3)m_2c_2\sin\theta_2}{d_2 + d_3} \tag{B.5}$$

$$CONS_{22} = \frac{J_{213}}{d_2 + d_3} \tag{B.6}$$

$$CONS_{23}$$
$$= \frac{-J_{211}\cos\theta_2\,\dot{\theta}_1\dot{\theta}_2 + J_{212}\sin\theta_2\,\dot{\theta}_1 + J_{223}\left(\dot{\theta}_1^2\cos^2\theta_2 - \dot{\theta}_2^2\right)\sin\theta_2}{d_2 + d_3}$$
$$+ \frac{+J_{212}\dot{\theta}_1\dot{\theta}_2 + J_{213}\dot{\theta}_1^2\sin\theta_2\cos\theta_2 - \dot{\theta}_1\dot{\theta}_2\cos\theta_2\,(J_{233} - J_{222})}{d_2 + d_3} \tag{B.7}$$
$$+ \frac{-(c_2 - d_3)m_2g\cos\theta_2}{d_2 + d_3}$$

$$F_{12A2} = \ddot{\theta}_1 CONS_{21} + \ddot{\theta}_2 CONS_{22} + CONS_{23} \tag{B.8}$$

Substituting F_{12C1} and F_{12C2} into (2.53) to solve for F_{011}.

$$F_{011} = m_1c_{azi2}\ddot{\theta}_1 + \left(-m_2c_2\cos\theta_2\,\ddot{\theta}_1 + m_2g\sin\theta_2\right)\cos\theta_2$$
$$- \left(F_{12A2} + m_2c_2\sin\theta_2\,\ddot{\theta}_1 + m_2g\cos\theta_2\right)\sin\theta_2 \Rightarrow$$
$$F_{011} = (m_1c_{azi2} - m_2c_2)\ddot{\theta}_1 \tag{B.9}$$

Substituting F_{12C1}, F_{12C2} and F_{011} into (2.59) to expressing the resultant equation in terms of $\ddot{\theta}_1$ and $\ddot{\theta}_2$.

$$J_{133}\ddot{\theta}_1 = T_{01a} - c_{01d}\dot{\theta}_1 - c_{azi2}\left((m_1c_{azi2} - m_2c_2)\ddot{\theta}_1\right)$$
$$- (d_2 - c_{azi2})(F_{12A1}\cos\theta_2 - F_{12A2}\sin\theta_2)$$
$$+ (d_3 + c_{azi2})\left(\left(-m_2c_2\cos\theta_2\,\ddot{\theta}_1 + m_2g\sin\theta_2 - F_{12A1}\right)\cos\theta_2\right.$$
$$\left. - \left(m_2c_2\sin\theta_2\,\ddot{\theta}_1 + m_2g\cos\theta_2 - F_{12A2}\right)\sin\theta_2\right) \Rightarrow$$

$$\ddot{\theta}_1(J_{133} + (d_3 + c_{azi2})m_2c_2\cos\theta_2)$$
$$= T_{01a} - c_{01d}\dot{\theta}_1 - c_{azi2}\left((m_1c_{azi2} - m_2c_2)\ddot{\theta}_1\right)$$
$$- F_{12A1}(d_2 + d_3)\cos\theta_2 + F_{12A2}(d_2 + d_3)\sin\theta_2 \Rightarrow$$

$$\ddot{\theta}_1(J_{133} + (d_3 + c_{azi2})m_2c_2\cos\theta_2)$$
$$= T_{01a} - c_{01d}\dot{\theta}_1 - c_{azi2}\left((m_1c_{azi2} - m_2c_2)\ddot{\theta}_1\right)$$
$$- \left(\ddot{\theta}_1CONS_{11} + \ddot{\theta}_2CONS_{12} + CONS_{13}\right)(d_2 + d_3)\cos\theta_2$$
$$+ \left(\ddot{\theta}_1CONS_{21} + \ddot{\theta}_2CONS_{22} + CONS_{23}\right)(d_2 + d_3)\sin\theta_2 \Rightarrow$$

$$\begin{aligned}\ddot{\theta}_1(J_{133} + (d_3 + c_{azi2})m_2c_2\cos\theta_2 + c_{azi2}(m_1c_{azi2} - m_2c_2)\\ + CONS_{11}(d_2 + d_3)\cos\theta_2\\ - CONS_{21}(d_2 + d_3)\sin\theta_2)\\ + \ddot{\theta}_2(CONS_{12}(d_2 + d_3)\cos\theta_2\\ - CONS_{22}(d_2 + d_3)\sin\theta_2)\\ = T_{01a} - c_{01d}\dot{\theta}_1 - CONS_{13}(d_2 + d_3)\cos\theta_2\\ + CONS_{23}(d_2 + d_3)\sin\theta_2\end{aligned} \tag{B.10}$$

Defining the dependent variables so that (B.10) can be expressed as follows.

$$\begin{aligned}CONS_{31} = J_{133} + (d_3 + c_{azi2})m_2c_2\cos\theta_2\\ + c_{azi2}(m_1c_{azi2} - m_2c_2)\\ + CONS_{11}(d_2 + d_3)\cos\theta_2\\ - CONS_{21}(d_2 + d_3)\sin\theta_2\end{aligned} \tag{B.11}$$

$$\begin{aligned}CONS_{32} = CONS_{12}(d_2 + d_3)\cos\theta_2\\ - CONS_{22}(d_2 + d_3)\sin\theta_2\end{aligned} \tag{B.12}$$

$$\begin{aligned}CONS_{33} = -\left(T_{01a} - c_{01d}\dot{\theta}_1 - CONS_{13}(d_2 + d_3)\cos\theta_2\right.\\ \left. + CONS_{23}(d_2 + d_3)\sin\theta_2\right)\end{aligned} \tag{B.13}$$

$$\ddot{\theta}_1CONS_{31} + \ddot{\theta}_2CONS_{32} + CONS_{33} = 0 \tag{B.14}$$

Substituting F_{12C1}, F_{12C2} and F_{011} into (2.66) to expressing the resultant equation in terms of $\ddot{\theta}_1$ and $\ddot{\theta}_2$.

$$\begin{aligned}\ddot{\theta}_1(-J_{213}\sin\theta_2 - J_{223}\cos\theta_2) + \ddot{\theta}_2(J_{233}) - J_{213}\cos\theta_2\,\dot{\theta}_1\dot{\theta}_2 \\ + J_{223}\sin\theta_2\,\dot{\theta}_1 + J_{212}\left(\dot{\theta}_1^2\cos^2\theta_2 - \dot{\theta}_1^2\sin^2\theta_2\right) \\ + \dot{\theta}_1^2\sin\theta_2\cos\theta_2\,(J_{211} - J_{222}) \\ - J_{213}\dot{\theta}_1\dot{\theta}_2\cos\theta_2 + J_{223}\dot{\theta}_1\dot{\theta}_2\sin\theta_2 \\ - \left(T_{12a} - c_{12d}\dot{\theta}_2\right) = 0\end{aligned} \tag{B.15}$$

Defining the dependent variables so that (B.16)(B.15) can be expressed as follows.

$$CONS_{41} = -J_{213}\sin\theta_2 - J_{223}\cos\theta_2 \tag{B.16}$$

$$CONS_{42} = J_{233} \tag{B.17}$$

$$\begin{aligned}CONS_{43} = -J_{213}\cos\theta_2\,\dot{\theta}_1\dot{\theta}_2 + J_{223}\sin\theta_2\,\dot{\theta}_1 \\ + J_{212}\left(\dot{\theta}_1^2\cos^2\theta_2 - \dot{\theta}_1^2\sin^2\theta_2\right) \\ + \dot{\theta}_1^2\sin\theta_2\cos\theta_2\,(J_{211} - J_{222}) \\ - J_{213}\dot{\theta}_1\dot{\theta}_2\cos\theta_2 + J_{223}\dot{\theta}_1\dot{\theta}_2\sin\theta_2 \\ - \left(T_{12a} - c_{12d}\dot{\theta}_2\right)\end{aligned} \tag{B.18}$$

$$\ddot{\theta}_1 CONS_{41} + \ddot{\theta}_2 CONS_{42} + CONS_{43} = 0 \tag{B.19}$$

(B.14) and (B.19) can be expressed in matrix representation as follows.

$$\begin{bmatrix} CONS_{31} & CONS_{32} \\ CONS_{41} & CONS_{42} \end{bmatrix}\begin{bmatrix}\ddot{\theta}_1 \\ \ddot{\theta}_2\end{bmatrix} = -\begin{bmatrix} CONS_{33} \\ CONS_{43}\end{bmatrix} \tag{B.20}$$

Expanding the (B.20) to involve gimbal angular velocity terms,

$$\begin{bmatrix} 0 & 1 & 0 & 0 \\ 0 & CONS_{31} & 0 & CONS_{32} \\ 0 & 0 & 0 & 1 \\ 0 & CONS_{41} & 0 & CONS_{42}\end{bmatrix}\begin{bmatrix}\dot{\theta}_1 \\ \ddot{\theta}_1 \\ \dot{\theta}_2 \\ \ddot{\theta}_2\end{bmatrix} = -\begin{bmatrix}\dot{\theta}_1 \\ CONS_{33} \\ \dot{\theta}_2 \\ CONS_{43}\end{bmatrix} \tag{B.21}$$